Probing the role of transmembrane domain interactions in Toll-like receptor signaling

by

James Isaac Godfroy III

B.S., University of Notre Dame, 2009

A thesis submitted to the

Faculty of the Graduate School of the

University of Colorado in partial fulfillment

of the requirements for the degree of

Doctor of Philosophy

Department of Chemical and Biological Engineering

2015

This thesis entitled:
Probing the role of transmembrane domain interactions in Toll-like receptor signaling
written by James Isaac Godfroy III
has been approved for the Department of Chemical and Biological Engineering

_____
Prof. Hubert Yin

_____
Prof. Theodore Randolph

_____
Prof. Amy Palmer

Date _____

The final copy of this thesis has been examined by the signatories, and we find that both the content and the form meet acceptable presentation standards of scholarly work in the above mentioned discipline.

Godfroy III, James Isaac (Ph.D., Chemical and Biological Engineering)

Probing the role of transmembrane domain interactions in Toll-like receptor signaling

Thesis directed by Prof. Hubert Yin and Prof. Theodore Randolph

Membrane proteins account for approximately 30% of the human proteome, are the therapeutic target of nearly 60% of current pharmacological agents, yet account for <1% of all solved structures. This lack of information on membrane proteins extends from the difficulty in studying transmembrane domains due to their inherent insolubility and instability outside of membrane mimetics. New methods to study these domains are critical for advancing the understanding of membrane protein signal transduction.

The Toll-like receptor (TLR) family of membrane proteins serve as critical sensors of infection for the innate immune system. As mounting evidence suggests that the transmembrane domain is a critical region in several protein families, we hypothesized that this was also the case for TLRs. Using a biochemical and biophysical approach in membrane mimetic systems, we were the first to report the role of isolated transmembrane domain interactions in TLR oligomerization. We showed that all TLR transmembrane domains were capable of homotypic interactions. We also demonstrated that the TLR2 transmembrane domain preferentially interacted with the transmembrane domains of its heterotypic signaling partners, TLR1 and TLR6.

To better understand the role of transmembrane domain interactions in biologically relevant membranes, we utilized acceptor photobleaching Förster resonant energy transfer to image the involvement of individual domains in TLR assembly in live cells. This technique is a simple, rapid approach to screen for both homotypic and heterotypic interactions in native protein environments. Results suggest that TLR2-TLR1 and TLR2-TLR6 transmembrane domains are interacting heterotypically in native cell membranes.

To better screen TLR signaling pathways for novel therapeutic intervention, we established a genetic reporter in native immune cells, monocytes and T-cells, for monitoring TLR signaling

activity. Monocytes specifically responded to TLR2 agonists and T-cells were specific for TLR5 agonists. Utilization of these cell lines allowed for screening of transmembrane domain libraries to investigate the potential of regulating TLR2 and TLR5 signaling through transmembrane domain interactions. Furthermore, they allowed for validation of small molecule therapies to treat TLR related diseases.

Dedication

To my parents for their endless support in all my endeavors.

To my friends for all the enjoyable adventures.

Acknowledgements

I would like to first thank my advisors, Hubert Yin and Ted Randolph, for the help, encouragement, and guidance on this project throughout my time in graduate school. I would also like to thank Amy Palmer and her lab for all of the assistance they have provided in my endless quest for the perfect images and FRET experiments. I would also like to thank my committee members, Joel Kaar and Stephanie Bryant, for the general support and guidance they have provided.

I also have to acknowledge all the great support staff that have significantly improved the day to day work as a graduate student. First, I would like to thank Theresa Nahreini for all her help in cell culture, flow cytometry, and the general daily discussions. I would also like to thank Joe Dragavon in the microscope core facility for his assistance with all the imaging experiments. I also can never say enough about the assistance Dominique de Vangel has provided for meeting all the graduate school deadlines and getting everything organized.

To all past and present Yin lab members, I have greatly appreciated the support in learning new techniques, running experiments, and discussing science in general. You have made my time in lab much more enjoyable with the friendly banter. I also appreciate all of the undergraduate students who have spent time with me working on various portions of this project.

I would like to thank my friends for making my time here enjoyable. I've had several great ski trips, numerous soccer games, and late night lifting sessions which have all provided me a nice distraction from lab work.

Lastly, I would like to thank the two most important people, my parents, for all their support and encouragement.

Contents

Chapter

Tables

Table

Figures

Figure

Chapter 1

Introduction

Portions of this chapter have been published as M. W. Lluis, J. I. Godfroy III, and H. Yin "Protein engineering methods applied to membrane protein targets" *Protein Engineering, Design & Selection* 26:91-100 **2013**. [134]

1.1 Membrane Proteins

Membrane proteins are estimated to account for 15-40% of the proteins encoded by the human genome based on hydropathy analysis [195, 1]. These membrane proteins are vital to cellular regulation, metabolism, and homeostasis by actions through various signaling receptors, transporters, ion channels, and enzymes. Involved in so many critical cellular processes membrane proteins are a high-priority target for drug design, currently accounting for nearly 60% of current pharmaceutical targets [228]. A specific subset of membrane proteins, transmembrane proteins, have some portion of their polypeptide chain that traverses the cellular membrane. Transmembrane proteins are considered critical gatekeepers for directly or indirectly inducing a biochemical response making them particularly interesting drug targets [215]. A specific signaling receptor class of transmembrane proteins, G-protein coupled receptors, currently account for nearly 30% of the membrane protein drug targets [163]. Even though these transmembrane proteins are considered such high-priority drug targets, there is a dearth of structural and biochemical information for them. This lack of information stems from the inherent insolubility and instability of transmembrane domains making for extremely difficult expression and purification of these open reading frames using recombinant

systems [98, 144]. The inherent difficulty in generating crystals for membrane proteins means that there are very few solved structures, less than 1% of known protein structures, preventing structure-function relationships from being obtained [220]. This lack of structural information means other methods for studying structure-function relationships are needed to understand membrane protein interactions.

In this thesis, we have advanced methods to investigate transmembrane protein-protein interactions, with the first proof of concept for studying heterotypic interactions in native membrane environments rather than traditional membrane mimetics (Chapter 3). During these studies, we expanded the understanding of transmembrane domain interactions, by investigating a family of proteins, Toll-like receptors, in which the role of the transmembrane domain had previously not been studied, and proving that they interact (Chapter 2). This chapter will provide an overview of the current field of transmembrane domain interactions and an overview of the Toll-like receptor family interactions and signaling as well as the clinical importance of developing new therapies to target Toll-like receptor interactions.

1.2 Transmembrane Domain Protein Interactions

Not only is there a lack of structural information on membrane proteins, but there is still a major question about what role the transmembrane domain itself has in protein function. It was long thought that transmembrane domains did not mediate specific protein-protein interactions, rather these domains served simply as a passive anchor to the lipid bilayer [151]. This thought has undergone a paradigm shift as it has recently been demonstrated that the transmembrane domain itself can specifically promote protein-protein interactions [151, 110]. These transmembrane domain interactions are often highly specific, arising from structural motifs that allow for noncovalent interactions to stabilize the helix-helix contacts. Typical driving forces include van der Waals packing interfaces, polar residues for ionic interactions, and hydroxylated amino acids for hydrogen bonding [151, 110]. Various methods have been used to elucidate the types of motifs that might contribute to the specificity of transmembrane domain interactions [224].

Transmembrane domain interactions can be classified in two broad categories [151]:

(1) static contacts between transmembrane helices involved in assembly of protein complexes; and

(2) regulated transmembrane interactions in signal transduction that can switch oligomeric state or conformation in response to stimuli.

These two types of interactions are demonstrated by multiple classes of transmembrane proteins. A brief overview of some receptor classes that utilize these different mechanisms will be outlined to highlight the important role transmembrane domains play in the assembly of active signaling complexes.

1.2.1 Static Transmembrane Domain Interactions

1.2.1.1 Glycophorin A

The most extensively studied transmembrane domain has been that of the glycophorin A (GpA) membrane protein from erythrocyte cells. It was originally found that fusions of the GpA transmembrane domain with the monomeric nuclease A protein from *S. aureus* were predominantly dimeric in the presence of sodium dodecyl sulfate detergent [120]. It was further found that the GpA transmembrane domain could dimerize in bacterial membranes [111], and that this interaction is strongly driven by a consensus motif, LIxxGVxxGVxxT [17]. An examination of membrane proteins found that an overrepresented sequence motif is a pattern of small residues (Gly, Ala, or Ser) spaced at the *i* and *i+4* positions of an α-helix (Small-xxx-Small) with a preference for β-branched residues (Val, Ile) at the neighboring positions $i\pm1$, $i\pm2$ [190], as is seen in that for the GpA transmembrane domain motif. Point mutations in the GpA interaction motif identified the glycine residues as being critical for oligomerization [178, 44]. This lead to the proposal that the Small-xxx-Small motif generates a groove on one face of the transmembrane helix for van der Waals packing of the much larger β-branched residues. More recent studies have shown that in mammalian mimetic systems the GpA transmembrane domain can dimerize [22, 186].

1.2.1.2 Immune Receptor Complexes

The T-cell receptor complex consists of seven single-pass transmembrane proteins, that form an important complex for adaptive immune responses [4]. Early reports showed the presence of polar residues in the transmembrane domains were critical for proper trafficking and assembly of the T-cell receptor complex [136, 179]. These transmembrane domain interactions led to the development of a transmembrane core peptide containing the two critical charged residues, GL**R**ILLL**K**V. This core peptide was capable of inhibiting T-cell receptor activation as well as B-cell and NK-cell function [137, 83]. Utilizing a fluorescently labeled core peptide and fluorescent monoclonal antibodies against proteins in the T-cell receptor complex, it was shown by confocal microscopy that this core peptide localized at the plasma membrane with clustered T-cell receptors [217]. It is likely this peptide changes the ability of transmembrane domains to interact for proper receptor assembly. Transmembrane peptides derived from NK cell activating receptors carrying similar charged residues were also shown to inhibit NK cell cytotoxicity *in vitro* at comparable levels to the core peptide [212]. It is not surprising that the core peptide is capable of altering these interactions, as many receptors involved in immune responses contain buried polar residues [151, 141], indicating the importance of electrostatic interactions in transmembrane domains for proper receptor assembly in immune cells.

1.2.1.3 Epstein-Barr Virus

Epstein-Barr virus is a ubiquitis herpes virus involved in mononucleosis infection, Burkitt's lymphoma, and Hodgkin's disease. A multipass transmembrane protein, latent membrane protein 1 (LMP-1), is an essential component of the viral process that immortalizes B-cells so the virus can propagate. LMP-1 activates the same pathway as CD40 for cell survival and proliferation, but unlike CD40, LMP-1 does so in a ligand independent trimeric complex. Initial studies on the individual transmembrane domains showed propensity for oligomerization in SDS-PAGE gels, with transmembrane domain 5 being most likely to oligomerize in a trimeric complex [184]. Analysis

of transmembrane domain 5 indicated the presence of a buried polar residue, aspartic acid. This aspartic acid was shown to be critical for the trimerization of LMP-1 with mutations of this residue greatly reducing oligomerization potential and potentiating signaling capability in live cells [184].

1.2.2 Switchable Transmembrane Domain Interactions

1.2.2.1 Integrin Receptors

The integrin family of receptors are eukaryotic cell-surface proteins that are activated by heterotypic interactions between α and β subunits. There are multiple heterotypic interactions that occur between the 18 α subunits and 8 β subunits that mediate several cell regulation processes [188, 151]. Analysis of all human integrin subunits indicated that every receptor except for one of the β subunits contained a Small-xxx-Small motif at a similar depth in the membrane [188]. Using bacterial reporter assays for the various subunit transmembrane domains, it has been shown that a preference exists for homotypic over heterotypic interactions [188, 239]. This suggests that while the TMDs have interaction potential, the extracellular domain plays a critical role in forming the active heterodimeric complex. It is possible that the TMDs are in a homotypic state preventing activation and driving apart this interaction results in the active complexes. Another possibility is that the weak heterotypic interactions of the transmembrane domains are stabilized by extracellular domain interactions, and homotypic transmembrane domain interactions switch the complex to an active state.

The computational design of synthetic integrin peptides suggest that the heterocomplex is holding the receptors inactive, and homotypic interactions lead to the active state. The computational design of peptides that have optimized the packing interface of integrin α_{IIb} and α_v showed specific interactions with the native integrin against which they were designed [230]. Furthermore, it was shown that the addition of these designed peptides led to specific activation of the expected heterodimeric complexes, $\alpha_{IIb}\beta_3$ or $\alpha_v\beta_3$, at comparable levels to the known agonists [230, 19]. These results suggest that switching from heterotypic to homotypic interactions at the transmem-

brane domain is important for integrin activation. This switch can be accomplished through ligands binding the extracellular domain or through synthetic peptides targeting transmembrane domains [229, 230, 19].

1.2.2.2 Receptor Tyrosine Kinases

Receptor tyrosine kinases (RTKs) are a large family of proteins composed of a single transmembrane domain, an extracellular ligand binding domain, and an intracellular kinase domain. Binding of ligand causes a conformation change that leads to phosphorylation of the kinase domains [73]. The RTKs consist of several subfamilies including epidermal growth factor receptors (EGFRs), fibroblast growth factor receptors (FGFRs), platelet-derived growth factor receptors (PDGFR), and insulin or insulin-like growth factor receptors [124]. Bacterial reporter systems show that the transmembrane domains of RTKs encode for self interactions of varying propensity [51]. Many of the RTK interactions are significantly weaker than that seen for GpA (section 1.2.1.1) in the same system. However, RTKs exist in a monomer-dimer equilibrium at physiological conditions and likely require weaker dimerization for tightly controlled regulations [124]. It is thought that the transmembrane domains contribute rather significantly to this equilibrium [73] as multiple mutations in the transmembrane domains of these receptors are linked to disease [151].

The EGFR subfamily consists of four members that are important for cell growth and differentiation. Multiple studies have looked at the ability of the receptor transmembrane domains to oligomerize in bacterial membranes [148, 51]. The results show varying levels of interaction potential depending on the reporter used. Clustering of the full-length EGFR on the cell surface showed a small portion of the receptor was already dimeric prior to ligand addition, upon ligand addition the EGFR receptors clustered at a much higher percentage [54]. The EGFR receptor ErbB2 has a known oncogenic mutation in its transmembrane domain, Val664Glu, that introduces a polar residue in the center of the membrane. It has been shown in plasma membrane derived vesicles that this mutation leads to a higher propensity for dimerization [171], thus stabilizing the active complex. Furthermore, peptides derived from the transmembrane domain of ErbB2 could

specifically inhibit signaling if they were expressed endogenously or synthesized chemically [11]. In combination, these results show the importance of the transmembrane domains in EGFR activation and disease states.

The FGFR subfamily also consists of four members, that recognize over 20 different fibroblast growth factor ligands. These receptors are involved in cell proliferation and survival, and skeletal development making them an attractive area of therapeutic targeting [97, 124]. Several pathogenic mutations exist in FGFRs and have been traced to mutations in the transmembrane domain [97, 151]. Initial studies of these receptor transmembrane domains in bacterial membranes showed a very weak propensity for interactions compared to other RTKs [51]. Biophysical assays confirmed the weak interaction for FGFR3 transmembrane domains in the absence of extracellular domains and ligands [127]. However, FRET studies in plasma membrane vesicles suggest that the transmembrane domain oligomerizes and that the extracellular domain partially inhibits this interaction to prevent activation [23]. Further studies on FGFR3 by FRET found that one of the oncogenic mutations in the transmembrane domain, Gly380Arg, leads to a small increase in the stability of the dimeric complex [172]. The majority of the FGFR family oncogenic mutations occur in the transmembrane domain and introduce a charged polar residue or a cysteine residue [151]. As charged residues play a key role in transmembrane assembly, it is likely that these mutations act by stabilizing the active dimeric complex.

The PDGFR subfamily consists of five members, that control cell growth, differentiation, and development. The two main receptors, PDGFαR and PDGFβR, recognize specific growth factors depending on if they exist as a homodimer or heterodimer. The homodimer has been shown to be rather strongly formed by isolated transmembrane domains in bacterial membranes [51]. The PDGFβR interacts not only with itself, but it is also the target of oncogenic proteins that transform cells for survival. One oncoprotein that does this is the bovine papillomavirus E5 protein, a 44 amino acid transmembrane protein, that directly binds the transmembrane domain of PDGFβR [202].

The insulin subfamily has only two receptors, but they play a critical role in glucose transport

and glycogen synthesis, with defective function being a key cause of diabetes [124]. Unlike other RTKs, insulin receptors are known to be constitutively dimeric with a heterotetrameric receptor composed of dimers of the α and β subunits [119]. The insulin receptor transmembrane domains were shown to interact in bacterial membranes [51], and peptides derived from the insulin receptor transmembrane domain could specifically activate endogenous insulin receptors in the absence of insulin [119]. This transmembrane peptide could also activate an insulin receptor with a mutation that prevents it from binding insulin, indicating that it acts through a different mechanism, likely at the transmembrane domain [119].

Taken together, all these interactions show the importance of the transmembrane domains in oligomeric association and transmission of signals from the extracellular milieu to the inside of the cell. The importance of transmembrane domain interactions in proper assembly of immune receptor complexes (see section 1.2.1.2) provided much interest in investigating transmembrane domain interactions in the innate immune receptors, specifically, Toll-like receptors.

1.3 Toll-like Receptors

Toll-like receptors (TLRs) are a major class of proteins involved in the innate immune response, first identified in 1997 as a homolog to the *Drosophilia* protein, Toll, which was involved in fungal infections. TLRs act as a first line of defense against invading pathogens and provide a critical link to the adaptive immune system [146]. Unlike the adaptive immune system, which can take weeks to refine antibodies for pathogen clearance, TLRs recognize conserved patterns in bacterial pathogens to mount an immediate immune response. However, evidence has indicated that improper regulation of TLR signaling is associated with various diseases [161]. The link of TLRs to progression in cancer, infectious disease, autoimmune disorders, and allergies have made them an area of active research.

In humans there are ten known functional TLRs expressed in a variety of tissues and cell types, with highest expression seen in leukocytes [235]. TLRs are expressed in two different subcellular locations, the plasma membrane and endosomal compartments. These locations are critical for

pathogen recognition and accessibility, signal transduction, and avoidance of self recognition. The cell surface receptors (TLRs 1, 2, 4, 5, 6, and 10) recognize components of bacterial cell walls and endosomal receptors (TLRs 3, 7, 8, and 9) recognize bacterial and viral nucleic acids [101].

1.3.1 Toll-like Receptor Signaling

Every TLR shares a common structural motif,

(1) multiple, 19-25, extracellular Leucine rich repeats involved in ligand recognition,

(2) a single-pass transmembrane domain, and

(3) a Toll-Interleukin 1 receptor (TIR) intracellular signaling domain,

which all play critical roles in assembly and propagation of the TLR signaling complex. For pathogen recognition by TLRs it is known they must form a homodimer or heterodimer, as evident by the solved crystal structures for TLR extracellular domains with their PAMPs. Crystal structures have been solved of the ligand bound state for TLR2/TLR1 [91], TLR2/TLR6 [91], TLR3 [133], TLR4 [167], TLR5 [85], TLR8 [205], and TLR9 [157]. While the crystal structure of dimers all share a similar M-shaped structure with closely approaching C-termini, it is important to note that each ligand binds a distinctive interface [50]. It is also important to note that the binding of ligand brings the C-termini of the extracellular domains closer together, as evidenced by the TLR8 apo crystal structure [205]. It is proposed that through the juxtaposition of the C-termini the TLR TIR domains are also able to undergo homotypic interactions, forming a nucleation site to recruit adaptor proteins [50].

Intracellularly, there are five TIR domain containing adaptor proteins used by TLRs, MyD88, MAL, TRIF, TRAM, and SARM [160]. MyD88 and the adaptor MAL is used by all TLRs, except for TLR3, which uses TRIF and the adaptor TRAM [57]. The MyD88 adaptor protein is composed of the C-terminal TIR domain and an N-terminal death domain (DD) which are linked by a flexible intermediate domain [57]. Conserved DD homotypic interactions are critical for signal propagation as MyD88 DDs are able to associate with DDs of the Ser/Thr kinase IRAK family [50]. A structure

of the death domain interactions between MyD88 and IRAKs was solved and showed assembly of a large left-handed helical complex held together by three different, yet conserved, DD interactions [130]. This helical assembly Myddosome is composed of four distinct layers. The top layer is composed of two MyD88 DDs, followed immediatelly by four more MyD88 DDs, which interact with four IRAK4 DDs, and finally four IRAK2 DDs [130]. The initial ligand binding by TLRs is thought to recruit MyD88 to the membrane where it can reach a high enough concentration to oligomerize its DDs and act as a nucleation site for the assembly of IRAK4 [50]. It is believed that the assembly of the Myddosome presents an oligomeric complex for IRAK kinase activity through autophosphorylation of IRAK4 which can then phosphorylate IRAK2 [130, 50].

The phosphorylation of IRAK1/2 domains leads to recruitment of TRAF6 to the membrane [50]. TRAF6 is recruited through TRAF6 interaction motifs that are present in the MAL and TRIF TIR domain containing proteins [160]. TRAF6 oligomerization lends itself to E3 ubiquitination ligase activity with K63-linked polyubiquitin chains being added to IRAK1/2 and TRAF6 itself [50]. Interactions with polyubiquitin chains recruit other downstream signaling components, like TAK1, which upon activation autophosphorylates and can then in turn activate IKK complexes through phosphorylation [50]. The activation of IKK complexes allows for phosphorylation of the inhibitory subunit of IκB [152]. This phosphorylation event targets IκB for degradation by the proteasome, allowing release of NF-κB from this complex [152]. NF-κB is then free to translocate into the nucleus, where it binds target sequences for activation of gene transcription [152]. This gene transcription leads to the hallmark signals of TLR activation - proinflammatory cytokines, including TNF-α and various interleukins [100]. These chemokines and cytokines upregulate costimulatory molecules on specific antigen-presenting cells, providing a direct link between the innate and adaptive immune systems [100].

1.3.2 Toll-like Receptors in Disease and Therapeutic Interventions

The direct link between the innate and adaptive immune systems makes TLRs an interesting therapeutic target, with active research occurring in both academia and industry. The role of TLRs

in disease initiation and progression are still not fully understood, but they have been experimentally linked to various conditions. For example, TLR4 activation has been linked to septic shock [161], while TLR2 activation has been implicated in lupus [161], rheumatoid arthritis [64, 198], and diabetes [36, 129]. Other TLRs have also been suggested to be involved in several disease states [30, 213]. Mice that are deficient in particular TLRs have demonstrated the importance of their regulation in inflammatory diseases such as arthritis, multiple sclerosis, and inflammatory bowel disease [77]. The critical importance of TLRs in various diseases has created an area of focus for new and emerging therapeutic strategies [161, 30, 107, 96].

As TLRs are central to the innate immune response pathway, there is much interest in new antagonist and agonist therapies. Antagonists are desirable due to TLR activation occurring early in the inflammation cascade [77]. Only a few compounds have been developed as antagonists, since they usually suffer from specificity problems. Those that have been specific, such as TAK-242 and Eritoran for TLR4 induced septic shock treatment, have failed in Phase III clinical trials [96]. Agonist therapies are much more common due to the known ligands for activating TLRs. There is also more interest in agonists as they can be used in a wider range of treatment options, including as vaccine adjuvants, cancer therapies, allergic diseases, and infectious diseases. The vaccine adjuvant market is the most studied with one compound for TLR4 being clinically approved [96]. A small molecule agonist for TLR7 and TLR8, imiquimod, has also been approved for the treatment of genital warts and non-melanoma skin cancers [77].

1.3.3 TLR Transmembrane Domain Involvement in Trafficking and Signaling

The structures of every component in the TLR signaling pathway have been solved in varying detail [50, 152], except for the transmembrane domain region of Toll-like receptors. A better understanding of TLR transmembrane domain interactions is needed to aide in the understanding of how the ligand binding induces the necessary changes in TIR domain conformation to recruit the remaining signaling adaptor proteins. Evidence suggests that the transmembrane domains are a contributing factor in the trafficking and signaling of TLRs. For example, TLR4 is a known cell

surface protein, but by expressing chimeric constructs of TLR4 utilizing the transmembrane and TIR domains of the other TLRs, the TLR4 extracellular domain localized and responded to LPS in cellular compartments according to the expected localization of the TLR transmembrane and TIR domains used [156]. Later evidence suggested this localization may be specifically dependent on the transmembrane domain interactions, as the TLR3, TLR7, TLR8, and TLR9 transmembrane domains regulate trafficking through interactions with the UNC93B1 chaperone in the ER [197, 16, 117]. Another ER chaperone, PRAT4A, has been found to regulate trafficking of the cell surface TLRs [216, 199], with a point mutant near the C-terminus of the TLR1 transmembrane domain (I602S) greatly affecting proper localization of the receptor [69].

Transmembrane domains are likely not only important for trafficking, but also signaling. CD4 and integrin nucleated TLR transmembrane and TIR domains showed that even in forced dimers only specific homotypic and heterotypic pairs of TLRs could activate NF-κB signaling [164, 237]. Additionally, chimeric constructs of TLR4 could only respond to LPS if cooperative transmembrane and TIR domains were expressed, i.e. TLR2 and TLR1 together, not just TLR2 or TLR1 [156]. Furthermore, the TLR4 extracellular domain was shown to be a negative regulator for signaling as TLR4 was constitutively active if only the transmembrane and TIR domains were expressed in cells [166]. This evidence suggests that the transmembrane domain plays a role in the TLR signaling pathway, but experimental evidence to specifically determine what function they play is lacking. Herein, we report several methods that have advanced the understanding of Toll-like receptor transmembrane domain interactions.

First, we used common membrane mimetic systems to study TLR transmembrane domain interactions. In these experiments, it was shown that the TLR transmembrane domains are capable of specific interactions (Chapter 2). After discovering these interactions we wanted to study if these isolated transmembrane domain interactions still occurred in a native membrane context and played a role in TLR signaling through conformational changes. To probe these questions, we adopted a live-cell Förster resonance energy transfer imaging technique to look at the interactions of various synthetic TLR constructs (Chapter 3). Preliminary evidence suggests that the TLR2

heterotypic interactions occur in the native membrane environment, but further work is needed to strengthen this conclusion. Lastly, as TLRs are important therapeutic targets, several reporter cell lines to investigate TLR signaling were developed. Using these new reporter cells, various transmembrane domain libraries and small molecules were studied to determine the effect they had on TLR signaling (Chapter 4). Taken together we have advanced the field on understanding TLR interactions, specifically related to the previously understudied transmembrane domains, and added to the toolbox for studying membrane protein-protein interactions.

Chapter 2

Isolated Toll-like receptor transmembrane domains are capable of oligomerization

This chapter has been published as J. I. Godfroy III, M. Roostan, Y. S. Moroz, I. V. Korendovych, and H. Yin. "Isolated Toll-like receptor transmembrane domains are capable of oligomerization" *PLoS ONE.* 7:e48875, **2012**. [84]

2.1 Abstract

Toll-like receptors (TLRs) act as the first line of defense against bacterial and viral pathogens by initiating critical defense signals upon dimer activation. The contribution of the transmembrane domain in the dimerization and signaling process has heretofore been overlooked in favor of the extracellular and intracellular domains. As mounting evidence suggests that the transmembrane domain is a critical region in several protein families, we hypothesized that this was also the case for Toll-like receptors. Using a combined biochemical and biophysical approach, we investigated the ability of isolated Toll-like receptor transmembrane domains to interact independently of extracellular domain dimerization. Our results showed that the transmembrane domains had a preference for the native dimer partners in bacterial membranes for the entire receptor family. All TLR transmembrane domains showed strong homotypic interaction potential. The TLR2 transmembrane domain demonstrated strong heterotypic interactions in bacterial membranes with its known interaction partners, TLR1 and TLR6, as well as with a proposed interaction partner, TLR10, but not with TLR4, TLR5, or unrelated transmembrane receptors providing evidence for the specificity of TLR2

transmembrane domain interactions. Peptides for the transmembrane domains of TLR1, TLR2, and TLR6 were synthesized to further study this subfamily of receptors. These peptides validated the heterotypic interactions seen in bacterial membranes and demonstrated that the TLR2 transmembrane domain had moderately strong interactions with both TLR1 and TLR6. Combined, these results suggest a role for the transmembrane domain in Toll-like receptor oligomerization and as such, may be a novel target for further investigation of new therapeutic treatments of Toll-like receptor mediated diseases.

2.2 Introduction

Toll-like receptors (TLRs) are an important class of proteins involved in the innate immune response, providing the first line of defense against microbes by recognizing pathogen-associated molecular patterns (PAMPs) [146]. These receptors also play a significant role in priming adaptive immune responses [146]. TLRs are type I transmembrane proteins that consist of three domains: (1) an extracellular domain made of Leucine-rich repeats that recognizes specific PAMPs, (2) a single transmembrane domain (TMD), and (3) an intracellular Toll-interleukin 1 receptor (TIR) domain that is required for downstream signal transduction [146]. These receptors are widely conserved across species, with humans having ten known functional TLRs [101]. TLRs can be generally divided into two subgroups based on their cellular location and PAMP recognition (Figure 2.1). The first subgroup is the cell surface receptors composed of TLR1, TLR2, TLR4, TLR5, TLR6, and TLR10, which recognize components of bacterial cell walls [101]. The second subgroup consists of TLR3, TLR7, TLR8, and TLR9, which are expressed in intracellular compartments like endosomes, and recognize bacterial and viral nucleic acids [101].

Over the past decade, extensive work has been done to understand TLR structure, ligand recognition, signaling, and role in diseases. It is known that active TLRs function as either a homodimer or heterodimer, as evident by the crystal structures for TLR extracellular domains with their PAMPs for TLR2/TLR1 [91], TLR2/TLR6 [91], TLR3 [133], TLR4 [167], TLR5 [85], TLR8 [205], and TLR9 [157]. It is also known that the dimerization of TIR domains is required for the

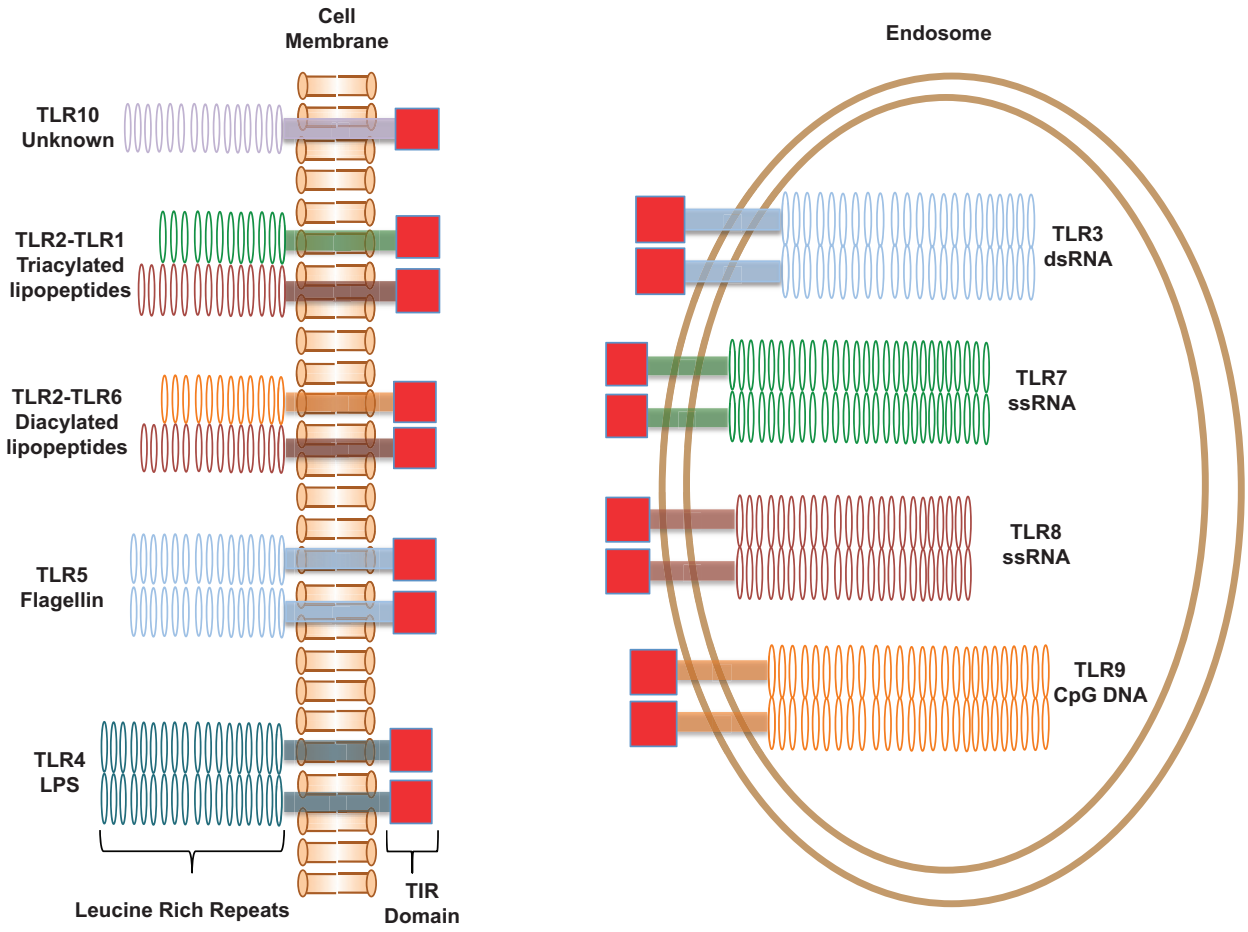

Figure 2.1: Toll-like receptors.
A schematic representation of the human Toll-like receptors. TLRs consist of three domains, an extracellular Leucine-rich repeat domain that recognizes the ligand, a single-pass transmembrane domain, and an intracellular TIR domain for signaling. Signaling is activated by the formation of either homodimers or heterodimers as depicted. TLRs are typically broken down into two classes, cell-surface receptors that recognize bacterial cell wall components, and endosomal receptors that recognize bacterial and viral nucleic acids.

recruitment of various adapter proteins to initiate a signaling pathway [100]. All TLRs, except for TLR3, signal through a MyD88-dependent pathway that activates NF-κB and produces proinflammatory cytokines [100]. TLR3 signals through the TRIF pathway that produces type I interferons as well as proinflammatory cytokines [100]. Due to the outcome of their signaling pathway, the TLRs are a double-edged sword because they provide important protection from bacterial and viral pathogens, but dysregulation can lead to several disease states [161]. For example, TLR4 activation has been linked to septic shock [161], while TLR2 activation has been implicated in lupus [161], rheumatoid arthritis [64, 198], and diabetes [36, 129]. Other TLRs have also been suggested to be involved in several disease states [30, 213]. The critical importance of TLRs in various diseases has created an area of focus for new and emerging therapeutic strategies [161, 30, 107, 96].

Our interest in TLRs is to study and understand the roles of the TMDs in TLR activation. Recent research has suggested that the TMDs of proteins not only function to anchor the protein to the membrane, but that they can also play a pivotal role in membrane protein oligomerization [110]. The important role of the TMD has been demonstrated on the integrin family of proteins [239, 128, 19, 230, 188], receptor tyrosine kinases [127, 149, 51], receptor-like protein tyrosine phosphatases [25], G-protein coupled receptors [153, 7], and other receptors [184, 47, 27, 183]. These reports indicate that TMD association can either be (a) the driving force for the required oligomeric state, or (b) the location of a conformational change that relates ligand binding to signal transduction.

Recent findings have demonstrated a possible role of the TMD in TLR activation [133, 166, 209, 113, 71, 237]. First, it has been shown that by forcing the TMD and TIR domains of TLRs to be in a dimeric complex using constitutively dimeric extracellular domains, it is possible to activate the NF-κB pathway as well as other known TLR gene promoters in the absence of ligands [71, 237]. Second, FRET studies demonstrated that TLR9 existed as preformed dimers in the cell membrane and underwent small conformational changes upon ligand addition [113]. Third, structural modeling using the TLR3 extracellular domain and TLR10 TIR domain suggested a close proximity between TMD domains in the dimeric complex that could allow for the TMD region to associate [133]. Last,

recent studies on TLR4 have demonstrated the importance of the tight coupling of the extracellular domain and TIR domain to the TMD as a requirement for signaling [209], and that the TLR4 extracellular domain prevents constitutive dimeric activation of TLR4 in the absence of ligand [166]. Based on these findings and the fact that the TLRs are single pass membrane proteins that are known to form functional homo- and heterodimers we asked whether TLR TMDs are capable of oligomerization in a manner analogous to the native TLRs. Interestingly, such a hypothesis is also supported by the fact that for the two pairs of heterodimeric TLRs (TLR2/1, TLR2/6), the transmembrane domain sequences of TLR1 and TLR6 are almost identical (Table 2.1) due to recent evolutionary divergence [108, 94], suggesting that their TMD regions possibly contribute to their association with TLR2. Our results demonstrate that isolated TLR TMDs are indeed capable of oligomerizing and have higher propensity for TLR interactions previously identified [133, 167, 91, 95, 113, 71, 67, 164]. Studies of whether such findings apply to the full length TLRs are currently ongoing. Nonetheless, a good correlation with existing structural and functional data has been observed, implying that interactions between TLR TMDs may be biologically relevant. As such, our findings may provide new targets for the development of chemotherapeutics for diseases wherein dysregulated TLR signaling is implicated.

2.3 Materials and Methods

2.3.1 Toll-like Receptor Transmembrane Domain Construction

As the transmembrane domain sequence is not known from crystal structures or experiment, we used hydrophobic analysis to determine the most likely consensus sequence for use in our studies. Briefly, the 10 human TLR protein sequences were accessed in FASTA format using the UniProt database (accession codes Q15399, O60603, O15455, O00206, O60602, Q9Y2C9, Q9NYK1, Q9NR97, Q9NR96, Q9BXR5) and analyzed to find the potential transmembrane domains. The programs used for predicting transmembrane domains were TMHMM, TMPred, SOSUI, DAS, and Mobyle, which were all accessed from the ExPasy topology prediction section (ca.expasay.org/tools).

Table 2.1: ToxR transmembrane domain sequences

TMD	**Sequence**
GpA	gnras**LIIF***G***VMA***G***VIGTIL**gslin
TLR1	gnras**ITLLIVTIVATMLVLAVTVTSLCSYL**gslin
TLR2	gnras*A***LVS***G***MCC***A***LFLLILLTGVLC**gslin
TLR3	gnras**LFFMINTSILLIFIFIVLLIHF**gslin
TLR4	gnras**TIIGVSVLVVSVVAVLVYKFYF**gslin
TLR5	gnras**FSLFIVCTVTLTLFLMTILTVT**gslin
TLR6	gnras**ITLLIVTIGATMLVLAVTVTSLCIYL**gslin
TLR7	gnras**LILF***S***L***S***I***S***V***S***LFLMVMMTASHL**gslin
TLR8	gnras**VTAVILFFFTFFITTMVMLAALA**gslin
TLR9	gnras**FALSLL***A***V***A***L***G***L***G***VPMLHHL**gslin
TLR10	gnras**ALLIVTIVVIMLVL***G***LAV***A***FCCL**gslin
TMD5	gnras**WQLL***A***FFL***A***FFL***D***LILLIIALYL**gslin
Integrin α_{IIb}	gnras**WVLV***G***VLG***G***LLLLTILVLAMW**gslin

Lowercase residues are encoded by the reading frame of the plasmid constructs, capitalized bold residues are the transmembrane domain sequences studied. GpA is the glycophorin A transmembrane domain previously studied and known to have strong homotypic interactions [111, 17, 131]. TLR1-TLR10 are the transmembrane domains of the specified Toll-like receptor as identified by hydrophobic analysis. Sequences of GpA, TLR2, TLR7, and TLR9 all contain potential Small-XXX-Small motifs that have been indicated as bold italicized letters. TMD5 and Integrin α_{IIb} are unrelated TMD receptors used for studying TLR specificity.

Residues that were identified by more than 60% of the software programs as part of the TMD were chosen as the consensus transmembrane sequences for all further studies.

2.3.2 ToxR Assay Plasmid Construction

Plasmids for this assay, pTox7 and pTox6 [78], and the competent *E. coli* strain, FHK12 [45], were kindly provided by D. Langosh, Technische Universit Mnchen, Germany. The pTox7 plasmid was modified by insertion of a single base (t) after the BamH1 site to keep the proper reading frame for the designed transmembrane sequences. Oligonucleotides from Integrated DNA Technologies encoding the designed TLR1-10 TMD constructs were ligated into the Nhe1/BamH1 restriction sites of both plasmids. Mutant constructs for TLR2 were generated using site-directed mutagenesis kits (Stratagene). DNA sequencing (Genewiz, Inc., NJ) validated proper TMD insertion and reading frame.

2.3.3 Homotypic ToxR Interactions

Briefly, the ToxR plasmids containing the TMD of interest (200 ng) were transformed into chemically competent FHK12 *E. coli* (200 μL) by incubating on ice for 30 min, heat shock at 42°C for 90 s, incubation on ice for 2 min, and addition of SOC media (800 μL) followed by incubation with shaking for 1 h at 37°C. This transformation mixture (50 μL) was then spread on LB agar plates containing cholaramphenicol (30 μg/mL) and ampicillin (100 μg/mL) and grown overnight at 37°C. Single colonies were selected from the plates in triplicate and added to 5 mL of LB media containing cholaramphenicol (30 μg/mL), ampicillin (100 μg/mL), and arabinose (0.0025%). These cultures were incubated overnight (16-20 h) with shaking at 37°C. The β-galactosidase activity was monitored using a Beckman Coulter DTX 880 plate-reader. First 5 μL of each culture was plated $>$ 6 times in a clear 96-well flat bottom culture plate (Sarstedt) containing 100 μL of Z-buffer/chloroform (1% β-mercaptoethanol, 10% chloroform, 89% Z buffer: 1 M sodium phosphate, 10 mM potassium chloride, 1 mM magnesium sulfate, pH 7.0). The cell densities of each well were recorded by measuring the OD595. Bacteria were lysed by the addition of 50 μL Z-buffer/SDS (1.6%

sodium dodecyl sulfate w/v in Z-buffer) and shaking at 28°C for 10 min. Enzymatic activity was measured by adding 50 μL of Z-buffer/ortho-Nitrophenyl-β-galactosidase (ONPG) (0.4% ONPG w/v in Z-buffer) and monitoring the reaction at 405 nm for a period of 20 min at 30 s intervals. Miller units were calculated using the equation:

$$MillerUnits = \frac{\frac{OD_{405}}{time}}{OD_{595}} 1000 \tag{2.1}$$

Western blotting was performed with antiserum recognizing the maltose-binding protein moiety of the constructs (Abcam). Data were normalized to GpA Miller Units and protein expression levels using ImageJ (NIH) as reported previously [44].

2.3.4 Heterotypic ToxR Interactions

For heterotypic interactions one plasmid containing a functional ToxR domain (200 ng) and a second plasmid containing a non-functional ToxR* domain (200 ng) were co-transformed into chemically competent FHK12 *E. coli* (400 μL) by incubating on ice for 30 min, heat shock at 42°C for 90 s, incubation on ice for 2 min, and addition of SOC media (1600 μL) followed by incubation with shaking for 1 h at 37°C. This transformation mixture (50 μL) was then used to spread LB-agar plates containing cholaramphenicol (30 μg/mL), kanamycin (33 μg/mL), and ampicillin (100 μg/mL) and grown overnight at 37°C. Single colonies were selected from the plates and grown in 5 mL LB media containing cholaramphenicol (30 μg/mL), kanamycin (33 μg/mL), ampicillin (100 μg/mL), and arabinose (0.0025%) overnight (16-20 h) with shaking at 37°C. Analysis of activity was monitored as described in homotypic ToxR assays. Western blotting was done in the same manner as the homotypic ToxR assay with one band appearing for the functional ToxR construct and a second band for the nonfunctional ToxR* construct. Data were normalized to poly-Leu* Miller Units and corrected for varying protein expression levels using ImageJ (NIH) as previously reported [44].

2.3.5 Peptide Synthesis

All peptides were synthesized at a 0.1 mmol scale on a Rink Amide resin with a loading capacity of 0.36 mmol/g using a CEM Liberty automated synthesizer with a Discovery microwave module. To increase the solubility of these highly hydrophobic peptides in polar solvents a KK sequence motif was added to both the N- and C-termini of the peptides. For all fluorophore labeling, a 6-atom flexible spacer was added to the N-terminus. The TLR2 peptide was labeled with FITC using aminohexanoic acid as the spacer using previously reported conditions [230]. The TLR1 and TLR6 peptides were labeled with coumarin using two glycines as the spacer following previously reported coupling methods [19]. For all peptides, side chain deprotection and cleavage from the resin was done using a mixture of trifluoroacetic acid/water/1,2-ethanedithiol/thioanisole/phenol/triisopropylsilane (81.5:5:5:2.5:1 v/v) at room temperature under a N_2 blanket for 2 h. The crude peptides were collected by precipitation with cold (-20°C) diethyl ether. The peptides were then purified on an Agilent 1200 series semi-preparative reverse phase high-performance liquid chromatography system with a Vydac Protein C4 column using a linear gradient of solvent A (Millipore water with 0.1% trifluoracetic acid) and solvent B (6:3:1 isopropanol/acetonitrile/water containing 0.1% trifluoroacetic acid). The identities of the purified peptides were confirmed by MALDI-TOF mass spectrometry on a Voyager-DE-STR Biospectrometry Workstation (Perseptive Biosystems). All peptides were lyophilized using a Labconoco FreeZone 4.5 freeze drier to yield the purified peptides as their TFA salts.

2.3.6 Circular Dichroism

CD measurements were performed on a ChirascanPlus spectrometer (Applied Photophysics) using a quartz cuvette with a 1.0 mm path length. C14-Betaine (3-(N,N-Dimethylmyristylammonio)-propanesulfonate, Sigma) and peptides were co-dissolved in 2,2,2-trifluoroethanol. The organic solvent was removed by drying to a thin film using N_2 and further dried overnight under reduced pressure to remove all traces of TFE. Samples were resusupended in a 20 mM HEPES buffer, pH

7.4, yielding a final C14-Betaine concentration of 10 mM. Peptide concentrations were determined using the Beer-Lambert law with coumarin absorbance at 400 nm using ϵ_{400} of 39,300 M^{-1} cm^{-1} [192] and FITC absorbance at 495 nm using ϵ_{495} of 68,000 M^{-1} cm^{-1} (Invitrogen). Peptides were prepared such that final concentrations were in the 5-10 μM range. All CD spectra were measured at 25°C with a step size of 1 nm and are reported as the average of 9 scans. Data were not collected below 200 nm due to the high voltage and background noise from the C14-Betaine buffer. Helical content was determined using CDNN [14].

2.3.7 Self-Quenching Assay

Fluorescence self-quenching was used to directly probe the homotypic interactions of the synthetic peptides. Fluorescently labeled peptides and C14-Betaine were co-dissolved in 2,2,2-trifluoroethanol. The organic solvent was removed using a N_2 stream to generate a thin film of the peptide/detergent mixture and then dried over night under reduced pressure to remove all traces of organic solvent. The samples were resuspended in a 100mM HEPES buffer, pH 7.4. Four stock solutions were prepared with final C14-Betaine concentrations of 0.15 mM, 1 mM, 5 mM, and 10 mM. Peptide concentrations of these samples were determined by UV-VIS and adjusted with the corresponding C14-Betaine only buffers such that all peptide concentrations were 1 μM. These samples were mixed in a black 96-well plate to obtain a range of peptide:detergent ratios at a fixed peptide concentration and varied detergent concentrations. Samples were allowed to equilibrate in the 96-well plate at room temperature for 2 h before measurement using a Beckman-Coulter DTX 880 Multimode Detector plate reader. The samples labeled with coumarin were excited at 360 nm and the emission filter set at 460 nm. The sample labeled with FITC was excited at 485 nm and the emission filter set at 535 nm. Each data point is blank corrected for the corresponding C14-Betaine only signal and are the average of 3 different readings. To scale the data from 0 to 1, the initial data point was averaged and set to be zero by subtracting from all further readings, and the data points that are in the plateau region were averaged and then all values were divided by this average to get a maximum of 1. The untransformed data were fit using the Hill equation

using OriginPro 8.6 to get a K_d with the first reading being fixed as the initial signal.

2.3.8 Förster Resonance Energy Transfer

FRET was used to directly probe the heterotypic association of the synthetic peptides. FRET experiments were performed on a Horiba Fluorolog-3 using a 0.3 cm path length cuvette. Peptides and C14-Betaine (1 mM) were co-dissolved in 2,2,2,-trifluoroethanol and dried under N_2 to generate a thin film of peptide/detergent. Samples were resuspended in 100 mM HEPES, pH 7.4. Samples were titrated such that the coumarin TLR1 or TLR6 peptide concentration was fixed at 20 nM and the fluorescein TLR2 peptide concentration varied. Data were collected with an excitation wavelength of 415 nm and emission spectra were collected from 440-600 nm, with slit widths of 3 nm for both excitation and emission. Reference samples containing only fluorescein tagged TLR2 were used for calculating net FRET signals that were used in the data analysis. Data were fit using the Hill equation in OriginPro 8.6.

2.4 Results

2.4.1 TLR Transmembrane Domain Interactions in *E. coli* Membranes

To demonstrate proof of concept for TLR TMD interactions in both a homotypic and heterotypic manner, we used the established ToxR reporter assay [111, 131] to qualitatively assess TLR TMD interactions. The fusion proteins used in this assay consist of an extracellular maltose binding protein, which properly orients the construct to the periplasm, the TMD of interest, and a cytoplasmic cholera toxin transcriptional activation domain, ToxR. Driven by TMD-TMD interactions, dimeric ToxR domains bind the cholera toxin promoter, which induces expression of a reporter enzyme, β-galactosidase. Various plasmid constructs for this assay make it possible to monitor both homotypic [111] and heterotypic [131] interactions that are driven by TMD-TMD association (Supplementary Figure A.1).

We first investigated homotypic interactions because the majority of the TLR family members

function as homodimers. All TLR TMDs demonstrated high propensity for homotypic interactions (Figure 2.2) showing 45%-85% of the activity of the positive control, glycophorin A (GpA).

The TMD of GpA was used as a positive control since it has been previously demonstrated to have a very strong homotypic interaction [111, 17, 44]. A construct that does not encode a TMD and is not capable of any TMD association (ΔTM) was used as the negative control to demonstrate the background signals [78]. This ΔTM construct consists of the same maltose binding protein and ToxR domain, but lacks a TMD for proper membrane insertion (Supplementary Figure A.2) [76]. Statistical analysis using the Tukey-Kramer test was performed to analyze any significant differences between all possible pairs of average interaction potentials (Supplementary Table A.2). All TLR TMDs were statistically different from the negative control ($p < 0.0001$), indicating that the TMD-TMD interactions observed were unlikely due to systemic errors or artifacts. Among the TLRs, no discernible differences in grouping based on statistical analysis at $p=0.05$ were indicated as all receptors belonged to multiple groups, except for TLR1, which with the lowest interaction potential among the family of receptors only existed in one group (Supplementary Table A.1).

Next, we investigated heterotypic interactions of the TLRs. We specifically studied TLR2, TLR1, and TLR6 because they are cell surface expressed receptors known to form functional heterodimers. To determine the ability of these three cell surface TLRs to have specific heterotypic interactions, we studied the ability of the TLR1, TLR2, and TLR6 TMDs to interact with the TLR receptors also expressed at the cell surface; namely, TLR1, TLR2, TLR4, TLR5, TLR6, and TLR10. We monitored these interactions using a dominant-negative ToxR assay (Supplementary Figure A.1) which works by having a second TMD expressed with a non-functional ToxR* intracellular domain. This ToxR* domain is incapable of binding the ctx promoter making any interactions with this second expressed TMD unable to produce the reporter enzyme. As such, any interaction between the functional ToxR and non-functional ToxR* TMDs will result in a reduction in signal output.

We saw a similar trend for all three TLR TMDs in the heterotypic interactions, as TLR2, TLR1 and TLR6, all showed that they had a strong propensity to interact with TLR1, TLR2, TLR6, and TLR10, but not with TLR4 or TLR5 (Figure 2.3). Furthermore, these TMDs did not

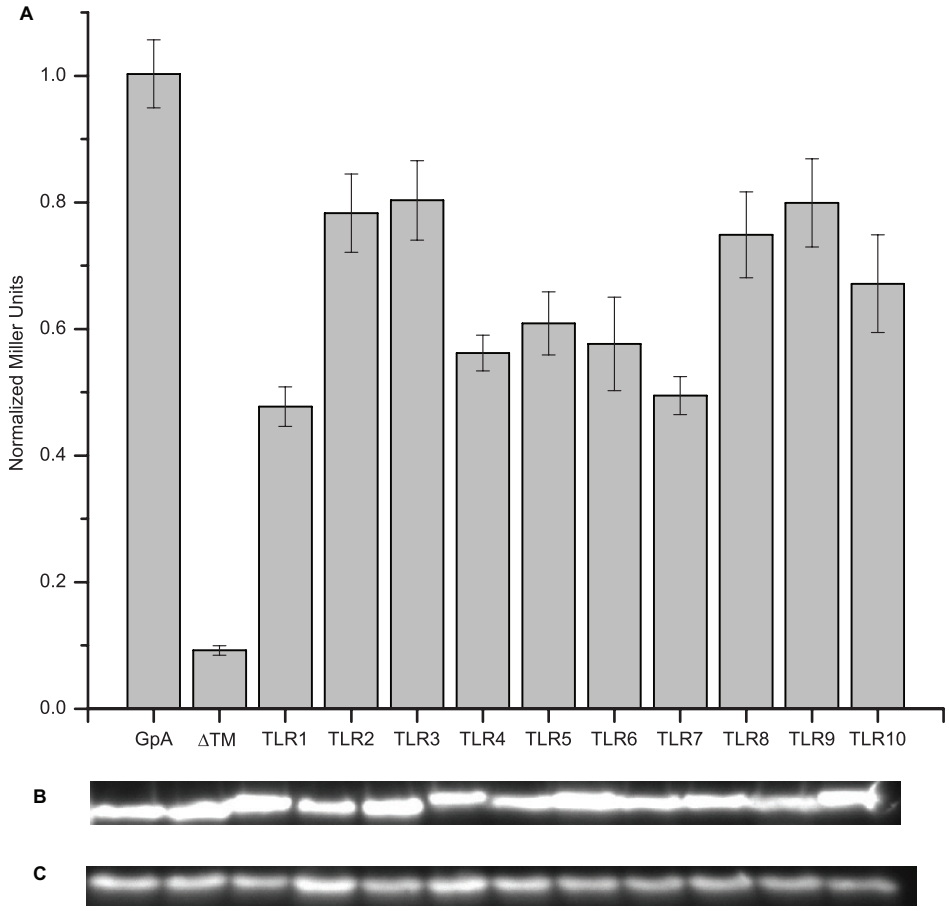

Figure 2.2: Toll-like receptor transmembrane domain interactions.
(A) The ToxR assay was used to study homotypic interactions of the TLR TMDs. A chimeric protein expressing the TMD of interest was monitored through β-galactosidase activity. In all cases, we saw that the TLRs have interaction potential solely from TMD-TMD interactions. Each TLR TMD interaction measurement analysis was performed on 3 technical replicates with >6 measurements for each replicate. Error bars depict the standard error of the mean (n - Supplementary Table A.1). Western blots staining for MBP were performed to monitor expression levels of the constructs (B) chimeric maltose binding protein expression, 70 kDa, (C) endogenous maltose binding protein expression, 45 kDa. All samples were normalized to the GpA signal and expression levels. Significant differences were determined by use of the Tukey-Kramer test with all TLRs being significantly different than the negative control.

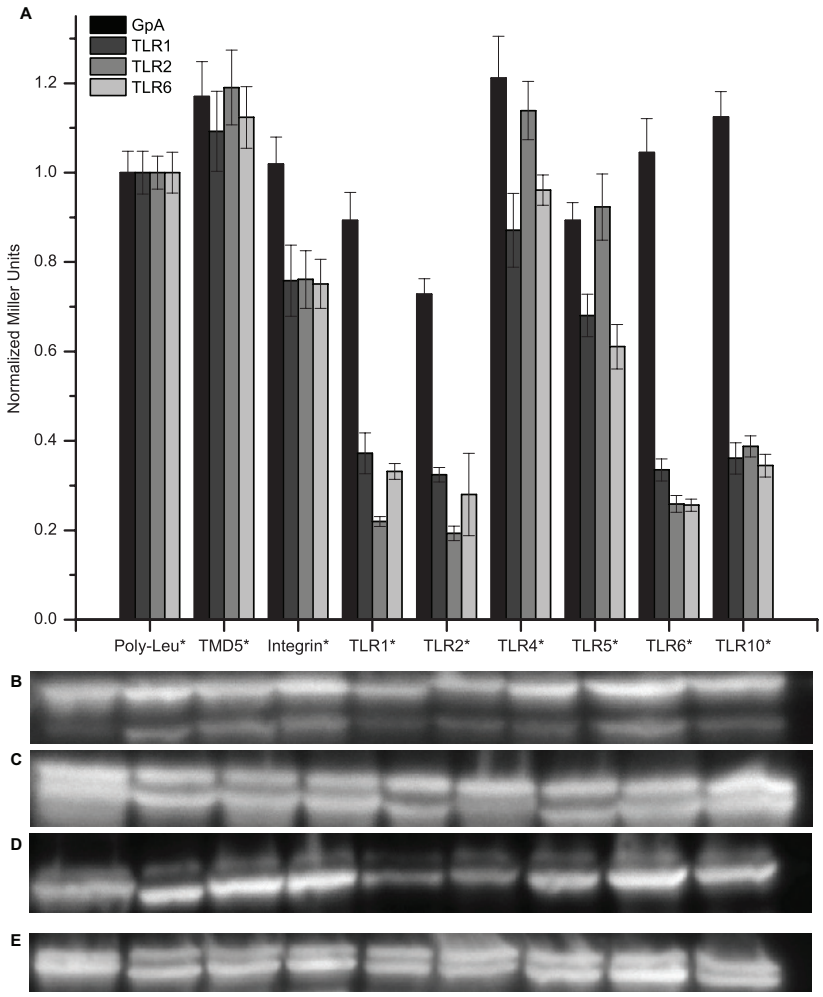

Figure 2.3: Plasma membrane Toll-like receptor heterotypic interactions.
(A) A dominant-negative ToxR assay was used to study heterotypic interactions of the plasma membrane TLRs. Two TMDs were encoded in the FHK12 *E. coli* reporter strain, one with a functional ToxR domain and one with a nonfunctional ToxR* domain. Interaction between the two different TMDs leads to a reduction in signal from that seen for homotypic interactions. The TMDs for GpA, TLR1, TLR2, and TLR6 were used with the functional ToxR domain while TMDs for poly-Leucine, TMD5, integrin α_{IIb}, TLR1, TLR2, TLR4, TLR5, TLR6, and TLR10 were used with the nonfunctional ToxR* domain. Interactions were most prominent for the TLRs known to have heterotypic interactions - TLR2-TLR1 and TLR2-TLR6. TLR10 also showed strong interactions with TLR2. We also saw interaction with the same TMD further validating the homotypic interactions. Moderate interaction was seen with other TMDs that could be attributed to non-specific interactions from similar TMD motifs as completely unrelated receptors showed similar levels of knockdown. Each dominant phenotype was done in 3 technical replicates with each negative phenotype and >6 measurements made for each replicate. Error bars depict the standard error of the mean (n - Supplementary Tables A.3, A.5, A.7, and A.9). Western blots staining for MBP were performed to monitor expression levels of the constructs with the upper band being functional ToxR chimeras, 70 kDa, and the lower band being nonfunctional ToxR* chimeras, 65 kDa (B) GpA, (C) TLR1, (D) TLR2, and (E) TLR6. Significant differences for the same dominant phenotype were determined by use of the Tukey-Kramer test.

show high interaction propensity with TMDs from completely unrelated receptors, TMD5 from latent membrane protein 1 and integrin α_{IIb}, or with the negative control TMD of poly-Leu. Co-expression of poly-Leu as the negative ToxR* construct with a functional ToxR construct resulted in the same signal as that seen when the functional ToxR domain was expressed alone (data not shown). Therefore, poly-Leu was used as the normalization standard of 1. The strongest interactions belonged to the heterotypic interactions among TLR1, TLR2, TLR6, and TLR10, with all combinations showing >60% reduction in signal from the homotypic interaction. The same high level of knockdown was seen for the same receptor, i.e. TLR1-TLR1*, validating the homotypic signal we had seen. Interestingly these sequences, TLR1, TLR6, and TLR10, demonstrated the highest sequence similarity (Table 2.1) and belong to the same TLR subfamily as TLR2 [94], implying biological relevance of such an observation. Statistical analysis using the Tukey-Kramer test demonstrated TLR1, TLR2, TLR6, and TLR10 always belonged to the same grouping classification, and that classification was statistically different from all other interactions seen (Supplementary Tables A.5-A.10). To further verify that the interaction we saw was specific, we looked at the ability of the TLR TMDs to form heterotypic interactions with unrelated transmembrane receptors and with the GpA TMD expressed as the dominant phenotype. With GpA as the dominant phenotype, we saw no significant reduction for any TMD based on statistical groupings (Supplementary Tables A.3-A.4) except TLR2, which showed a weak knockdown of 30%. The TLR1, TLR2, and TLR6 TMDs all showed a weak interaction, 30-40% knockdown, with both the integrin α_{IIb} and TLR5 TMDs, but no interaction with TMD5 or TLR4 (Supplementary Tables A.5-A.10).

2.4.2 Synthetic Transmembrane Peptide Homotypic Interactions

To quantify the interaction propensity demonstrated by the ToxR assay, we synthesized peptides for the TLR1, TLR2, and TLR6 TMDs. Synthetic TMD truncations have been widely used to study protein interactions in membrane mimetic systems (e.g. micelles) and may provide useful information on protein assembly in membrane bilayers [193, 41, 53]. These TLR TMD peptides were monitored by circular dichroism in the presence of detergent micelles and found to

adopt a helical conformation (Figure 2.4). The helical content of the peptides was determined to be >99% for all three synthetic peptides (Supplementary Table A.11), indicating the micelles are a suitable mimetic system for further studies.

These transmembrane peptides were fluorescently labeled with either fluorescein or 7-hydroxycoumarin, which have been previously demonstrated to exhibit fluorescence self-quenching upon interaction and do not contribute to the peptide interactions [37]. An apparent dissociation constant (K_d) can be determined from self-quenching interactions by varying the amount of detergent present for a fixed peptide concentration. At low detergent:peptide ratios, the TMD peptides are driven to interact; however, gradually increasing the amount of detergent present at a fixed peptide concentration will cause the TMDs to dissociate. Then, at some critical detergent:peptide ratio, the interaction is completely disrupted and the fluorescence plateaus. For the TLR peptides we saw that TLR1 and TLR6 showed relatively weak interactions, and TLR2 showed a moderate interaction (Figure 2.5). Fitting the data results in apparent dissociation constants, K_d, in terms of a dimensionless detergent:peptide ratio (molar fraction) as this ratio, instead of the bulk concentration, is more relevant to TMD peptide association. For TLR1 the K_d was determined to be 645.63 ± 49.08, for TLR6 the K_d was determined to be 883.57 ± 86.92 and for TLR2 the K_d was determined to be 4475.5 ± 637.9. These molar fraction values fall within the known ranges of TMD interactions [47] and classify the TLR1 and TLR6 homotypic interactions as weak, and the TLR2 homotypic interaction as moderately strong. Further experiments were performed using sedimentation equilibrium analytical ultracentrifugation (SE-AUC) to determine oligomeric states of the TLR2 and TLR6 peptides. The TLR2 peptide was well modeled by a monomer-dimer-tetramer equilibrium (Supplementary Figure A.3) and the TLR6 peptide was well modeled by a monomer-dimer equilibrium (Supplementary Figure A.4) which indicated that these peptides formed oligomers in a micellar environment.

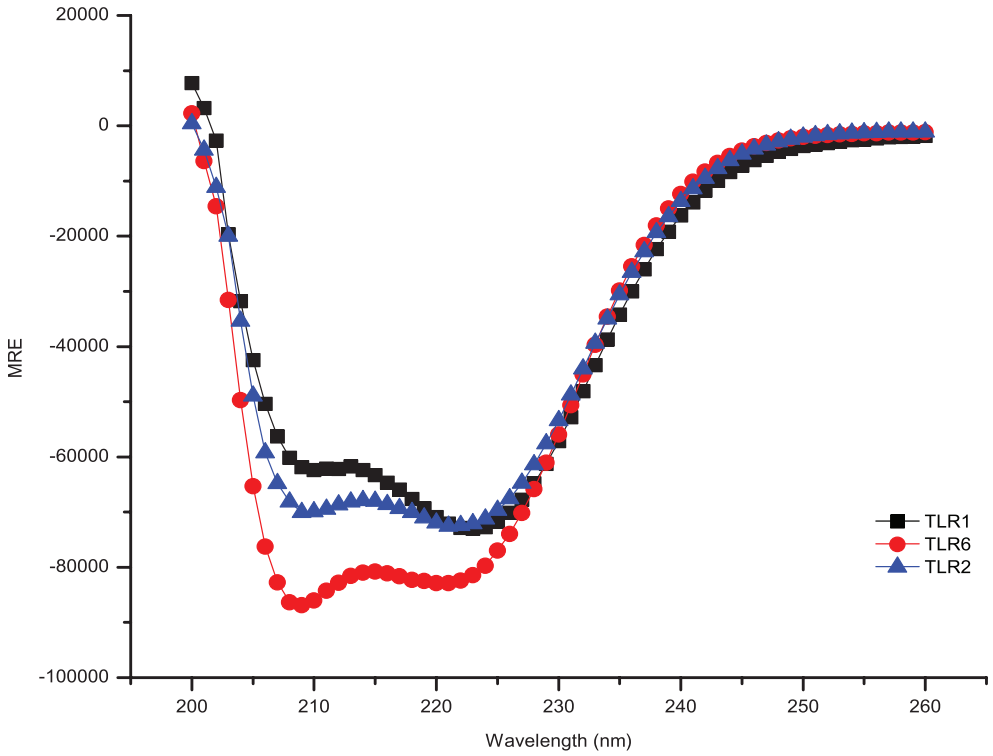

Figure 2.4: Circular dichroism spectra of TLR1, TLR2, and TLR6 synthetic TMD peptides. Far-UV spectra of the synthetic TMD peptides at concentrations ranging from 5-10 μM in the presence of 10 mM C14-betaine detergent micelles. Spectra were collected at 25 °C with a step size of 1 nm and are the average of 9 scans. All peptides had helical content >99% (Supplementary Table A.11) as determined using CDNN [14]

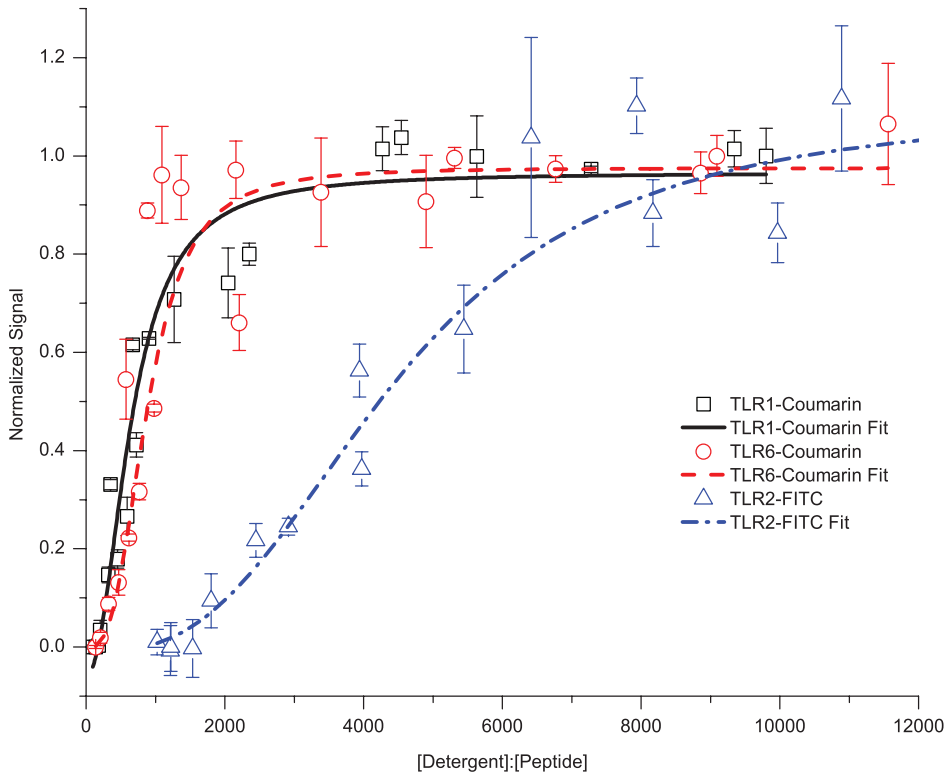

Figure 2.5: TLR1, TLR2, and TLR6 homotypic interactions by fluorescence self-quenching. Synthetic TMD peptides were fluorescently tagged with fluorescein (TLR2) or coumarin (TLR1, TLR6). Homotypic interaction affinity was studied by changes of fluorescence intensity at different molar ratios of detergent to peptide. All samples were fixed at a peptide concentration of 1 μM, while the detergent concentration was varied. Increasing detergent competes off the TMD-TMD interactions and leads to an increase in fluorescence signal. TLR1 and TLR6 exhibit similar behavior characteristic of weak interactions as indicated by rapid release of quenched fluorescence with K_d of 645.63 $\pm$ 49.08 and 883.57 $\pm$ 86.92 respectively. TLR2 exhibits a different behavior indicative of a moderate interaction as it gradually releases quenched fluorescence with K_d of 4475.49 $\pm$ 637.86. Each data point is a minimum of 3 measurements from 3 different sample preparations. Error bars are standard deviations of the measurements. K_d were determined using the Hill Equation [194].

2.4.3 Synthetic Transmembrane Peptide Heterotypic Interactions

Using the same TLR1, TLR2, and TLR6 peptides, as described above, we were able to monitor the heterotypic interactions between TLR2-TLR1 and TLR2-TLR6 using a previously reported Förster resonance energy transfer (FRET) assay [230]. The titration of a fluorescein-labeled TLR2, FRET acceptor, into a 7-hydroxycoumarin labeled TLR1 or TLR6, FRET donor, resulted in the reduction of the donor emission and an appearance of the acceptor emissions, demonstrating that these transmembrane peptides have heterotypic interactions (Figure 2.6). Fitting these data as described previously [127, 149, 194], it is possible to get dissociation constants. The dissociation constant for the TLR2-TLR1 interaction was 230.8 ± 20.0 nM of acceptor labeled peptide and for TLR2-TLR6 it was 286.5 ± 14.8 nM of acceptor labeled peptide (Figure 2.6C). To make these dissociation constants comparable to the apparent dissociation constants determined by self-quenching we divided these values by the fixed detergent concentration of 1 mM to yield 4332.0 ± 410.7 and 3490.4 ± 190.1 for the TLR2-TLR1 and TLR2-TLR6 interactions, respectively. SE-AUC was also used to investigate the oligomeric state of the TLR2-TLR6 heterotypic interaction. Analysis showed that the molecular weight of the species decreased for TLR2 when in the presence of TLR6, suggesting that these peptides are also interacting (Supplementary Figure A.5).

2.4.4 TLR2 Mutational Analysis for Interface Determination

After demonstrating that the TLR2 TMD is capable of both homotypic and heterotypic interactions, we investigated residues that might be responsible for these interactions. As previous works have identified structural motifs that can be involved in TMD-TMD interactions [151, 110], we examined the TLR2 TMD sequence and found that it contained an extended Small-XXX-Small motif (Table 2.1, where Small can be Ala, Gly, or Ser) that has been reported to facilitate TMD dimerization [151]. Further analysis also revealed that the TMDs of TLR2, TLR1, TLR6, and TLR10 contained luminal Cys residues (Table 2.1). To investigate if these residues were involved in the homotypic or heterotypic interactions we performed site-directed mutagenesis at key positions

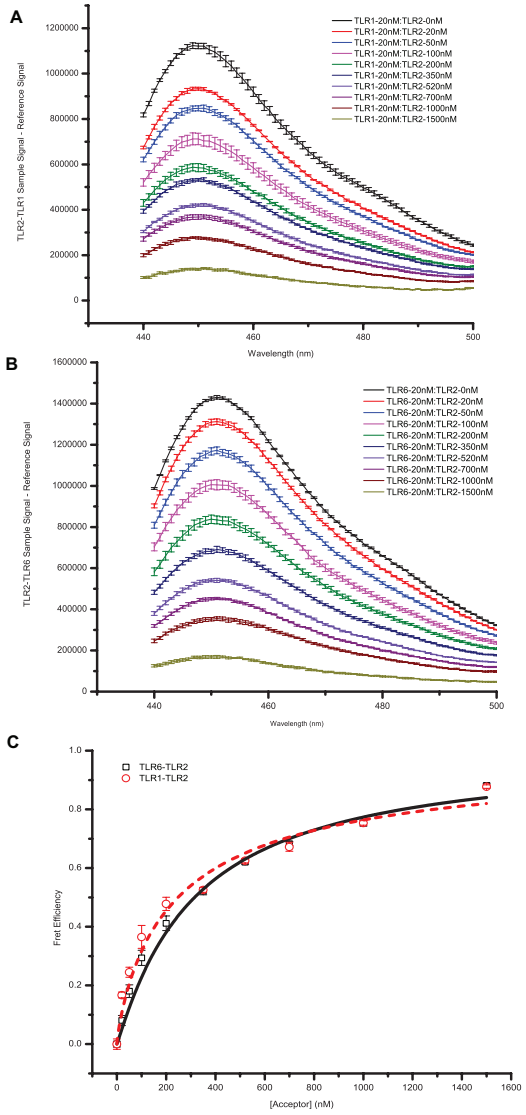

Figure 2.6: TLR2-TLR1 and TLR2-TLR6 heterotypic interactions measured by Förster resonance energy transfer

Synthetic TMD peptides were co-incubated in micelles with the FRET donor concentration fixed to be 20 nM and the FRET acceptor concentration varied from 0-1500 nM. The donor was excited at 415 nm and emission was monitored from 440-600 nm. Only donor emission is shown as the excitation-emission separation led to a high background signal seen in the acceptor channel. (A) TLR2-TLR1 donor channel. (B) TLR2-TLR6 donor channel. (C) FRET efficiency based on decrease in donor signal at increasing acceptor concentrations. Fitting these curves yields a TLR2-TLR1 interaction of $K_d = 4332.0 \pm 410.7$ (in molar fraction unit) and a TLR2-TLR6 interaction of $K_d = 3490.4 \pm 190.1$.

in the TLR2 TMD Gly593Val, Ala597Val, and Cys609Ile and tested these mutants in both homotypic and heterotypic ToxR assays. The results suggest that these mutations were not critical for TLR2 homotypic interactions since no mutation demonstrated significant difference from the wild type TLR2 TMD (Figure 2.7A). As a control for the effect of a point mutation on TMD interactions, we used TMD5 of latent-membrane protein 1, which has been previously studied in our laboratory and demonstrated that the Asp150 was critical for interaction [184]. For heterotypic interactions, the Ala597Val and Cys609Ile mutations played a role in heterotypic interactions since both mutations were capable of reducing the ToxR inhibition demonstrated by the native TLR2 TMD (Figure 2.7B).

2.5 Discussion

Membrane proteins account for nearly 30% of all proteins encoded in the genome and are involved in many diverse cell processes [110, 151, 62]. Previous work with TLRs has investigated the potential of the TLR TMDs and TIR domains to activate signaling pathways or gene promoters when a chimeric protein contains an extracellular domain forcing these domains into a dimeric state [71, 237]. While these data suggest that the TLRs are activated when in a dimeric state, and it has been proposed that the dimerization of the TIR domains is required for recruitment of adapter proteins in signal transduction [165], it provides no information about the role of the TMD in this dimeric interaction. Our data shows, for the first time, that isolated TLR TMDs are capable of oligomerizing both homotypically and heterotypically, showing preference for the known interaction partners of each TLR in the absence of the extracellular domain and TIR domain. These results provide critical evidence on the role of TMD interactions for the TLR family of the innate immune system and suggest that this short region of the protein likely plays an important role in the assembly and function of the receptors.

In terms of native interactions, the isolated TMDs were sufficient to recapture the known behaviors of the full-length proteins as well as provide evidence for others that are still unclassified. All TLR TMDs were capable of forming homotypic interactions (Figure 2.2). These results are

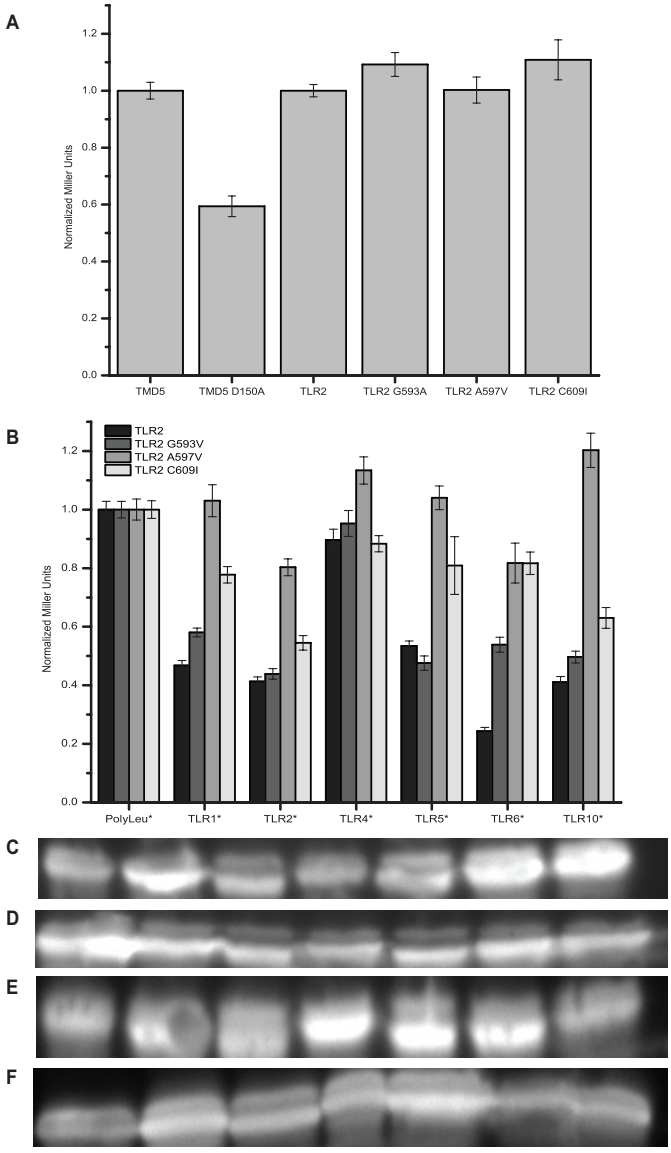

Figure 2.7: Toll-like Receptor 2 interaction interface studied by mutagenesis
TLR2 residues were mutated to study effects on homotypic and heterotypic interactions using the ToxR assay. These mutations were at positions identified in the sequence as likely interaction locations. (A) Homotypic interactions of point mutations show no difference in interaction potential from wild-type TLR2 TMD. (B) Heterotypic interactions of point mutations show the potential importance of both the Ala597 and Cys609 positions for heterotypic interactions. Western blots staining for MBP were performed to monitor expression levels of the constructs with the upper band being functional ToxR chimeras, 70kDa, and the lower band being nonfunctional ToxR* chimeras, 65 kDa, (C) TLR2, (D) TLR2 G593V, (E) TLR2 A597V, and (F) TLR2 C609I. All signals were normalized to the expression levels of GpA.

promising as crystal structures exist showing the extracellular domain of TLR3 [133] and of TLR4 [167] as a homodimer with their respective ligands. Additionally, a computer model based on homology modeling of the TLR3 extracellular domain and TLR10 TIR domain proposed that the TMDs could be in close proximity to interact [133]. We saw agreement with this model as the TLR3 TMD showed a very high homotypic interaction potential. It has also been shown using fluorescence lifetime FRET of CFP tagged TLR9 that TLR9 exists as a preformed dimer in cell membranes and undergoes conformational changes upon binding of its ligand [113] suggesting that the TMD may be in close proximity prior to ligand activation. The ToxR assay result demonstrated that the TLR9 TMD has a very high propensity for homotypic interactions, indicating it could be a contributing factor to the pre-formed TLR9 dimers found in cells. The TLR1, TLR6, and TLR10 receptors are not known to have functional homodimers; however, TLR1 and TLR6 are known to form functional heterodimers with TLR2 [91, 95, 164] and while TLR10 pathogen recognition is still unknown, it has recently been proposed to also form a heterodimer with TLR2 [70, 67]. These known and proposed heterotypic interactions of TLR1, TLR6, and TLR10 with TLR2 were verified using our heterotypic ToxR assay (Figure 2.3). The strongest heterotypic interactions were seen for the known heterotypic pairs of TLR2-TLR1 and TLR2-TLR6, as well as for the proposed TLR2-TLR10 interaction. The heterotypic interaction of TLR1, TLR2, and TLR6 with its own TMD provides further evidence for the ability of these receptors to also interact homotypically. We also saw a strong heterotypic interaction with TLR1-TLR6, TLR1-TLR10, and TLR6-TLR10 combinations, which is likely due to the high sequence similarity among these TMDs (Table 2.1) making these interactions analogous to the homotypic interactions. Alignments of the TLR TMD sequences showed that no TMD pairs had >25% sequence identity except for TLR1-TLR6 which has 92% sequence identity with only 2 residues different between the sequences, TLR1-TLR10 which had 50% sequence identity, and TLR6-TLR10 had 46% sequence identity. This homology is not surprising as TLR1, TLR6, and TLR10 are all on the same gene locus in humans and are the most recently diverged in phylogenetic trees [94, 108].

As a comparison, we observed weak heterotypic interactions with GpA-TLR2, TLR1-Integrin

α_{IIb}, TLR2-Integrin α_{IIb}, TLR6-Integrin α_{IIb}, TLR1-TLR5, and TLR6-TLR5 (Figure 2.3). The GpA-TLR2 and all TLR-Integrin α_{IIb} interactions can likely be explained by the presence of a similar Small-xxx-Small motif in the TMD sequences of GpA, TLR2, and Integrin α_{IIb} (Table 2.1). This motif and neighboring residues have been shown to be critical for GpA TMD interactions [44], so it is highly probable that this motif is the cause for these weak interactions. The TLR1 and TLR6 interactions with TLR5 do not appear to share any structural motifs, but as we are only looking at the isolated TMDs of these receptors, one possible explanation could be that other regions of the protein might prevent such an interaction from occurring in the context of full-length proteins. Our reasoning is based on the evidence that the extracellular domain serves as a negative regulator for interactions in other transmembrane proteins [166, 23]. One example is for a receptor-tyrosine kinase, fibroblast grown factor receptor 3 (FGFR3), whose transmembrane domain has been shown to interact independently of ligand and extracellular domains using both ToxR and biophysical assays [127, 51]. It was recently shown that the FGFR3 extracellular domain has a repulsive contribution to the overall dimerization energetics and prevents ligand-independent activation [23]. In addition to this, recent evidence reveals a similar trend for TLR4 [166]. It was shown that TLR4 without an extracellular domain, or with a small monomeric extracellular domain, was constitutively active. However, if the extracellular domain was bulky and monomeric, TLR4 was not constitutively active or responsive to LPS. Only with the presence of the TLR4 extracellular domain was the receptor not constitutively active and responsive to LPS [166]. These findings suggest that although some TLR TMDs demonstrate a weak heterotypic interaction potential with unexpected partners, other factors might prevent this interaction in a native context. Further studies would be needed to elucidate what are these factors contributing to the weak interactions seen.

The use of synthetic transmembrane peptides provided an alternative means to probe the interactions of TLR TMDs. We chose to focus on the TLR2, TLR1, and TLR6 TMD family as these receptors provided a method to validate both homotypic and heterotypic interactions that we saw in the ToxR assays. Additionally, the TLR2 heterodimeric receptors have been associated

with a myriad of diseases that still have unmet clinical needs [161] making this a highly interesting subfamily of TLRs. Using self-quenching and FRET studies, it was possible to determine the affinity of the various TLR2, TLR1, and TLR6 interactions. For homotypic interactions, the increase in fluorescence for TLR1 and TLR6 at low peptide to detergent ratios suggested the interaction was easily driven apart while the increase in TLR2 fluorescence at higher peptide to detergent ratios suggested a stronger interaction (Figure 2.5). The differing interaction strengths were validated by data fitting as the K_d were 645.63 $\pm$ 49.08, 883.57 $\pm$ 86.92, and 4475.5 $\pm$ 637.9 in terms of molar fractions for TLR1, TLR6, and TLR2 respectively. These molar fraction values are in a good agreement with previously reported TMD interactions [230, 47, 44, 5]. For heterotypic interactions we saw a FRET signal for both TLR2-TLR1 and TLR2-TLR6 (Figure 2.6) are also moderately strong from the respective K_d of 4332.0 $\pm$ 410.7 and 3490.4 $\pm$ 190.1. In addition to these assays, sedimentation equilibrium analytical ultracentrifugation was performed on the TLR2 and TLR6 peptides to determine oligomeric states. The TLR2 peptide showed a high molecular weight species when fit (Supplementary Figure A.3) that was well modeled by a monomer-dimer-tetramer equilibrium. The TLR6 peptide also showed a high molecular weight species when fit (Supplementary Figure A.4) that was well modeled by a monomer-dimer equilibrium. Also when TLR2-TLR6 were in the same sample cell, we again saw a high molecular weight species, but this species was smaller than that for TLR2 alone (Supplementary Figure A.5) that suggests TLR2 and TLR6 were interacting. The results from synthetic peptide studies of TLR1, TLR2, and TLR6 validated the interactions observed in our ToxR assays and lends further support to the ability of the TLR TMDs to associate and potentially drive receptor assembly.

To further understand the TLR TMD interactions, we examined their sequences (Table 2.1) for any structural motifs that could provide further insight into the homotypic and heterotypic behavior as it has been demonstrated that certain structural motifs and residues are over represented in transmembrane segments and can play a pivotal role in protein-protein interactions [151, 110]. The first interesting results of this analysis was that of the strongly homotypic interactors, TLR2, TLR7, and TLR9 all contained a Small-xxx-Small motif, where small residues are considered to

be Gly, Ala, or Ser. This motif occurs in over 66% of known membrane helical pairs [151] and is known to be a critical interface for the GpA dimerization and other high-affinity TMD interactions [111, 78, 44]. While this motif is commonly found in interacting transmembrane domains, it does not guarantee high interaction propensity by itself. The residues around this motif are also important in terms of stabilizing the packing interface [110]. As TLR2 showed both strong homotypic and heterotypic interactions (Figures 2.2, 2.3, 2.5, 2.6, and Supplementary Figures A.3, A.5), mutating residues in this interface for TLR2 would determine any role of the Small-xxx-Small motif in these interactions. Mutational analysis of potential interface residues, demonstrated that this Small-xxx-Small motif was only important for the heterotypic interactions, and was not critical for homotypic interactions (Figure 2.7), suggesting that TLR2 potentially has multiple interfaces for oligomerization. Further investigations to identify and characterize the entire TLR2 TMD interface would be needed before determining the Janus interface that is critical for the previously unseen homotypic capability of TLR2.

In conclusion, we demonstrated that the TLR TMDs possess a wide range of interaction potentials and are able to recapture the known behavior of the native proteins. This work indicates a pivotal role of the TMDs in TLR dimerization, a region of this family of proteins that had previously not been studied in the same depth as the extracellular domain and TIR domain. Given the importance of TLRs in the innate immune response and its relationship to several chronic disease states, understanding the roles of TLR TMDs can provide critical insights into assembly and function of these receptor complexes and provide potential ways to regulate TLR interactions that may lead to the discovery of novel therapeutics.

Chapter 3

Studying interactions of Toll-like receptor transmembrane domains in mammalian membranes

3.1 Introduction

Toll-like receptors (TLRs) are a critical component of innate immunity, acting as the first responders to viral and bacterial infections [146]. These receptors are evolutionary conserved germline encoded proteins, that exist in multiple species, with humans having 10 known functional receptors. Each Toll-like receptor is a type I transmembrane protein composed of three unique domains:

(1) an extracellular domain composed of multiple Leucine rich repeats involved in pathogen recognition;

(2) a single transmembrane domain; and

(3) an intracellular Toll-Interleukin-1 receptor (TIR) domain involved in downstream signal transduction.

Toll-like receptors are broken down into two classes based on cellular localization [101]:

(1) cell-surface expressing receptors including TLR1, TLR2, TLR4, TLR5, TLR6, and TLR10, that are involved in the recognition of bacterial cell wall components, and

(2) receptors expressed on intracellular compartments, like endosomes, including TLR3, TLR7, TLR8, and TLR9, that are involved in the recognition of bacterial and viral nucleic acids.

Structural studies have long focused on the extracellular domain, the intracellular domain, and downstream signaling complexes involved in the Toll-like receptor signaling pathway [231]. Crystal structures have been solved for the extracellular domains of TLR2/TLR1 [91], TLR2/TLR6 [91], TLR3 [133] TLR4 [167], TLR5 [85], TLR8 [205], and TLR9 [157] in complex with ligands, demonstrating the active signaling complexes for TLRs are homodimeric or heterodimeric. Only the TLR8 extracellular domain has been solved in an apo conformation, without ligand, which demonstrated the existence of a preformed dimer that underwent a conformational change upon ligand binding [205]. For transmembrane proteins, it is thought that ligands can induce a signal by either changing the oligomeric state of the protein, or by inducing conformational changes in the protein [151]. In regards to TLRs, it has been proposed that the cell surface receptors undergo a change in oligomeric state upon ligand addition, but the endosomal receptors are preformed dimers that undergo conformational changes upon ligand addition [57]. We propose that the Toll-like receptors at the cell surface also exist as preformed dimers and undergo conformational changes upon ligand addition to initiate signaling events.

Evidence for the potential of all Toll-like receptors to exist as preformed dimers is supported by the fact that isolated transmembrane domains of TLRs were capable of oligomerizing in bacterial membranes without any contribution from extracellular domain driven interactions [84]. In order to study TLR transmembrane domain interactions in native membrane environments, it is important that the transmembrane domains are properly localized. It has been shown that transmembrane domains for TLRs are indeed critical for trafficking. First, It was shown that the extracellular domain of TLR4, when coupled to other TLR transmembrane and TIR domains, only localized to the plasma membrane if it was fused with another plasma membrane expressing TLR transmembrane and TIR domain [156]. Additional evidence for the importance of this region in trafficking is that the TLR3, TLR7, TLR8, and TLR9 transmembrane domains only traffic correctly to endosomes through transmembrane domain interactions with the UNC93B1 chaperone in the ER [197, 16, 117]. Another ER chaperone, PRAT4A, has been found to regulate trafficking of the cell surface TLRs [216, 199], with a point mutant near the C-terminus of the TLR1 transmembrane domain (I602S)

greatly affecting proper localization of the receptor [69]. Evidence also supports the importance of the TLR transmembrane domains in signal initiation. First, the TLR4 extracellular domains only responded to LPS if the transmembrane and TIR domain chimeras were expressed in complimentary signaling pairs, indicating that the transmembrane and TIR domains are critical for signal propagation [156]. Secondly, it has been shown that the TLR4 extracellular domains acts as an inhibitor of signaling, as expression of just the TLR4 transmembrane and TIR domains leads to constitutive signaling [166]. These results suggest that the various domains play important roles in oligomerization, trafficking, and signaling.

To elucidate the contribution of the various domains (extracellular, transmembrane, and intracellular) to Toll-like receptor oligomerization, trafficking, and signaling, suitable mammalian membrane systems for studying these interactions needed to be developed. Current methods to study membrane protein interactions in native environments are severely limited. The earliest methods use Förster resonance energy transfer (FRET) with fluorescently conjugated antibodies or ligands against the protein of interest. For example, early studies on epidermal growth factor receptor using donor photobleaching FRET with a fluorescent ligand showed that the ligand induces some dimerization of the receptor, but predominantly causes a change in conformation for activation [54]. Initial studies on the Interleukin-2 (IL-2) receptor used fluorescent antibodies and flourescent activated cell sorting (FACS) to show that the three subunits of the IL-2 receptor are a preformed heteromer that undergoes subtle conformation changes in the presence of various cytokines [33]. While useful, these methods do not allow one to study contributions of individual domains. Also, highly specific molecular probes, like antibodies, are required for the protein of interest, which for the study of integral transmembrane domain interactions, do not exist.

With the advance in fluorescent proteins, genetically encoded fluorescent tags have become a common alternative to fluorescently labeled dyes and antibodies [132]. Fusing a fluorescent protein to proteins of interest allows them to be studied in native environments without exogenous agents. Interactions can be measured by attaching a suitable FRET pair to two proteins that are thought to interact, and monitoring energy transfer.

There are several ways to measure FRET [88]. The most common method is sensitized emission because of its ease of setup; however, it also has the drawback of being the least sensitive measure of FRET and requires the most controls [170]. Another common method is photobleaching FRET [170], in which high intensity laser is used to completely bleach the acceptor fluorescent protein and the change in emission intensity of the donor fluorescent protein is monitored. The advantage of photobleaching is that it provides a definitive measure of FRET, but a major downside is the irreversible change in the sample [170].

Herein, we report on the use and development of FRET reporter systems for imaging transmembrane domain interactions in mammalian membranes. One suitable mimetic for studying membrane proteins is the use of plasma membrane derived vesicles [191], a method that has been used extensively to study homotypic interactions among membrane protein receptors [126, 22, 23, 186]. We utilized these plasma membrane derived vesicles to measure heterotypic interactions of transmembrane domains for the first time. As a faster approach to screen for heterotypic interactions, we adopted a photobleaching FRET method for use in live-cell imaging experiments.

3.2 Materials and Methods

3.2.1 Plasmid Constructs

All constructs were cloned into pcDNA3.1(+) (Invitrogen), kindly provided by Dr. Amy Palmer (University of Colorado, Boulder), using the NheI and XbaI restriction sites in the multiple cloning site. Assembly was performed using standard restriction enzyme digestion or Gibson Assembly methods [63]. Control plasmids for expressing FGFR3 extracellular and transmembrane domains were provided by Dr. Kalina Hristova (Johns Hopkins) with both EYFP and mCherry fluorescent proteins. TLR constructs were PCR amplified from genomic DNA (Qiagen DNeasy Blood & Tissue Kit) extracted from U-937 monocytes (ATCC CRL 1593.2). All assembled constructs were sequence verified (Genewiz).

3.2.2 Confocal Microscopy

For all imaging experiments, transfections were carried out in HEK 293T cells (ATCC CRL-3216) maintained in Dulbecco's modified Eagle's medium supplemented with 10% fetal bovine serum, 100 U/mL penicillin, and 100 mg/mL streptomycin. Cells were seeded at a density of 20% confluency in the dish or well being used for the experiment. The next day wells were transfected with equivalent amounts of EYFP and mCherry expressing plasmids using TransIT-2020 according to the manufacturer's specifications (Mirus).

3.2.2.1 Sensitized Emission FRET in Plasma Membrane Derived Vesicles

Vesiculation of cells was carried out to isolate plasma membrane fractions using previously reported methods [126, 191]. Briefly, 24 hours post-transfection cells were washed three times with PBS containing 0.75 mM $CaCl_2$ and 0.5 mM $MgCl_2$ (CM-PBS). Cells were then incubated in vesiculation buffer, CM-PBS containing 25 mM formaldehyde and 0.5 mM 1,4-dithiothreitol, for 2 hours at 37 °C. Glycine solution in PBS was added to a final concentration of 0.125 M to quench the formaldehyde. Supernatant was transferred to a 4-well Nunc Lab-Tek II chambered coverslip (Fisher) for imaging.

Images were collected on a Nikon A1R confocal microscope using a dual laser, 3-filter cube set. The EYFP donor and sensitized FRET channels were imaged using a 488 nm laser line with the EYFP donor channel collecting emission from a 525/50 filter and the FRET channel emission using a 600/50 filter. The mCherry acceptor channel was imaged using a 561 nm laser line with a 650 LP filter. All images were collected using a 1.30 numerical aperture 40X oil objective lens.

3.2.2.2 Acceptor Photobleaching FRET in Live Cells

Live cell photobleaching was performed by washing cells 24 hours post transfection three times with PBS. Cells were then placed in live-cell imaging solution (20mM HEPES, 140 mM NaCl, 2.5 mM KCl, 1.8 mM CaC_2, 1.0 mM $MgCl_2$, pH 7.4) to maintain cell-viability at ambient conditions for up to four hours. Cells were analyzed on a Nikon A1R confocal using an EYFP filter

cube (488 nm laser, 525/50 filter) and an mCherry filter cube (561 nm laser, 600/50 filter) with a 1.30 numerical aperture 40X oil objective lens. Laser power was maintained below 2% to avoid photobleaching of samples while finding cells in the focal plane. Individual cells were zoomed on to limit the focal area being photobleached. The photobleaching scan consisted of:

(1) five scans using the EYFP filter cube at low power ($Donor_{pre}$),

(2) one scan using the mCherry filter cube at low power ($Acceptor_{pre}$),

(3) 10 scans using the mCherry filter cube at full power to bleach the acceptor,

(4) one scan using the mCherry filter cube at low power ($Acceptor_{post}$), and

(5) five scans using the EYFP filter cube at low power ($Donor_{post}$).

If FRET occurred, donor intensity would increase after the bleaching of acceptor allowing FRET efficiency to be calculated according to the equation:

$$E_{FRET} = 1 - \frac{Donor_{pre}}{Donor_{post}}. \tag{3.1}$$

See Figure B.6 for a representative scan profile.

3.2.3 Fluorescent Protein Expression and Purification

To calibrate protein concentration to microscope intensity values, the EYFP and mCherry proteins needed to be expressed and purified. The EYFP and mCherry sequences were PCR amplified out of the FGFR3 plasmid constructs and cloned into the pET-15b NdeI and BamHI restriction sites. BL21(DE3) chemically competent cells were transformed with the plasmid of interest and plated on LB + Ampicillin (100 μg/mL) agar plates. Single colonies were inoculated in a 5 mL starter culture of LB media containing 100 μg/mL of ampicillin, and grown overnight at 37 °C and 250 rpm. These cultures were then transferred to flasks containing 250 mL of LB without antibiotic and allowed to grow at 37 °C and 250 rpm until the OD_{600} was between 0.4 and 0.6. Protein expression was induced with 1.0 mM isopropyl β-D-thiogalactopyranoside at this

time and the cells were allowed to grow for 4 hours before cell pellets were obtained by spinning down the cultures at 4500 rpm and 4 °C for 15 min. The bacterial pellets were lysed by sonication (MiSonix) and spun down at 15,000 rpm and 4 °C for 30 min. The soluble protein was isolated from the supernatant using Talon metal affinity resins (Clontech) following the manufacturer's protocol. The fluorescent proteins were concentrated using 10kDa MWCO centrifugal filters (EMD Millipore). Concentrated protein was verified using Coomassie stain and His-tag Western blots on 10% SDS-PAGE gels. Protein concentration was determined by absorption using a UV-Vis spectrophotometer (Beckman Coulter) with EYFP, ϵ_{513} of 83,400 M^{-1} cm^{-1}, and mCherry, ϵ_{587} of 72,000 M^{-1} cm^{-1}.

3.2.4 Localization Studies

3.2.4.1 Flow Cytometry Antibody Staining

To compare localization between the transiently expressed constructs and endogenous TLR expression, primary monoclonal antibodies against the extracellular domains of TLR1, TLR2, and TLR6 were purchased from Cell Signaling Technologies. The target cells are spun down, supernatant aspirated, and pellet resuspended in freshly made fixation buffer (4% paraformaldehyde, Fisher, heated at 60 °C to dissolve and dissociate in PBS). The cells are fixed at 37 °C for 15 min. Cells are then chilled on ice for 1 min before being spun down, resuspended in PBS and counted. $1x10^6$ cells are aliqouted into microcentrifuge tubes and washed three times with 1 mL incubation buffer (0.5% BSA, Fisher, in PBS), spinning down at 2000xg for 3 min after each wash. After the third wash, the cells are incubated with 100 μL of primary antibodies at a 1:100 dilution in incubation buffer. Primary antibodies are left to incubate for 1 hour at room temperature. Again cells are washed three times with incubation buffer. A fluorescent secondary antibody, 100 μL anti-rabbit IgG conjugated to phycoerythrin, PE, (Cell Signaling Technologies) diluted 1:200 in incubation buffer, was added to the cells and incubated for 30 min at room temperature. Cells were again washed three times with 1 mL incubation buffer before being suspended in 500 μL PBS

prior to analysis on a MoFlo Cytomation fluorescence activated cell sorter (Beckman Coulter).

Primary monoclonal antibodies against the GFP protein (Cell Signaling Technologies) were also used to verify EYFP transfected constructs. The EYFP reporter is fused to the C-terminus of all constructs, and as such is expected to be intracellular. To probe for intracellular localization, the cells being monitored were permeabilized after fixation with 90% ice cold methanol and incubated on ice for 30 minutes before continuing the protocol with primary antibody incubation as described above.

3.2.4.2 Confocal Microscopy Membrane Markers

A monoclonal antibody against wheat-germ agglutinin conjugated to AlexaFluor 647 (Invitrogen) was used to stain the plasma membrane. The antibody was incubated with cells in PBS for 15 min at 37 °C prior to suspension in live cell imaging solution. The WGA-AlexaFluor 647 antibody was imaged using a Cy5 filter cube (640 nm laser, 650 LP filter).

The endoplasmic reticulum was marked using a genetically encoded fluorescent protein with an ER retention tag. The construct contained the signal peptide from the ER protein BiP, fused to a KDEL-mCherry marker. This plasmid was kindly provided by Dr. Gia Voeltz (University of Colorado, Boulder). The plasmid was cotransfected in equal amounts with the protein of interest fused to an EYFP tag 24 hours prior to imaging.

3.3 Results and Discussion

3.3.1 Construct Assembly

To investigate TLR2 heterotypic assembly with TLR1 or TLR6, we generated a series of constructs with and without the extracellular and intracellular domains, fused to fluorescent proteins. The fluorescent proteins utilized were EYFP and mCherry, a system suitable for FRET measurements [126, 22, 23, 186]. The EYFP-mCherry FRET pair has a Förster radius of 5.6 nm [2], a suitable distance for studying TLR domains based on crystallographic distances. Each TLR con-

struct was cloned into the pcDNA 3.1(+) mammalian expression system for transient transfection of mammalian cells. The N-terminal domain of all constructs consisted of the endogenous signal peptide for TLR1, TLR2, or TLR6 to assist in recognition by the translocon for membrane protein folding and trafficking [223]. The remaining domains were chosen based on sequence annotations from the UniProt database (TLR2 - O60603, TLR1- Q15399, TLR6 - Q9Y2C9) shown in Table 3.1. Domains were extended in the case of the signal peptides, which were identified to include only the first 30 amino acids, for easier handling by PCR. Transmembrane domains were extended on both sides of the membrane to include flexible juxtamembrane regions in order to ensure complete spanning of the membrane bilayer. Each of the final constructs (Figure 3.1) could be co-transfected in mammalian cells to study the contribution of individual domains in the assembly of active TLR2 signaling heterodimers with TLR1 and TLR6. These constructs would also allow detection of conformational changes that may be induced upon ligand addition as is seen in other receptor families [49], as any changes in FRET efficiency of the EC+TM constructs in the presence versus absence of ligand would suggest conformational changes.

Table 3.1: TLR domain boundaries

Domain	**TLR2**	**TLR1**	**TLR6**
Signal Peptide	1-53	1-53	1-53
Extracellular Domain	54-580	54-579	54-575
Transmembrane Domain	581-638	580-634	576-639
TIR Domain	639-784	635-779	640-784

The domain boundaries are the amino acids over which the construct was PCR amplified for construct assembly. The signal peptide is typically shorter, but for ease of PCR handling it was extended to the junction that begins the first Leucine-rich repeat. The membrane spanning region of the transmembrane domain is shorter than that cloned here. Transmembrane domain segments were PCR amplified to include N-terminal and the C-terminal juxtamembrane regions to ensure the membrane was spanned in its entirety.

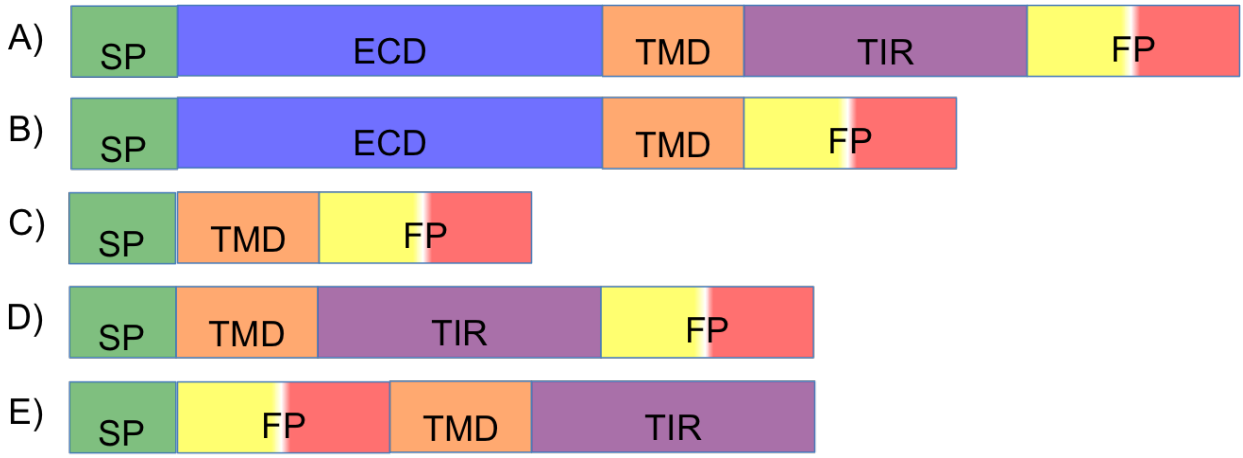

Figure 3.1: Plasmid constructs for studying domain contributions to TLR2 assembly.
Constructs were designed to investigate the role of each domain, extracellular (ECD), transmembrane (TMD), and intracellular (TIR) in TLR2 heterotypic assembly with TLR1 and TLR6. Each construct was tagged with a genetically encoded fluorescent protein, FP, that could act as a FRET donor (EYFP) or FRET acceptor (mCherry). The signal peptide (SP) at the native N-terminus of each TLR was used to direct localization to the plasma membrane. A) WT, B) EC+TM, C) TM, D) TM+TIR, E) FP-TM+TIR

3.3.2 Sensitized Emission FRET Interactions

Following previously reported FRET methodologies, we used plasma membrane derived vesicles to study the heterotypic interactions of the TLR constructs in native membrane environments. A sensitized emission FRET method using plasma membrane derived vesicles was previously reported for the studies of homotypic membrane protein interactions utilizing the GpA transmembrane domain [22], and the FGFR3 receptor [23]. Additionally, this method was able to discern the role of disease causing point mutations in the FGFR3 transmembrane domain as these mutations stabilized the association of the receptor [172, 171]. The advantage of using this system is that the transmembrane domains are in a native cellular environment that includes other proteins instead of an isolated transmembrane domain in detergent micelles or synthetic liposomes.

To utilize sensitized emission FRET in plasma membrane derived vesicles, appropriate controls must first be performed [170]. These controls include calculation of bleed-through coefficients for the donor, EYFP, and acceptor, mChery, in the FRET imaging channel. To quantify the FRET signal, calibration curves for accurately determining the concentration of protein expressed in each vesicle is critical. A correction factor must also be determined that relates the sensitized emission to donor quenching when acceptor is present.

3.3.2.1 Donor and Acceptor Bleed-Through Coefficient Determination

For any given FRET scan using sensitized emission, three contributions can appear in the FRET channel:

(1) direct donor emission (donor bleed-through, β_D),

(2) acceptor emission due to direct excitation (acceptor bleed-through, β_A), and

(3) sensitized acceptor emission due to FRET (I_{sen}).

The sensitized emission intensity can be directly calculated using bleed-through coefficient corrections according to the equation:

$$I_{sen} = I_{FRET} - \beta_D * I_{Donor} - \beta_A * I_{Acceptor} \tag{3.2}$$

where I_{FRET}, I_{Donor}, and $I_{Acceptor}$ are the intensities measured in the respective channel for each vesicle.

The donor bleed-through coefficient, β_D, is determined by expressing the donor only in vesicles and measuring the intensity recorded using the donor and FRET filter cube sets. The bleed-through value can then be calculated according to Equation 3.3.

$$\beta_D = \frac{I_{FRET}}{I_{Donor}} \tag{3.3}$$

In a similar manner, the acceptor bleed-through coefficient, β_A, can be determined by expressing the acceptor only in vesicles and measuring the intensity recorded using the FRET and acceptor filter cubes. The bleed-through value can then be calculated according to Equation 3.4.

$$\beta_A = \frac{I_{FRET}}{I_{Acceptor}} \tag{3.4}$$

Through expression of just EYFP in vesicles, Figure B.3, we determined $\beta_D = 0.24 \pm 0.07$, for this microscope system. Through expression of just mCherry in vesicles, Figure B.4, we determined β_A was 0.25 $\pm$ 0.06. These values were determined from measurements collected on three independent transfections and vesicle formations. The bleed-through values determined for our setup are in good agreement with values previously reported for this FRET pair on a similar microscope with similar settings [22].

3.3.2.2 Calibration of Donor and Acceptor Intensity

To accurately measure the protein concentration present in each vesicle, calibration curves were generated for donor and acceptor. The EYFP and mCherry proteins were expressed and purified from bacterial cells. Solutions of purified EYFP protein in vesiculation buffer were measured over a concentration range of 0-45 μM (Figure B.1) using the donor scan settings. Solutions of

purified mCherry protein in vesiculation buffer were measured over a concentration range of 0-90 μM (Figure B.2) using the acceptor scan settings. Several curves were collected at fixed laser power, but various gains, to cover a broader range of potential settings for imaging of the TLR constructs. The slopes of the respective lines provided calibration constants, i_D and i_A, for determining the apparent concentration of the donor,

$$C_{D,app} = \frac{I_{Donor}}{i_D} \tag{3.5}$$

and the actual concentration of the acceptor,

$$C_A = \frac{I_{Acceptor}}{i_A} \tag{3.6}$$

that are present in each vesicle. The donor concentration is apparent because in any system expressing both donor and acceptor, some of the donor fluorescence energy will be used to generate acceptor flourescence [170].

3.3.2.3 Correction of Donor Concentration due to Acceptor Quenching

The measured sensitized emission, I_{sen}, is proportional to the donor quenching, ΔI_{Donor}, due to FRET according to Equation 3.7. The proportionality constant, G_F, is the gauge factor which is specific for each microscope depending on the wavelengths of recorded emission for donor and acceptor, the ratio of quantum yields, and environment [126]. The utilization of plasma membrane vesicles eliminates the heterogenous environment and allows this value to be determined for quantification of the sensitized emission.

$$\Delta I_D = I_{Donor,corr} - I_{Donor} = G_F * I_{sen} \tag{3.7}$$

where $I_{Donor,corr}$ is the corresponding donor intensity in the absence of FRET, which is related to the actual donor concentration by $I_{Donor,corr} = C_D * i_D$.

To determine the G_F value, a plasmid encoding the fluorescent donor directly linked to the fluorescent acceptor is necessary, as the fixed donor-to-acceptor ratio is necessary for concentration calculations. Cells transfected with the linked EYFP-mCherry plasmid were vesiculated, and each

vesicle was scanned in the three channels to determine the sensitized emission (Equation 3.2). From the calibration curve values, the apparent donor concentration and acceptor concentration can be calculated from Equations 3.5 and 3.6. As acceptor is present, the actual donor concentration is being decreased by FRET, so $C_{D,app} < C_D$. However, it is known for the EYFP-mCherry construct that $C_D = C_A$ by design. Taking this into account, one can solve for G_F by relating Equations 3.7 and 3.2 with $I_{Donor,corr}$ to get:

$$G_F = \frac{C_D - C_{D,app}}{C_{D,app}} \frac{I_D}{I_{sen}} \tag{3.8}$$

where C_D is fixed to be C_A in this experimental design.

Measurements of the EYFP-mCherry fusion protein in vesicles on our microscope using the values we determined above for β_D, β_A, i_D, and i_A yielded G_F = -3.57 ± 1.11 (Figure B.5). This value indicates a non-physical process is occurring in the vesicles, namely $C_{D,app} > C_D$. For this negative value to be true the donor would have to be receiving energy from the acceptor, an impossible photophysical process. With the determined G_F value it is not possible to get quantitative values of sensitized emission using previously reported methods [126, 22]. While such quantitative values would be ideal, sensitized emission values can still be measured in the plasma membrane derived vesicles, they just can't be directly correlated to a FRET efficiency. Compared to reported values for β_D, β_A, i_D, and i_A, only the slopes of the lines for fluorescent protein concentration are significantly different [126], suggesting that something may be wrong with the standard curves generated for purified EYFP and mCherry proteins, or the concentrations determined by UV-vis spectroscopy.

3.3.2.4 Vesicle Production for TLR1, TLR2, and TLR6

The ability of the TLR1, TLR2, and TLR6 transmembrane domains to form both homotypic and heterotypic associations in bacterial membranes [84], suggests vesicles for both interactions should be studied. Therefore co-transfections with constructs for TLR2-TLR2, TLR1-TLR1, TLR6-TLR6, TLR2-TLR1, and TLR2-TLR6 were performed to make vesicles. This would allow the calculation of equilibrium constants for each interaction to be determined. As the heterotypic

system has three interactions in equilibrium, the homotypic interactions must be accounted for to determine the heterotypic association constant through coupled equilibrium relationships [73].

Expression of the TLR TM constructs in plasma membrane derived vesicles (Figure 3.2 A, C, and E) yielded vesicles similar to those seen for the fluorescent protein only constructs (Figure B.3, B.4, and B.5), namely, vesicles of uniform size and fluorescent intensity across the entire vesicle. These vesicles did not appear to demonstrate a membrane bilayer environment as reported elsewhere for plasma membrane proteins studied in plasma membrane derived vesicles [22, 186, 171] or for vesicles used to study lipid raft properties [123, 122]. Occasionally, a uniform vesicle would appear in the vesiculated solution for these TM only constructs, Figure 3.2 E, but they were very rare. These images suggest that the synthetic constructs are not trafficking properly to the plasma membrane and are instead localized in intracellular compartments. Indeed, if the live cells from which the vesicles were formed were first analyzed on the microscope, it was apparent that the proteins were partially localized to a membrane bilayer environment (Figure 3.2 B, D, and F). Early studies of plasma membrane derived vesicles by electron microscopy determined that vesicles produced via these chemical methods were not contaminated with intracellular organelles [189]. This suggests that the vesiculation process was creating artifacts in TLR localization, or that the constructs were stuck in the ER and not trafficked to the plasma membrane. This is not unfounded, as the vesiculation procedure uses high amounts of reducing agents and cross-linking reagents compared to those in a normal experiment [236]. To further investigate the TLR domain interactions in mammalian membranes, we modified our experimental setup to investigate interactions on live cells.

3.3.3 Acceptor Photobleaching FRET Interactions

Instead of using sensitized emission FRET in live cells, another common imaging method that can directly measure FRET efficiency without correction factors, acceptor photobleaching, was utilized [170]. The acceptor photobleaching concept arises as some donor fluorescence is quenched by FRET in the presence of an acceptor. By bleaching the acceptor fluorophore, the method by

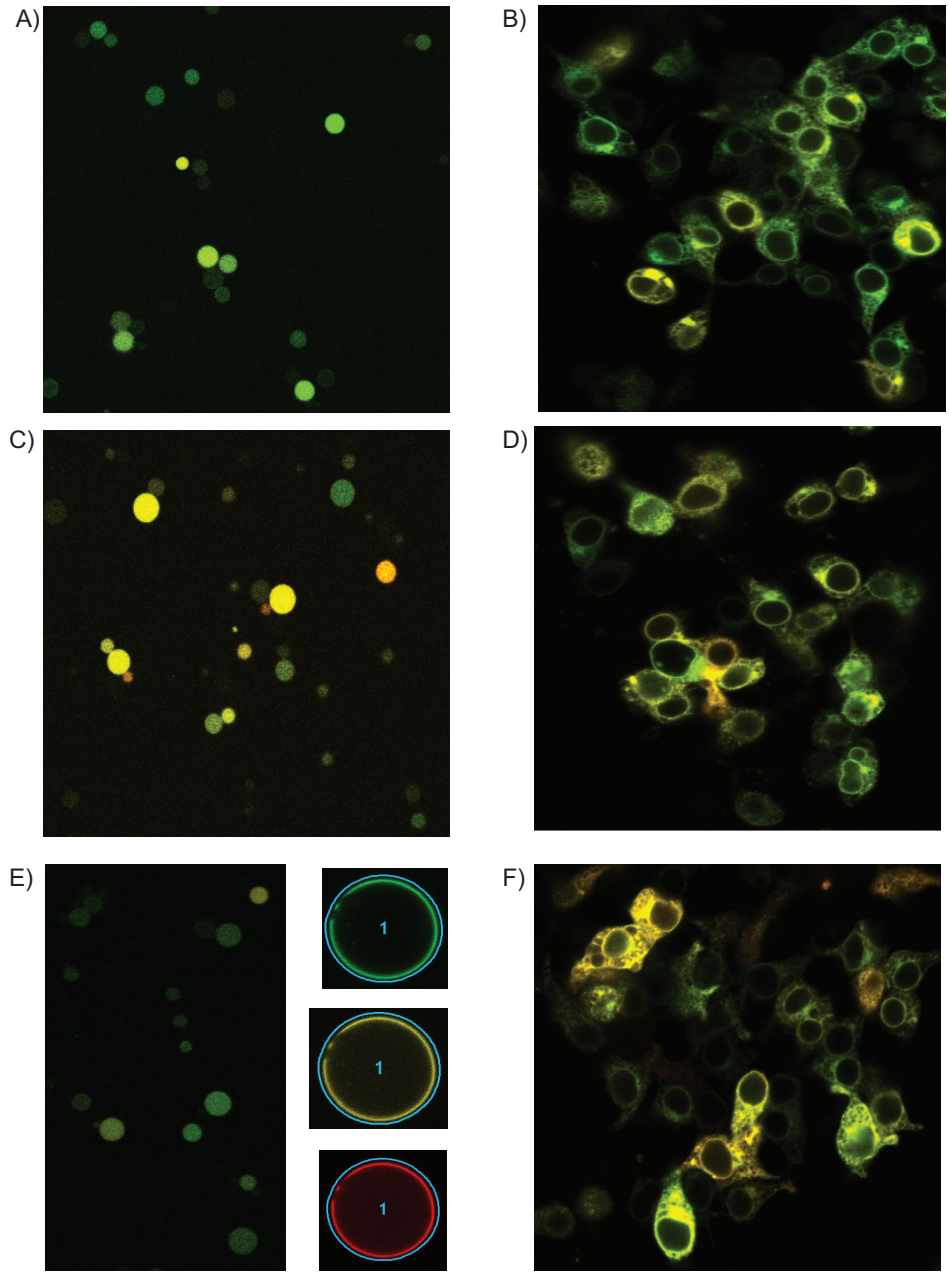

Figure 3.2: Comparison of fluorescence images of plasma membrane derived vesicles and live cells. A,B) Cells were transfected with pcDNA-TLR2-TM-FP plasmids and A) imaged after vesiculation, or B) imaged as live cells. C,D) Cells were transfected with pcDNA-TLR6-TM-FP plasmids and C) imaged after vesiculation or D) imaged as live cells. E,F) Cells were cotransfected with pcDNA-TLR2-TM-EYFP and pcDNA-TLR6-TM-mCherry and E) imaged after vesiculation or F) imaged as live cells. Vesiculated cells were predominantly uniform vesicles of fluorescence, but occasionally membrane only labeled vesicles were found (E). While vesicles appeared to be uniformly fluorescent, live cells showed distinct membrane localization. This could be due to artifacts of the vesiculation process, or improper localization of the synthetic constructs.

which donor energy is transferred to FRET emission is removed, and the donor flourescence emission energy must increase in proportion to the strength of the energy transferred during FRET. This donor dequenching can be measured as a FRET efficiency by relating the donor intensity before and after the bleaching process as shown in Equation 3.1.

The controls necessary in photobleaching experiments are to ensure that the photobleaching process does not also degrade the donor, and that the acceptor is bleached to <10% of its initial value [170]. For our system, we validated that the photobleaching scan conditions did not degrade the donor by expressing a donor only sample of our TLR constructs. In these experiments we typically saw <2% reduction in the donor channel signal over the time course of the bleaching experiment, which was comparable to that if we did not bleach and just continuously scanned the sample on the donor channel. We also optimized the time for photobleaching to ensure >90% of the acceptor intensity was bleached. The optimal bleaching time was found to be 10 scans with the 561 nm laser (Figure 3.3 A and B.6), as additional scans had minimal change in the acceptor intensity.

Cells were co-transfected with plasmids encoding the TLR2-TLR1 or TLR2-TLR6 transmembrane domains with both constructs being expressed as the donor and acceptor. These transfections yielded cells of uniform membrane intensity with the donor channel showing increases in fluorescent intensity after bleaching of the acceptor (Figure 3.3 A). For each interaction, >250 individual cells were analyzed to calculate FRET efficiencies (Figure 3.3 B, C). The FRET efficiencies from acceptor photobleaching assays ranged from 7-47%. The increase in signal with acceptor concentration suggests that interactions are occurring between transmembrane domains of TLR2-TLR1 (Figure 3.3 B) and of TLR2-TLR6 (Figure 3.3 C). However, it is important to note that FRET signals can arise from random interactions, especially in systems of overexpressed proteins similar to those shown here [87]. People have tried to assess the random contribution using simulations, but this requires accurate determination of the concentrations for each expressed construct in the membrane, and knowledge of the exact oligomeric state formed [103]. Neither of those parameters are known for this system as TLR transmembrane domains were previously shown to have higher order oligomeric

states present in membrane mimetics, Figures A.3-A.5 [84]. Therefore, alternative controls using a known transmembrane domain associating protein, like GpA or T-cell receptor, that does not have any heterotypic interactions with the TLRs, should be constructed and tested to determine the boundaries of interacting versus noninteracting species in this system. Only with these experiments can definitive claims be made about the association of TLR2 heterotypic transmembrane domain associations in mammalian membranes.

3.3.4 TLR1, TLR2, and TLR6 Membrane Trafficking and Localization

The difference in the appearance of the constructs in plasma membrane derived vesicles and live cells (Figure 3.2) led us to investigate the localization of the TLR2, TLR1, and TLR6 constructs. From the images analyzed, it was possible that the proteins were at the plasma membrane, or that they were retained by the translocon in the endoplasmic reticulum. By utilizing two common methods, flow cytometry and fluorescence microscopy, we could determine the distribution of receptors in each location.

3.3.4.1 Flow Cytometry Localization

The standard method for TLR localization in literature has been to use flow cytometry with antibodies against the extracellular domain [114, 115, 156]. In this regard, we used antibodies on cells transfected with TLR2 EC+TM-EYFP constructs to see if the receptors were trafficking to the surface or were maintained in intracellular compartments. Antibodies against the extracellular domain of TLR2 and the fluorescent protein, EYFP, were incubated with intact cells (Figure 3.4) to detect cell surface receptors, or with permeabilized cells (Figure 3.5) to detect all receptors, through use of a phycoerythin-conjugated secondary antibody. For both sets of experiments the untransfected cells incubated with the TLR2 primary antibody (Figure 3.4 A) or the EYFP primary antibody (Figure 3.5 A) and PE-secondary antibody were gated to indicate negative cells for threshold of interactions and transfection efficiency.

The TLR2 antibody was used identify positively transfected cells. Based on untreated cells,

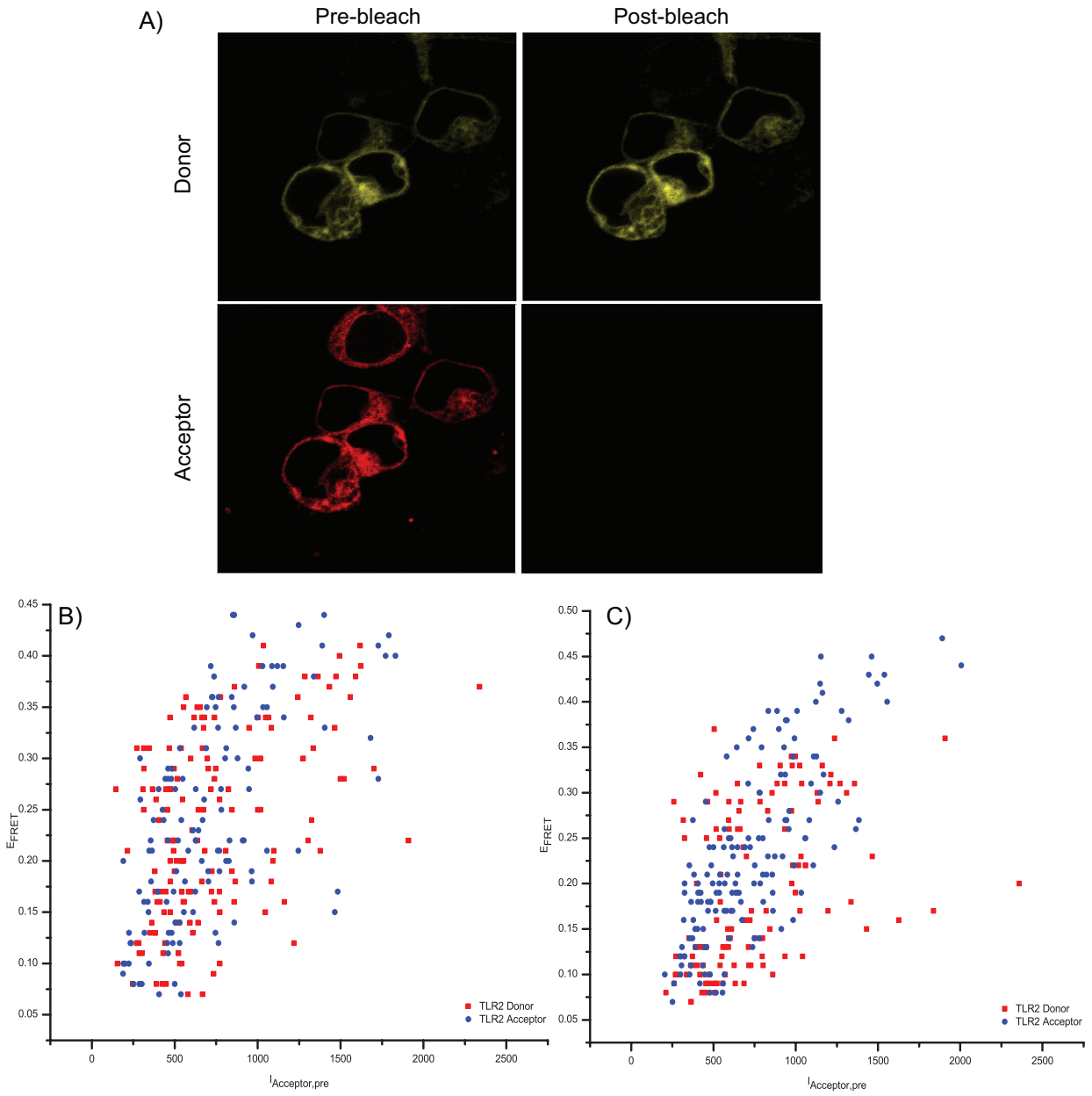

Figure 3.3: Acceptor photobleaching of TLR2-TLR1 and TLR2-TLR6 transfected cells.
Cells were transfected with TLR2 and TLR1 or TLR2 and TLR6. A) A representative image of a cell expressing both donor and acceptor constructs. The cell was bleached and an increase in the donor fluorescence signal was seen as the acceptor was completely bleached. B) TLR2-TLR1 TM only cells. C) TLR2-TLR6 TM only cells. All constructs were measured when expressed as the donor and the acceptor in three biological replicates with >250 individual cells analyzed. The increase in signal indicates the possibility of transmembrane domains undergoing heterotypic interactions in the cell. Red points correspond to transfections with TLR2 TM as the donor. Blue points correspond to transfections with TLR2 TM as the acceptor.

the right two quadrants, R3 and R5, indicate expression of the transfected plasmid, and anything in the upper right quadrant, R3, indicates binding of secondary antibody to the primary. For both cell treatments, the transfection efficiency was approximately 30% of the cell population. Based on intact cells for the TLR2 EC+TM construct, 55% of the transfected cells show trafficking to the membrane (Figure 3.4 B). For permeabilized cells, all transfected cells were not positively identified, but there was an increase to 70% of transfected cells stained for TLR2 (Figure 3.5 B). This increase in the percentage of all cells that were stained by the TLR2 primary for permeabilized (20.6%) compared to intact (16.5%) suggests that there is receptor distributed between both subcellular locations. Given that these antibodies had not previously been validated for flow cytometry, a standard 1:100 dilution was used. As not all transfected cells were identified by permeabilization perhaps more antibody is required to detect the amount of protein that is being over expressed.

The GFP antibody, which binds a conserved region in both GFP and EYFP, was used to stain for expression of the intracellular FP tag in transfected cells. This primary antibody showed unexpected binding as it had high signal for intact cells, which, based on the construct design, should always be found inside the cell, not at the surface. In both intact and permeabilized cells the entire population of transfected cells show binding by this antibody, with a large population of cells that weren't positive for transfection also showing increased secondary antibody binding signal (Figure 3.4 C and 3.5 C). Taken together it is unclear if the GFP antibody used is suitable for flow cytometry experiments.

3.3.4.2 Fluorescence Microscopy Localization

As flow cytometry experiments did not provide definitive evidence for the localization, confocal microscopy utilizing organelle specific reporters was tested. Common methods include the use of fluorescently conjugated antibodies or genetically encoded fluorescent proteins. TLR2, TLR1, and TLR6 are expected to traffic from the endoplasmic reticulum to the plasma membrane, so markers for these two organelles were used. Several commercial antibodies exist to target the plasma membrane. To visualize the plasma membrane, wheat germ agglutinin fluorescent antibody

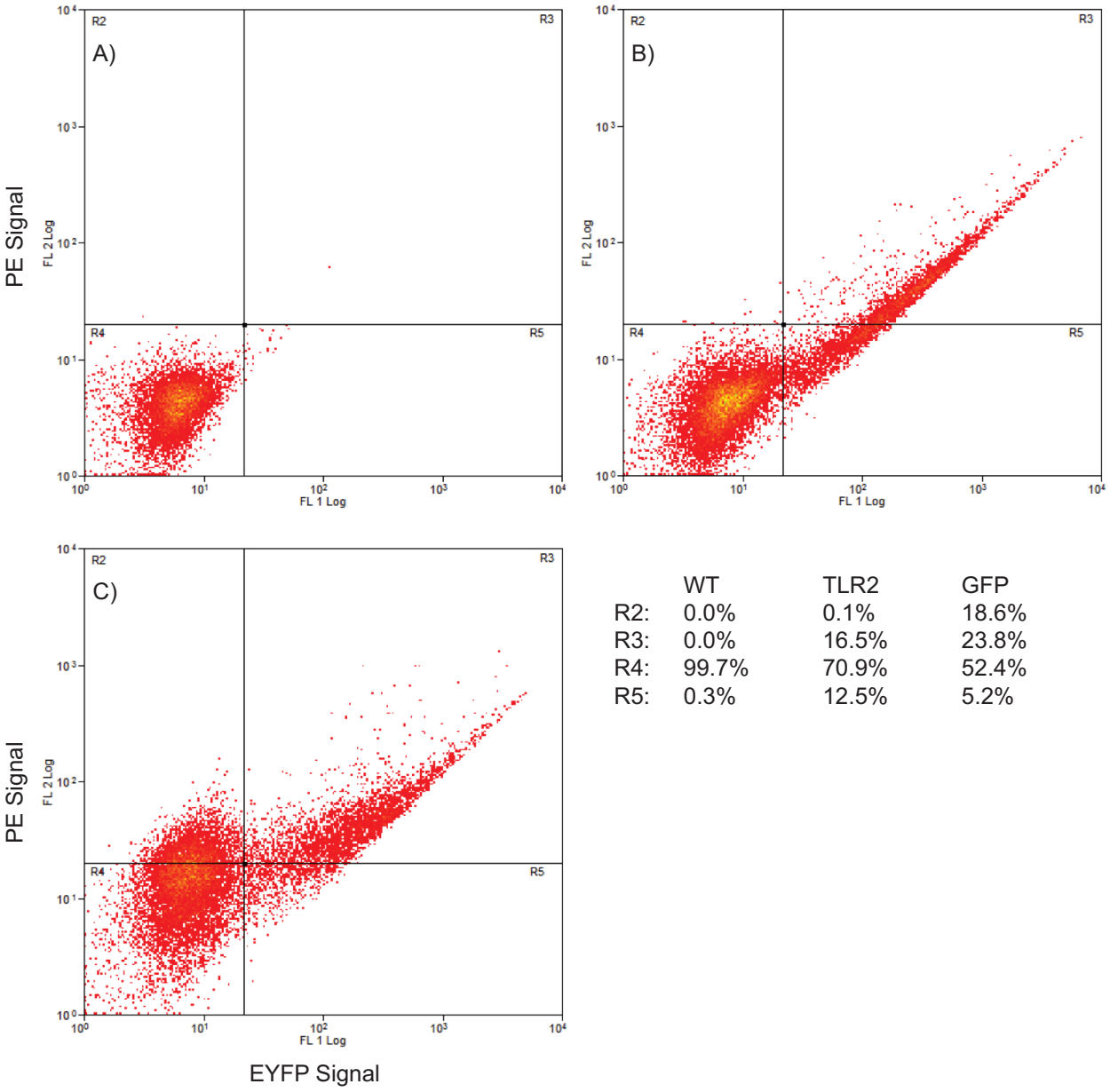

Figure 3.4: Flow cytometry profiles of permeabilized cells.
Flow cytometry for TLR2 and EYFP expression was checked in transfections of 293T cells using a TLR2-EC+TM-EYFP construct. Profile is broken down into quadrants: R2 - top left, R3 - top right, R4 - bottom left, R5 - bottom right. The upper half indicates binding of secondary antibody, PE signal. The right half indicates positively transfected cells, EYFP signal. A) Untransfected cells treated with isotype control primary and PE-conjugated secondary. B, C) Cells transfected with the pcDNA-TLR2-EC+TM-EYFP expression construct incubated with TLR2 (B) or GFP (C) primary antibody and PE-conjugated secondary.

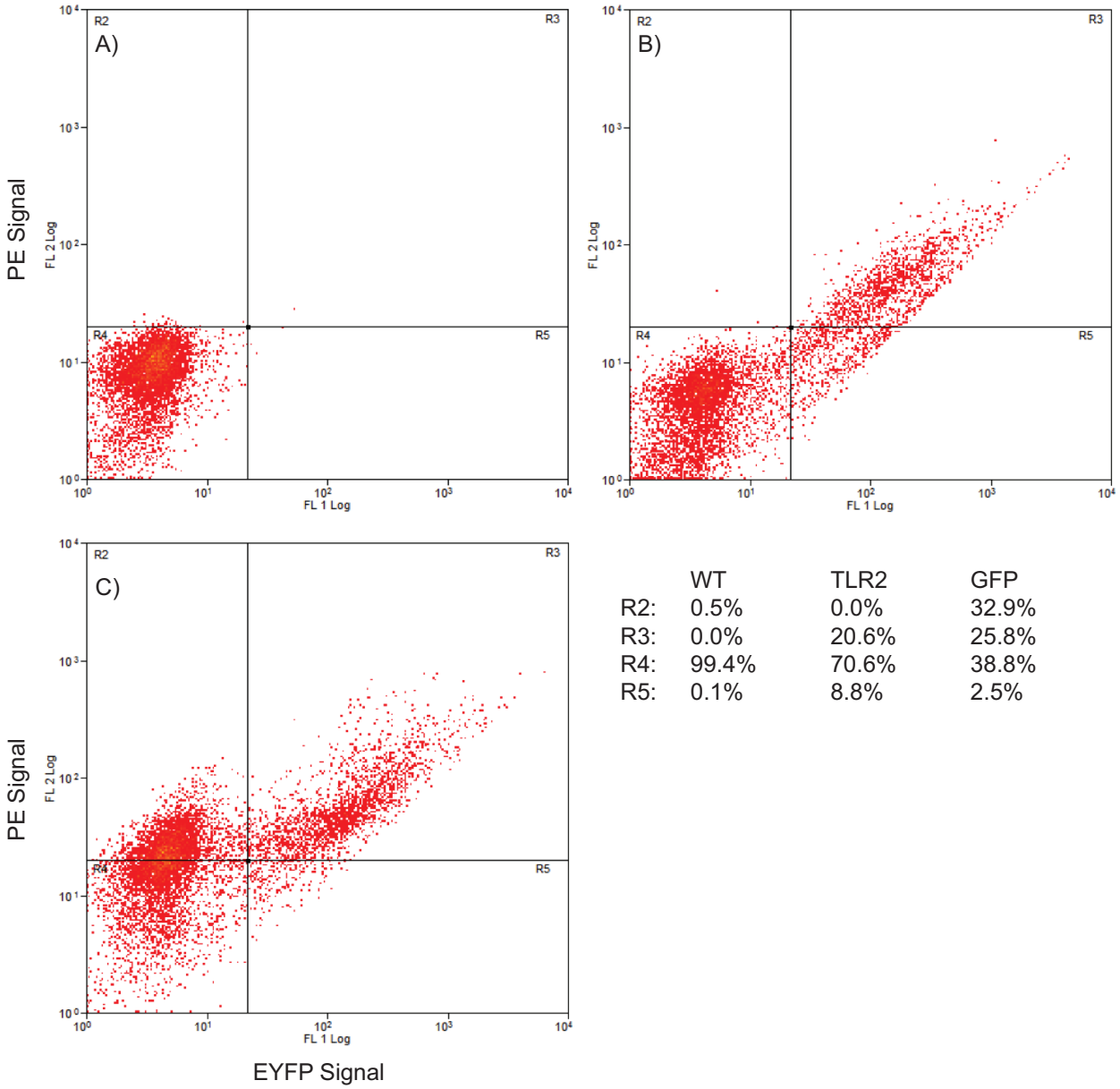

Figure 3.5: Flow cytometry profiles of fixed and permeabilized cells.
Flow cytometry for TLR2 and EYFP expression was checked in transfections of 293T cells using a TLR2-EC+TM-EYFP construct. Fixed and permeabilized cells allows for detection of all expressed protein regardless of localization. Profile is broken down into quadrants: R2 - top left, R3 - top right, R4 - bottom left, R5 - bottom right. The upper half indicates binding of secondary antibody, PE signal. The right half indicates positively transfected cells, EYFP signal. A) Untransfected cells treated with isotype control primary and PE-conjugated secondary. B, C) Cells transfected with the pcDNA-TLR2-EC+TM-EYFP expression construct incubated with TLR2 (B) or GFP (C) primary antibody and PE-conjugated secondary.

that binds to N-acetyl-D-glucosamine and sialic acid residues on the cell surface was used. Several groups have developed genetically encoded fluorescent protein sensors that are targeted to specific organelles [174]. To visualize the endoplasmic reticulum, a KDEL-mCherry fusion protein was used. Three TLR2-EYFP constructs, WT, EC+TM, and TM, (Figure 3.6) were co-transfected with the KDEL-mCherry endoplasmic reticulum marker in HEK 293T cells. Prior to imaging, these cells were stained with the fluorescent wheat germ agglutinin antibody to mark the plasma membrane. Visual inspection of these images clearly shows that the constructs are predominantly located in the ER with co-localization analysis using Imaris imaging sofware indicating that <10% of all EYFP intensity was found to be at the plasma membrane. From these results we concluded that the TLR constructs were not trafficking correctly in the over expression system.

Several alternative constructs were tested in an attempt to direct the trafficking to the plasma membrane. First, the signal peptide was changed to a stronger membrane localization tag, the IgG κ-chain leader sequence, used in commercial membrane display vectors. WT and TM constructs with the new signal peptide showed no difference in construct localization compared to the endogenous leader sequence. Second, the 3'UTR of membrane proteins has been reported to alter trafficking via a Rac1 dependent mechanism [12], and Rac1 has previously been shown to be important in TLR2 signaling [6]. Generation of constructs that included the endogenous 3'UTR of TLRs, WT-FP-3'UTR and FP-TM+TIR-3'UTR (modification of Figure 3.1 A and E), also did not show a change in localization by confocal microscopy. Additionally, in native immune cells, TLR2 was initially present at the cell surface but TLR1 and TLR6 were not; only after treatment with ligands were TLR1 and TLR6 present at the cell surface (Figure 4.4). We tried treating cells transfected with WT and EC+TM constructs in a heterotypic manner to determine if cell surface localization was somehow dependent on ligand recognition. Unfortunately, these constructs did not show any increase in the amount of construct localized that the plasma membrane by confocal microscopy.

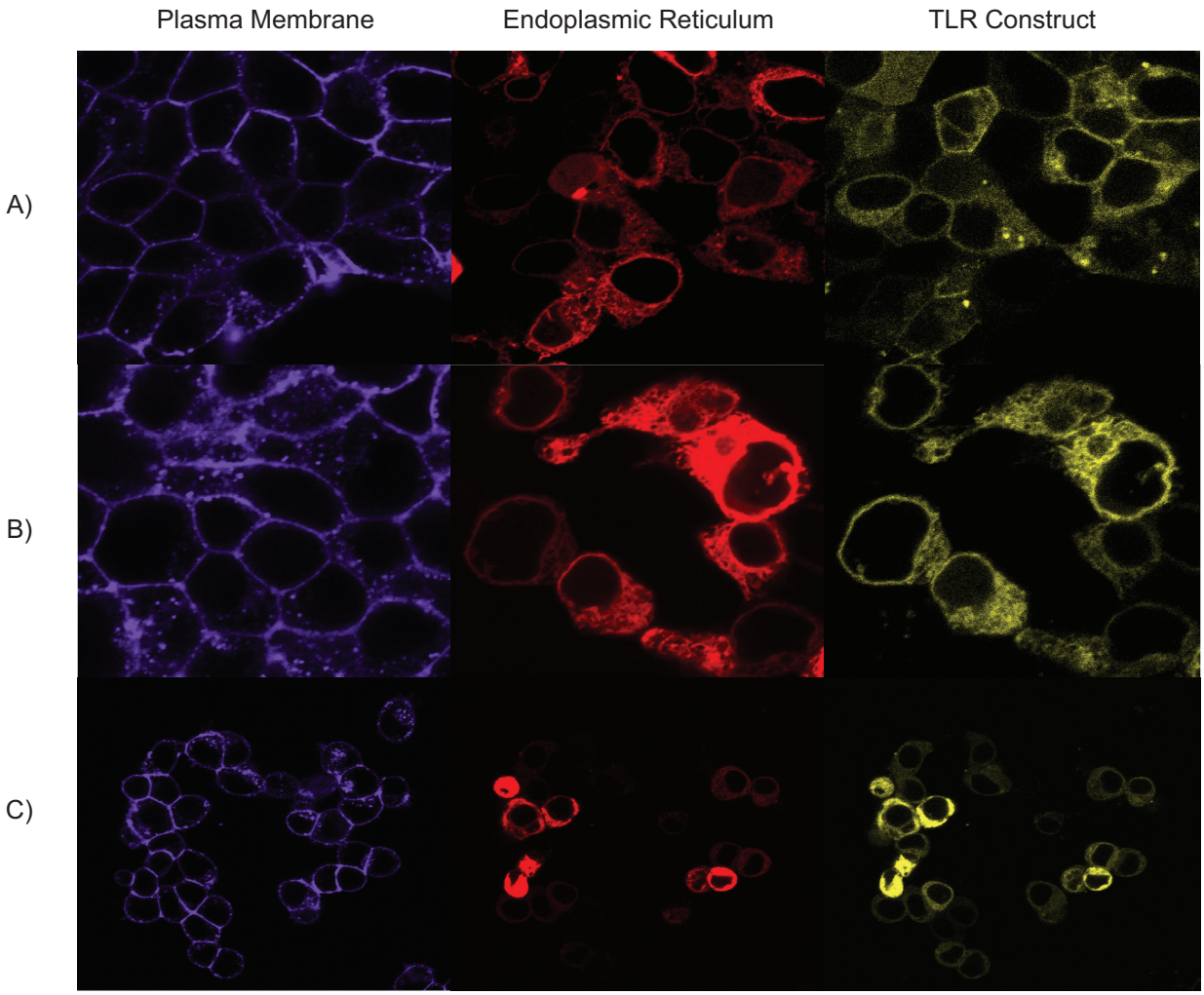

Figure 3.6: Microscopy analysis of TLR localization in transfected cells.
HEK 293T cells were transfected overnight with plasmids encoding a TLR construct of interest fused to EYFP and a plasmid encoding an ER-mCherry marker. After transfection, cells were incubated with a wheat germ agglutinin AlexaFluor 647 primary antibody for 15 min prior to imaging. Images were captured using specific laser lines and filter sets for each fluorophore. A) WT, B) EC+TM, and C) TM only constructs of TLR2.

3.4 Conclusions and Future Directions

Due to incomplete trafficking of TLRs to the plasma membrane we were unable to answer the question of whether the TLRs exist as preformed dimers in the cell membrane and undergo conformational changes upon ligand addition. However, we were able to look at the ability of TLR2 transmembrane domains to have heterotypic interactions in a native membrane environment. A previously reported method for quantitative sensitized FRET measurements was initially attempted, but the vesicles did not show proper uniform membrane intensity. We also calculated a nonphysical value for one of the key parameters, G_F, that relates the sensitized emission to a FRET efficiency. For those two reasons, we looked at transmembrane domain interactions in live-cell imaging experiments using acceptor photobleaching methods. Using acceptor photobleaching FRET we have preliminary evidence that the TLR2-TLR1 and TLR2-TLR6 transmembrane domains are interacting in native membrane environments. To make these claims stronger, proper controls for FRET and no FRET systems need to be established to determine if the signal intensity is a real FRET signal and not an artifact of overcrowding due to the over expression system. Such controls should include positive and negative interacting proteins for both homotypic and heterotypic scenarios. For positive interactions the well studied GpA and T-cell receptor domains would be ideal choices. It is also possible that by using the acceptor photobleaching method, a direct measure of FRET efficiency, the need to know G_F is eliminated so one could theoretically use the calculations for the plasma membrane derived vesicles to determine dissociation constants. Utilizing the equations derived for the sensitized emission quantification in plasma membrane derived vesicles, acceptor photobleaching FRET could provide a quicker way to determine these measurements. If one can accurately determine a calibration linking the fluorescence intensity in a membrane to absolute concentration of fluorescent proteins, for example [56], one would have accurate measurements of the total acceptor, $Acceptor_{pre}$ and donor, $Donor_{post}$, concentrations required to calculate dissociation constants.

Additionally, to address trafficking, one could use the CRISPR system to tag an endogenous

TLR with a fluorescent protein in immune cells and monitor trafficking in the presence and absence of agonists. It may be that additional chaperone proteins for TLR2, TLR1 and TLR6 are necessary to shuttle the constructs from the ER to the plasma membrane, as is seen for the endosomal TLRs [117], that are not expressed in the HEK cell line used for construct expression.

Chapter 4

Directed evolution of transmembrane peptides as regulators of Toll-like receptor signaling

4.1 Introduction

Membrane proteins account for approximately 30% of the genome, and are the target of nearly 60% of current pharmacological agents [195, 1, 228]. Transmembrane domains have come to be an important region for membrane protein interactions [151]. With a better understanding of these transmembrane interactions, the idea of transmembrane domains as therapeutic targets for signal regulation has expanded in recent years. The three commonly employed methods for using transmembrane peptides as targets of signaling include [193]:

(1) endogenous transmembrane regions, or truncations thereof;

(2) directed evolution of transmembrane domain libraries or native sequences, and

(3) computationally designed anti-membrane proteins.

In all of these methods the first requirement is the establishment that the transmembrane domain is involved in receptor assembly. In this regard, we have previously shown the ability of Toll-like receptor transmembrane domains to oligomerize [84].

The first method, utilizing endogenous transmembrane domains, is the simplest method as these regions can be built using solid-phase peptide synthesis [193]. Early studies on the β2-adrenergic G-protein coupled receptors demonstrated the ability of peptides based on transmembrane domain VI to control oligomeric states, indicating the critical role of this domain in protein

assembly [74]. Related studies on the D1 dopamine G-protein coupled receptor also showed that transmembrane peptides derived from the sequence of transmembrane domain VI could alter receptor function without altering oligomeric states [59]. Single pass membrane proteins, such as ErbB2 from the EGFR family, have shown that the transmembrane domain can be specifically regulated using endogenous transmembrane peptides as well [11, 10]. Additionally, studies on T-cell receptor oligomerization noted the importance of charged residues in the transmembrane domains for proper receptor assembly [136]. A short peptide derived from the T-cell receptor α chain containing these residues has been shown to inhibit cytotoxicity through T-cell receptor activation [137], as well as cytotoxicity of other immune receptors, such as NK cells and B-cells [83]. Transmembrane peptides of other immune complexes have also been shown to inhibit signaling [212]. The T-cell receptor transmembrane peptide has been modified in attempts to make it more therapeutic like [3], as there are multiple applications for regulating immune cell activation [140].

The second method, utilizing directed evolution, can either be used to modify a native structure for better interfacial contacts or start from a completely randomized library. Such methods were pioneered with the discovery that the oncogenic E5 protein of the bovine papillomavirus interacted specifically with the PDGFβR transmembrane domain through two critical hydrophobic residues [173, 202]. Using a directed evolution approach on this E5 backbone template several novel transmembrane peptide activators and inhibitors were developed. The E5 transmembrane domain was changed from an activator to an inhibitor of the PDGFβR by single amino acid mutations [169]. Randomized transmembrane peptides based on the E5 backbone could specifically activate the human erythropoietin receptor, but not the murine receptor [18, 26]. Transmembrane peptides inhibiting surface expression of a multipass membrane protein, the C-C chemokine receptor type 5 (CCR5), used in HIV infections, provide an alternative treatment option for HIV [187].

The third method, utilizing computational design algorithms, can be used to more rationally optimize packing interfaces of transmembrane peptide interactions. It has been well documented that transmembrane domains are involved in the assembly of integrin family homodimers and heterodimers [188, 239]. Using a computed helical anti membrane protein (CHAMP) method,

small transmembrane peptides against the α_{IIb} and α_V subunits were designed [230]. Design was performed by taking unrelated solved transmembrane crystal structures and threading the desired integrin sequence onto one chain of the structure and then optimization of all other amino acids for complementary packing in the target backbone was then performed on the remaining chain [230]. These computationally designed peptides resulted in high specificity for the desired receptor [230, 19].

Having shown previously the involvement of TLR transmembrane domains in oligomerization [84], we proposed that the transmembrane domains can be targeted to regulate the signaling pathway. Using both native transmembrane peptides and directed evolution approaches, we investigated the ability to regulate Toll-like receptor signaling via transmembrane domain interactions. We found that immune cells were unable to express the directed evolution libraries at the cell surface, preventing selection of any transmembrane activators or inhibitors. The establishment of reporter cells to screen these libraries however, have been beneficial for small molecule validation pursuits.

4.2 Materials and Methods

4.2.1 Reporter Cell-line Construction

U-937 monocytes (ATCC CRL-1593.2) and Jurkat T-cells (ATCC TIB-152) were virally transduced using the pGreenFire reporter vector with NF-κB transcription response elements (System Biosciences) to investigate Toll-like receptor responses. Both cell lines were maintained in RPMI-1640 medium supplemented with 10% fetal bovine serum, 100 U/mL penicillin, and 100 mg/mL streptomycin. The pGreenFire plasmid is a third generation HIV-based lentiviral vector that requires the coexpression of the HIV *gag, pol,* and *rev* genes for production of viral particles as well as a suitable pseudotyping envelope plasmid. The *rev* gene was encoded on the pREV plasmid (Addgene plasmid #12253). The *gag* and *pol* genes were encoded by the pMDL vector (Addgene plasmid #12251). The viral particles were pseudotyped using the vesicular stomatitis

virus envelope glycoprotein encoded by the pVSV-G plasmid (Addgene plasmid #8454).

The viral packaging cell line HEK 293T (ATCC CRL-3216) was grown and maintained in Dulbecco's modified Eagle's medium supplemented with 10% fetal bovine serum, 100 U/mL penicillin, and 100 mg/mL streptomycin. For virus production of the NF-κB reporter, HEK 293T cells were transfected in a 10 cm dish using a 6:1 polyethylenimine:plasmid DNA ratio. The viral vectors were combined in 1 mL OptiMEM (Invitrogen) using pGreenFire (4.33 μg), pREV (4.33 μg), pMDL (4.33 μg), and pVSV-G (2 μg). Viral particles were harvested 48-72 hours after transfection, filtered through a 0.22 μm filter, and concentrated overnight at 4 °C in a 8.5% PEG-8000 (polyethylene glycol, molecular weight 8000, Sigma) and 10 mM NaCl solution. Concentrated virus was spun down at 4 °C and 2000xg for 30 min before aspirating off the supernatant and suspending the viral pellet in 500 μL OptiMEM. The concentrated virus and polybrene (8 μg/mL) were added to target cells ($0.5 * 10^6$ cells in 500 μL complete growth media) for 48 hours, passaging target cells as necessary. After 48 hours, the growth media on the target cells was changed and the cells were allowed to grow until sorting for GFP expression using a MoFlo Cytomation fluorescence-activated cell sorter (Beckman Coulter). Cells were sorted for GFP expression using gates that excluded any cells with same GFP signal as non-transduced cells. GFP positive cells were then treated with TLR agonists (Invivogen) to determine if they expressed high enough levels of the receptor to turn on the NF-κB reporter. If the reporter was activated, further sorting was performed to select the highest expressing cells by collecting only the top 10% of responsive cells.

4.2.2 Flow Cytometry Cell Surface Staining

Primary monoclonal antibodies against the extracellular domains of TLR1, TLR2, and TLR6 were purchased from Cell Signaling Technologies to verify expression levels. The target cells are spun down, supernatant aspirated, and pellet resuspended in freshly made fixation buffer (4% paraformaldehyde, Fisher, heated at 60 °C to dissolve and dissociate in PBS). The cells are fixed at 37 °C for 15 min. Cells are then chilled on ice for 1 min before being spun down, resuspended in PBS and counted. $1 * 10^6$ cells are aliquoted into microcentrifuge tubes and washed three times

with 1 mL incubation buffer (0.5% BSA, Fisher, in PBS), spinning down at 2000xg for 3 min after each wash. After the third wash, the cells are incubated with 100 μL of primary antibodies at a 1:100 dilution in incubation buffer. Primary antibodies are left to incubate for 1 hour at room temperature. Again cells are washed three times with incubation buffer. A fluorescent secondary antibody, 100 μL anti-rabbit IgG conjugated to phycoerythrin (Cell Signaling Technologies) diluted 1:200 in incubation buffer, was added to the cells and incubated for 30 min at room temperature. Cells were again washed three times with 1 mL incubation buffer before being suspended in 500 μL PBS before analysis on a MoFlo Cytomation fluorescence activated cell sorter (Beckman Coulter).

4.2.3 Directed Evolution Library Sorting

An overview of the library screening is shown in Figure 4.1. For library transduction, on day 1 HEK 293T cells are plated at $5 * 10^6$ cells per 10 cm dish and immediately transfected with viral plasmids following the protocol as above except the viral plasmids are combined in a 5:3:2 ratio of pMSCVpuro:pCL-ECO:pVSV-G, where pMSCVpuro contains the library of interest (Table 4.1), pCL-ECO (Addgene#12371) expresses *gag/pol/env* genes, and pVSV-G is for pseudotyping. After 48 hr incubation with viral particles, target cells are selected for puromycin resistance (1 μg/mL). After complete selection (2-3 days), cells are plated in fresh media and allowed to recover for 2 days. Cells are treated with ligand on the third day post-selection and sorted on the fourth day. After sorting cells by collecting 10% of the desired population, the cells are grown to recover until $2 * 10^6$ cells are viable for genomic DNA recovery (Qiagen DNeasy Blood & Tissue kit). Inserts for the next library round are PCR amplified out of the gDNA using invariant regions of the library construct. UDv2 FWD: 5' TGCCTGGCCTCTCGAGGAACATAGCGTTAAC and UDv2 REV: 5' CGTGCACCTTGAATTCGCCGATCGCGGATCC. Library inserts were gel extracted after PCR (Omega Gel Extraction kit), digested with EcoRI and XhoI restriction enzymes and cloned into digested pMSCVpuro vector. To generate new library vectors, the ligated products were transformed in DH10β electrocompetent cells (Invitrogen), grown on ampicillin (100 μg/mL) plates, and all colonies were purified by midi-prep kits (Qiagen).

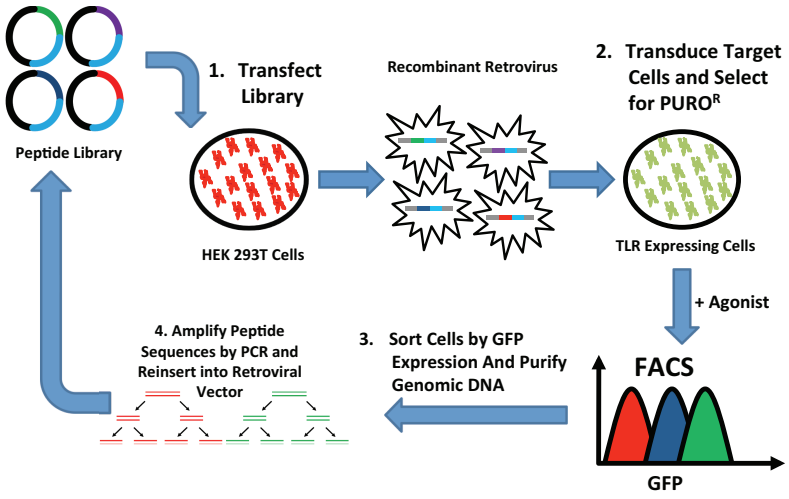

Figure 4.1: Directed evolution schematic overview.
The directed evolution process is composed of iterative rounds of library generation, selection, and diversification. First the library is constructed in a virus and transduced into a suitable cell line on which phenotypic selection is performed. After phenotypic selection, the genetic library is excised out of the cells and constructed to form the library for the next round.

4.3 Results and Discussion

4.3.1 Directed Evolution Library Screening

The directed evolution process is an iterative process of library diversification, phenotypic selection, and genotypic enrichment [134]. An overview of this process is highlighted in Figure 4.1. To utilize a directed evolution screen for Toll-like receptor transmembrane targeting, a reporter cell line needed to be constructed, and an initial library needed to be chosen.

4.3.2 Reporter Cell Construction

In order to screen for peptide and library activity, an adequate reporter cell line needed to be constructed that expressed only a single TLR signaling complex. As it has been established previously that TLR2 family expression is much higher in leukocyte cell lineages than other cell types [235], we selected a human monocytic cell line, U-937, for generation of reporter cells. T-cell receptors are also known to be strongly affected by a TLR5 agonist [31, 20], so a Jurkat T-cell line was established as another reporter cell line. Since TLR signaling culminates in NF-κB translocation to the nucleus [100], a NF-κB response element upstream of a green flourescent protein (GFP) was retrovirally inserted into U-937 cells or Jurkat cells.

Jurkat cells were tested for response to flagellin as several reports have indicated the importance of TLR5 in shaping the T-cell response [31, 20, 154, 58]. It has also been shown previously that the Jurkat cell line we have does not respond to TLR2 or TLR4 agonists, but they are activated in the presence of TLR5 agonist [207]. Initial insertion and sorting of the TLR5 response in Jurkat cells showed activation of the GFP reporter, agreeing with published reports, but minimal signal separation was seen (Figure C.1). Over the course of treating and sorting cells to enhance signal separation, the untreated cells developed two distinct fluorescent populations (Figure 4.2 A). The untreated cells were sorted based on the two fluorescent populations, low and high, yielding GFP reporter Jurkat cells with a strong response to the flagellin agonist (Figure 4.2 B, C). As multiple subclasses of T-cell receptors exist it is possible these two different responsive subsets are

different classes of $CD4^+/CD8^+$ T-cells that are responding to the agonist [31, 154]. While both populations show strong activation, the higher fold change between treated and untreated cells in the low fluorescent population as well as sharper peak distributions made them ideal for the library screen.

The TLR2, TLR1, and TLR6 receptors have all been shown previously to have high levels of mRNA in peripheral blood leukocytes, similar to U-937 monocytes, relative to spleen tissue [235]. In agreement with this, the reporter response was strongly activated by TLR2 agonists (Figure 4.3 A, B). To improve peak separation, activated cells were sorted multiple times with the top 10% of cells collected each round for further growth. After three rounds of sorting an approximate 2.5 fold change in signal was seen, with minimal peak overlap, and additional sorting did not improve this separation.

Leukocytes were also shown to have higher mRNA levels for TLR4, TLR5, and TLR8 [235]. A very minor change in signal was seen for TLR4 and TLR5 (Figure 4.3 C, D), but sorting out the top 1% of these activated cells did not lead to better signal after two rounds of sorting. No response was seen in the reporter cells when incubated with agonists for TLR3, TLR7/8, and TLR9 (Figure 4.3 E, F, G).

Differentiation of monocytes into macrophages using phorbol esters, such as phorbol myristate acetate, has been shown to improve responsiveness to the TLR4 agonist LPS [200]. We showed this TLR4 response was possible in U-937 differentiated macrophages, but the process of differentiation is terminal to the monocytic lineage and they cannot be propagated in culture. Thus, while we can see an improved TLR4 response in the macrophage lineage, they are unable to be applied to a library screen process.

Next, cell surface expression of the TLR2, TLR1, and TLR6 proteins on the sorted U-937 cells was validated by flow cytometry using antibodies against the respective extracellular domains. It was found that TLR2 was initially present on the cell surface, but TLR1 and TLR6 were not (Figure 4.4). After activation with a TLR2 ligand the TLR1 and TLR6 receptors expression levels were significantly upregulated, while TLR2 levels remained the same (Figure 4.4). These results suggest

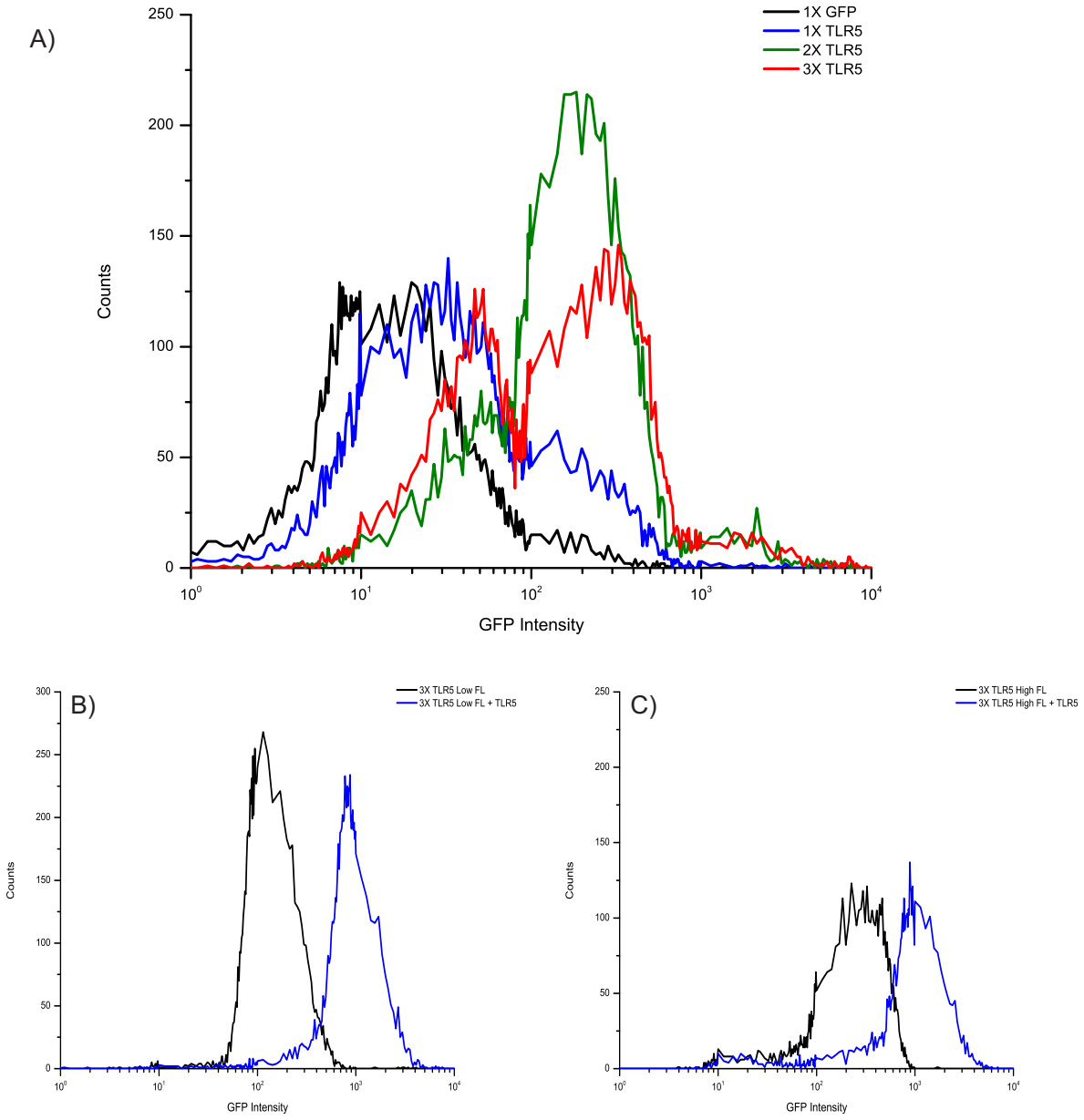

Figure 4.2: Jurkat response to TLR5 agonist flagellin after sorting.
Jurkat cells were stably transfected with a NF-κB reporter. A) Initial cell populations after sorting for GFP and three rounds of treatment with the TLR5 agonist flagellin (100 ng/mL). After the third treatment with flagellin and sorting for GFP activation, two populations of GFP fluorescent cells were detected. B, C) The third flagellin treatment of untreated cells were sorted by the initial GFP signal, low or high. These cells were then treated with agonist to determine response for the given population B) low fluorescence population and C) high fluorescent population. The better peak separation in the low fluorescence population made them ideal for library screening.

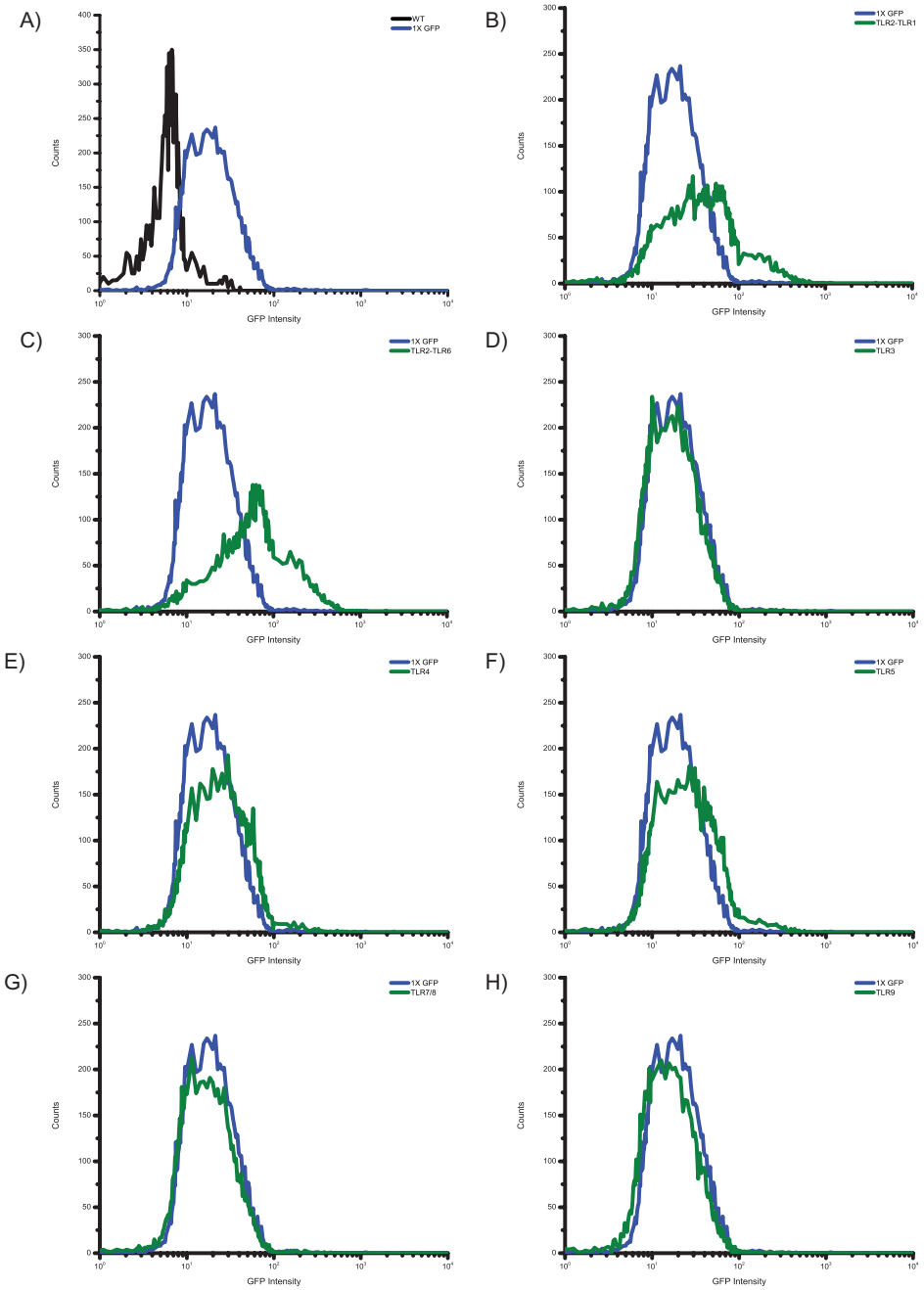

Figure 4.3: U-937 Toll-like receptor agonist response profile.
Ligands for every TLR were incubated with the U-937 GFP reporter cell line overnight. A. TLR2-TLR1 agonist, Pam3CSK4 (100 ng/mL), B. TLR2-TLR6 agonist, Pam2CSK4 (100 ng/mL), C. TLR4 agonsit, LPS (20 ng/mL), D. TLR5 agonist, flagellin (100 ng/mL), E. TLR3 agonist, poly-I:C (10 μg/mL), F. TLR7/8 agonist, R848, (5 μg/mL), and G. TLR9 agonist, ssDNA (5 μg/mL). Non-transduced cells were used as a baseline negative control for insertion of the NF-κB:GFP reporter.

that upon stimulation TLR1 and TLR6 expression is somehow upregulated to mount the necessary immune response. It has been demonstrated that some known trafficking proteins are upregulated upon TLR2 stimulation [6, 12]. It is possible that only a small portion of receptor complexes are initially at the cell surface and that upon activation receptor expression is upregulated to form higher-order assemblies that might be required for signal transduction [225].

4.3.3 Transmembrane Library Construction

Two libraries were initially chosen for screening. One based on the native TLR transmembrane domain sequences. The other library is based on the bovine papillomavirus E5 protein that is oncogenic through specific transmembrane domain interaction as previously reported [18, 202]. The use of the native transmembrane domain would allow for determination if this domain was critically involved in TLR signal propagation. As we had established a reporter cell line that would allow screening of TLR2 heterotypic interactions we chose the native sequence for the TLR2 transmembrane domain (Table 4.1). This library consisted of the predicted transmembrane residues, A589 - C608, of the TLR2 protein. We modified this sequence to include a Kozak consensus sequence upstream of a start codon with a hemagluttin (HA) tag on the N-terminus. Residues were also added to each termini to improve recognition and insertion into the membrane bilayer by the translocon [79, 80, 90].

The UDv2 library was based on the initial backbone of the bovine papilomavirus E5 oncoprotein that is known to interact with the transmembrane domain of PDGFβR [18, 202]. Using similar libraries generated from this backbone it was possible to specifically target receptors unrelated to the native receptor, usually within six rounds of directed evolutionary screening. It was shown that this library was able to activate the erythropoietin receptor [18, 26] and inhibit surface expression of CCR5, an HIV co-receptor for viral entry [187]. Deep sequencing of E5 library derivatives has shown them to contain nearly 300,000 unique sequences [142], a very small portion of the sequence space potentially covered by this library (10^{28}). The UDv2 library differed from those published in that the N-terminus of the E5 oncoprotein was replaced with a HA tag after

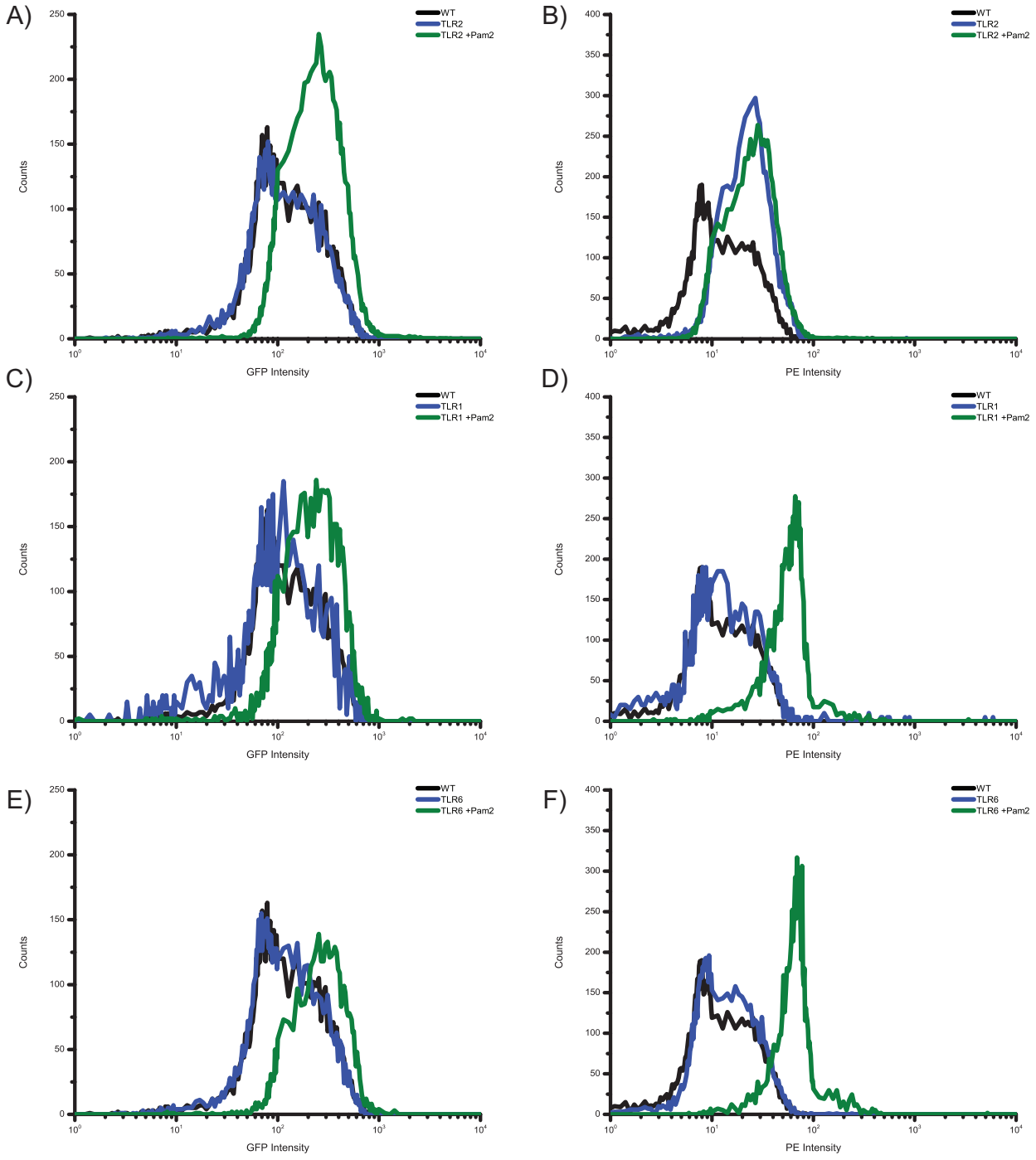

Figure 4.4: Cell surface expression of TLR1, TLR2, and TLR6 on U-937 cells.
To verify the expression of the receptors at the cell surface, primary antibodies for TLR1, TLR2, and TLR6 were incubated with the reporter cells in the presence and absence of a TLR2 agonist and detected using a PE-conjugated secondary. In the absence of agonist, only TLR2 was detectable at the cell surface. In the presence of agonist, all three receptors were highly expressed at the cell surface. A, C, and E) show the NF-κB reporter intensity for untreated and treated cells. B, D, and F) show the intensity of secondary antibody labeling. WT cells, black lines, were U-937 cells not sorted for TLR2 expression.

the start codon and every residue in the transmembrane domain was randomized, as well as the C-terminal juxtamembrane interaction residues.

Table 4.1: Directed evolution library starting sequences

Library Name	**Library Sequence**
TLR2	MG*YPYDVPDYA*GGPG**ALVSGMCCALFLLILLTGVLC**KPKK
UDv2	MA*YPYDVPDYA*DLPNLWF**XXXXXXXXXXXXXXXXXXXXXXXXX** YW***XX***FECSCTGLPF

The TLR2 library is composed of an N-terminal HA-tag, shown in italics, and the TLR2 transmembrane domain, shown in bold. The GGPG and KKPK residues at the termini have been shown to improve recognition by translocon elements for stable membrane insertion [90]. The UDv2 library is derived from the bovine papillomavirus E5 oncoprotein [18]. The N-terminus was modified from E5 to contain an HA-tag, shown in italics. The transmembrane domain, bold Xs, was randomized to encode hydrophobic residues 80% of the time using degenerate oligonuclueotides. Two other residues were randomized to avoid bias for E5 interactions of a polar residue located at the C-termus, bold and italicized Xs.

4.3.4 Transmembrane Library Screens

The two libraries, Table 4.1 were cloned into a retroviral expression vector, pMSCVpuro, that allows for selection of genetic insertion in the target cells by using puromycin antibiotic selection.

4.3.4.1 Native TLR2 Transmembrane Domain Library

The initial screen with the TLR2 library did not show any inhibition, raising the question as to if the transmembrane domain does play a role in TLR signaling. Previous reports have used synthetic peptides from the TLR2 transmembrane domain as a way to regulate signaling in mouse septic models [52]. First, we wanted to determine if the protein library was expressing. An antibody against the HA-tag was used to test whole cell lysates transduced with the library by Western blot. We saw the construct was expressing in the cells (Figure 4.5 A), but whole cell lysates do not provide any details as to whether or not the library is being trafficked to the correct location.

To determine if the library was trafficking to the plasma membrane, from where TLR2 signals [100], flow cytometry was performed using antibodies against the N-terminal HA-tag. The antibody

did not show any binding of an HA-tag by flow in untreated transduced cells (Figure 4.5 B), which suggests that the TLR2 transmembrane domain library is being expressed in the cells, but is not properly trafficking. If the library is not present at the plasma membrane, it cannot inhibit the TLR2 signal that is induced by agonist at that location.

4.3.4.2 UDv2 Directed Evolution Library Screen

The UDv2 library was screened in U-937 cells for potential inhibitors TLR2-TLR1 or TLR2-TLR6 of signaling. The initial library went through selection as shown in Figure 4.1. After the first round of library screening, four individual sublibraries were maintained as a way to detect enrichment of similar sequences in separate libraries generated from the same starting point. Previous reports on the use of similar libraries have shown the enrichment of activating or inhibiting sequences after 3-6 rounds of selection [18, 187]. After a similar number of directed evolution rounds we had not seen any enrichment of inhibitory sequences for TLR2-TLR1 screening (Figure 4.6) nor for TLR2-TLR6 screening (Figure 4.7).

To determine if the library was being maintained, each round of library was transformed and plated for selection of single colonies. The initial and second round library were the only ones that had sequencing results of the expected library construct form. This indicates that during the process of library construction from genomic DNA amplification the library was lost after the second round. This could be due to either nonspecific amplification from gDNA, or more likely from incomplete digestion of the backbone, as future rounds were still able to survive puromycin selection, and transformations yielded numerous colonies.

4.3.5 Small Molecule Inhibitors of TLR2-TLR1 Activation

While the reporter cells were generated to be utilized in directed evolution screens, the response to only a specific subset of TLR agonists makes them well suited for other uses. Our lab is interested in general mechanisms for regulating TLR signaling, the most common method being the use of small molecules. A small molecule screen previously identified activators of TLR2 signaling

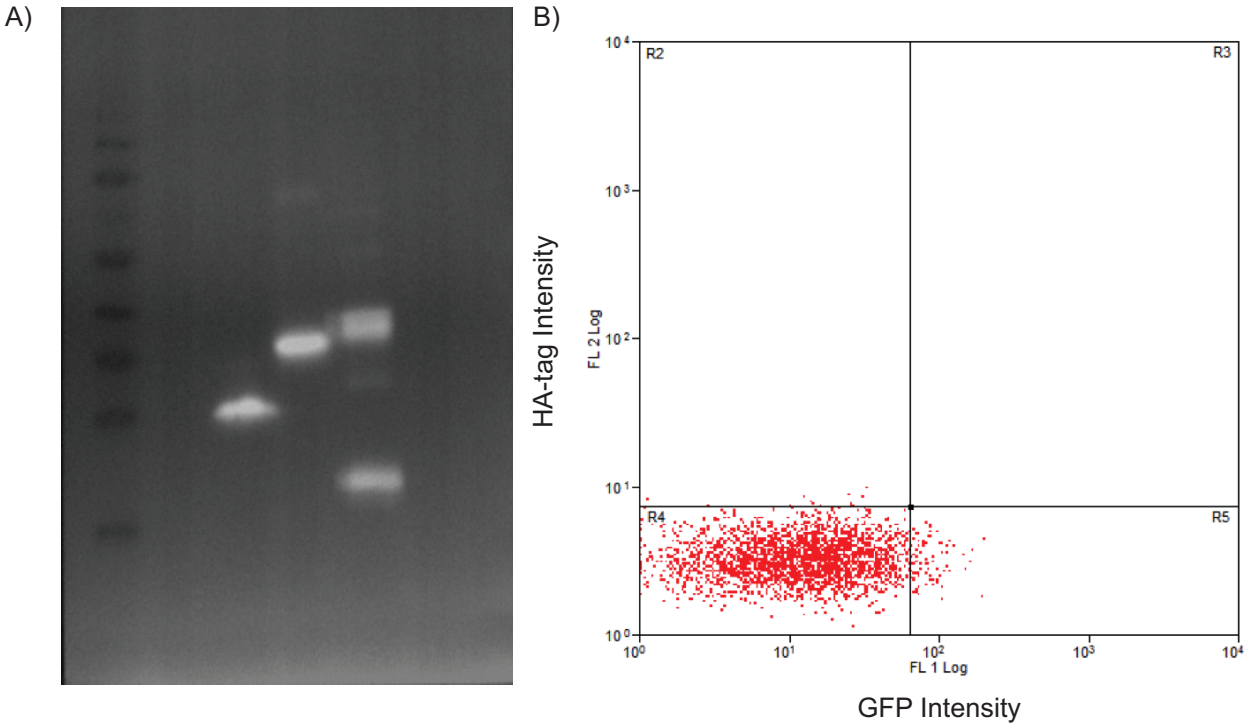

Figure 4.5: TLR2 transmembrane domain viral library expression.
A) Western blot against HA tag verifies the presence of the library. The Western is loaded as ladder, untransfected cells, library infected cells, control protein 1, control protein 2. This analysis is performed on whole cell lysate and does not tell location of library. B) Flow cytometry was performed with an anti-HA PerCP-CY5.5 conjugated primary antibody to determine if library was at the cell surface. Lack of signal in the Cy5.5 channel indicates that the library is not being trafficked to the correct cellular membrane.

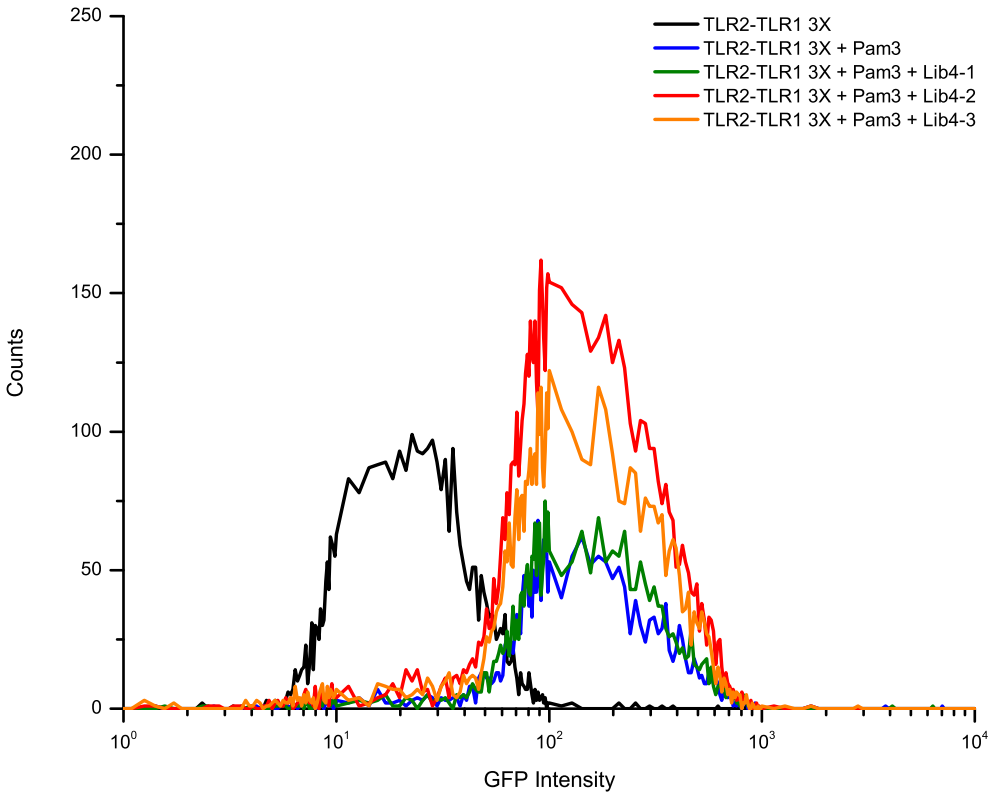

Figure 4.6: UDv2 fourth round directed evolution library against TLR2-TLR1.
Libraries from the initial UDv2 design were propagated through four rounds of the directed evolution process. As the library was screening for antagonists, the bottom 10% of activated cells were isolated in each selection round and used to grow the next library. After the fourth round, no change in signal was seen in cells containing the library when treated with the TLR2-TLR1 agonist Pam3CSK4 (100 ng/mL).

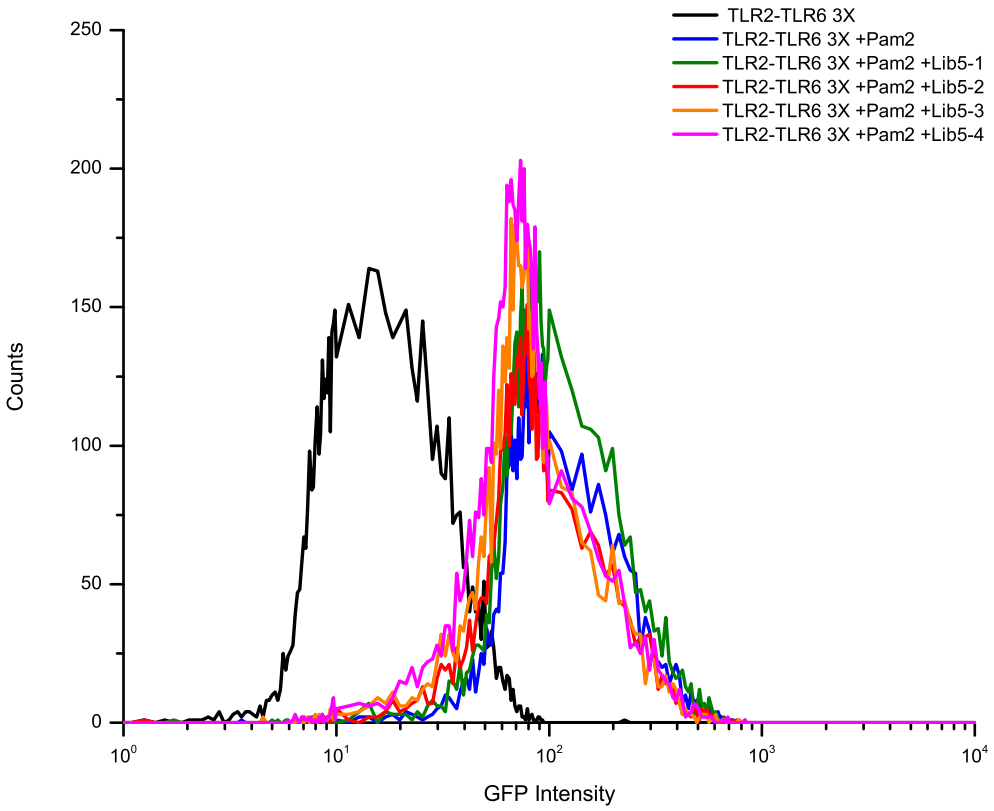

Figure 4.7: UDv2 fifth round directed evolution library against TLR2-TLR6.
Libraries from the initial UDv2 design were propagated through five rounds of the directed evolution process. As the library was screening for antagonists, the bottom 10% of activated cells were isolated in each selection round and used to grow the next library. After the fifth round, no change in signal was seen in cells containing the library when treated with TLR2-TLR6 agonist Pam2CSK4 (100 ng/mL).

[66]. Through structure-activity-relationship studies, this compound was improved upon to yield the most active compound CU-12-9 [24]. Using the U-937 reporter cells we were able to confirm the potent activity of a small molecule, CU-12-9, for TLR2 activation [24]. The small molecule showed activation of the receptor at as little as 1 μM CU-12-9. At 10 μM, this small molecule was as potent as known synthetic lipoprotein agonists (Figure 4.8). This is the first well-characterized small-molecule activator of TLR2, that is specific for the TLR2-TLR1 complex [24]. This small molecule has great potential for biomedical applications, specifically as next generation vaccine adjuvants.

4.4 Conclusions and Future Directions

The aim of discovering novel transmembrane peptides to regulate TLR signaling through directed evolution means was unsuccessful due to poor library propagation and localization. However, we did successfully construct TLR reporter cells in native immune cells. Current TLR reporter cells are kidney cells that do not natively express TLRs. These kidney cells have been transfected to stably express a single TLR construct of interest. The use of actual immune cells for studying TLR signaling is less likely to have artifacts due to the expression of accessory proteins like CD14 and CD36 and other adapter proteins [155, 234]. The goal of these cells was for testing transmembrane domain libraries for altering TLR signaling, but they can also be successfully utilized to analyze small molecule activators or inhibitors of TLR signaling. We were able to show a novel small molecule compound could activate immune cells as strongly as the current synthetic lipopeptide ligands, the first

There are several areas that need to be further addressed for this project. First, similar to the problems seen for TLR localization in Chapter 3, the ability of TLR transmembrane constructs to localize correctly is of critical importance to determining if the transmembrane domains are directly involved in TLR signaling. Second, optimization of the directed evolution process for next round generation is necessary to ensure stability of the library during screening. It is also important to validate the replacement of the E5 N-terminus with an HA-tag does not alter the trafficking of this

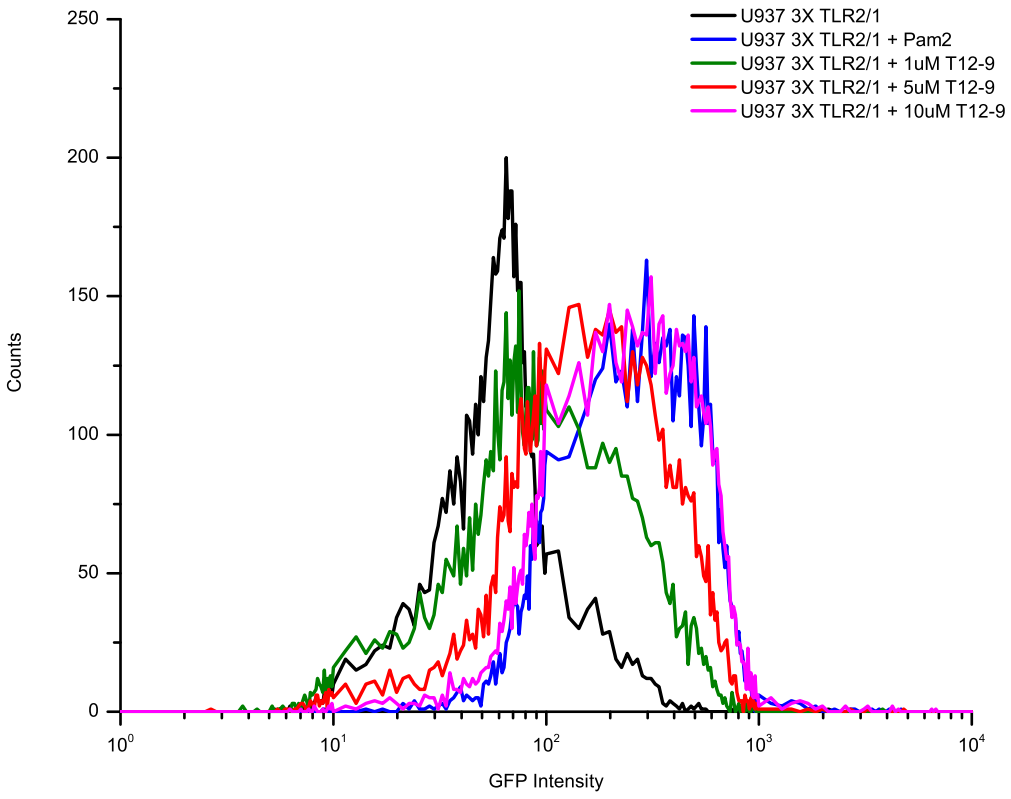

Figure 4.8: Small molecules can activate the TLR2 receptor complex.
U937 cells were incubated with 0, 1, 5, and 10 μM of compound CU-T12-9 to determine activation of the NF-κB:GFP reporter. The TLR2-TLR1 agonist, Pam3CSK4 (100 ng/mL, 66 nM) was used as the positive control for cell activation. It is shown that this small molecule can potently activate the TLR2-TLR1 complex using small molecules.

library to the plasma membrane. The published libraries from this E5 domain do not have this HA-tag.

Chapter 5

Conclusions

Toll-like receptor membrane proteins have been a major area of research in the field of immunology since their discovery in 1997 as components of the human innate immune system. Acting as sentinels of bacterial and viral infection, TLRs are critical in fighting off pathogens and preparing the adaptive immune system to respond if necessary. The majority of studies have focused on the extracellular domains and intracellular signaling proteins due to there ease of study. TLR transmembrane domains were long thought to be passive anchors, and the lack of experimental tools to study these regions left them unexplored.

In this thesis, we have studied the interaction potential of Toll-like receptor transmembrane domains for the first time. To accomplish this we have expanded on methods in the toolbox for transmembrane domain studies to more rapidly screen for transmembrane domain interactions in membrane environments using fluorescence microscopy and reporter cell lines.

5.1 Toll-like receptor transmembrane domains interact with high specificity

In Chapter 2, we demonstrated for the first time that transmembrane domains of the Toll-like receptor family could specifically interact. Using previously reported methods and techniques, we showed that every Toll-like receptor was capable of homotypic interactions, in good agreement with reported extracellular domain crystal structures. Prior to this work, people had only known that TLR transmembrane and TIR domains could interact by forcing extracellular domains to be dimeric [237, 71], or through ligand activation [156]. By isolating the TLR transmembrane domains,

whose sequences lack many of the common overrepresented structural motifs for transmembrane domain interactions [151, 110], we discovered that TLRs interact with high propensity through their transmembrane domains. Such a discovery has led to structural studies on the transmembrane domains in membrane mimetic systems. One such study solved the TLR3 transmembrane domain structure in detergent micelles, using solution state NMR, and found dimeric and trimeric states with two potential interfaces for these interactions [150]. This structure agrees with the data we have demonstrating that the TLR3 transmembrane domain had very strong homotypic interaction propensity. As methods of solution and solid state NMR advance in the upcoming years, it is likely that we will see more structures solved of TLR transmembrane domains in agreement with the transmembrane domain interactions we discovered.

Our studies were also the first report of TLR2 transmembrane domains having specific heterotypic interactions. It was long known that TLR2 was involved in heterotypic interactions with TLR1 or TLR6 as a means to recognize a wide variety of pathogens [164]. Furthermore the transmembrane domain and TIR domains for these receptors had to be present in pairs for signaling activation [156]. What we showed was that the transmembrane domains of these receptors had specific heterotypic interactions, and included the orphan receptor TLR10 as another heterotypic interaction potential. Other groups had proposed TLR10 to have roles in TLR2 interactions [70], and we provided the first direct evidence for this interaction at the transmembrane level. Further studies have lent credence to this interaction as TLR10 was found to potentiate proinflammatory cytokine production from TLR2 agonists only [162].

5.2 Microscopy techniques for rapid analysis of transmembrane domain interactions in mammalian membranes

In Chapter 3, we utilized two different microscopy techniques to measure the interaction potential of TLR transmembrane domains in mammalian membranes. A quantitative imaging FRET technique, using sensitized emission, to study transmembrane domain interactions in plasma membrane derived vesicles that has been previously reported [126, 22]. One significant drawback to this

method is that the production of vesicles requires the use of chemical crosslinking reagents, which could artificially influence the proteins of interest interaction potential. However, this method has been used to study the contributions of transmembrane and extracellular domains to dimerization [23], and the contribution of oncogenic mutations in transmembrane domains to receptor stability [171]. In all cases, this method had only been applied to homotypic interactions of transmembrane proteins, our aim was to adopt this method for studying the heterotypic interactions of TLR2. However, the microscope calibration required for this method resulted in a nonphysical value for the G_F parameter, preventing correlation of sensitized emission to FRET efficiency. Furthermore, the production of vesicles with TLR constructs did not yield uniform membrane intensity vesicles as was expected, leading us to explore other methods.

We adopted acceptor photobleaching FRET as a method to directly measure FRET efficiency as we were unable to determine this value using sensitized emission techniques. We also adopted live-cell imaging methods to eliminate cross linking and other potential artifacts in plasma membrane derived vesicles. Using this method we were able to preliminarily show that the TLR2-TLR1 and TLR2-TLR6 transmembrane domains undergo FRET in a mammalian membrane environment. This technique is one that we think could allow for a rapid identification of membrane protein interactions in native membrane environments, and would simplify the analysis required for heterotypic interactions.

5.3 Toll-like receptor construct localization

Throughout the studies using FRET (Chapter 3) we noted differential localization of the TLR expression constructs. We saw that these constructs were not localized at the plasma membrane by confocal microscopy. Although there could be a very small percent at the surface based on colocalization. Flow cytometry data for the same constructs did have detectable levels of plasma membrane expression, suggesting that some receptor may be appropriately trafficked. Additional constructs that used various signal peptides [75], or included endogenous 3'UTRs [12] did not alter the distribution of the TLRs from the ER to the plasma membrane.

It may be possible that additional trafficking proteins are required for TLR localization [199, 216, 69, 197, 117]. In a native immune cell line, U-937 monocytes, only TLR2 is present at the surface, with TLR1 and TLR6 being upregulated upon agonist treatment. This further suggests that additional trafficking proteins are required in the proper localization of TLRs to the plasma membrane, and that this process is controlled by exposure to agonists. Several known trafficking proteins have been shown to be upregulated by TLR2 agonists previously [6]. However, ligand treatment of the cells transfected with TLR2 WT or TLR2 EC+TM constructs did not lead to changes in plasma membrane localization. Without having proper localizaiton of the constructs we cannot determine if the receptors are preformed dimers that undergo conformational changes upon ligand binding, as the ligand is only accessible to the potentially small subset of constructs being trafficked to the membrane.

5.4 Reporter cell lines for studying Toll-like receptor signaling

In Chapter 4, we established new reporter cell-lines for utilization of studying Toll-like receptor signaling pathways. These cells were designed with the intention of screening a random, transmembrane domain library for potential regulators of TLR signaling via transmembrane domain interactions. The library based on the E5 bovine papillomavirus oncoprotein have been used previously in murine cells to activate or inhibit its known target, PDGFβR [202, 169], activate the erythropoietin receptor [18], or inhibit CCR5 expression and HIV coreceptor function [187]. The use of an unpublished library based on the E5 protein did not show any effect on TLR signaling in these cells. However, sequencing revealed this library was not intact starting with the third round library generation.

We also found that a library based on the native TLR2 transmembrane domain did not show any inhibitory effect. This was in conflict with reports that synthetic peptides based on the TLR2 and TLR6 transmembrane domains could specifically reduce TLR signaling from TLR2 agonists [52]. We discovered that the likely cause of this problem was the trafficking of the TLR2 library to the cell surface. It is possible that the N-terminal HA-tag on both the E5 and TLR2 libraries is

preventing proper trafficking of these libraries to the membrane where they would then be present to alter TLR signaling pathways.

Chapter 6

Future Directions

6.1 FRET Microscopy Experiments

The first item that needs to be addressed is the localization of the TLR synthetic constructs. Without trafficking to the plasma membrane, any interactions determined, will not provide an accurate representation of the functional signaling complex. As over expression systems can be a problem for causing proteins to be retained in the ER through stress. It may be possible to use a CRISPR based system in native immune cells by tagging the endogenous protein with a fluorescent protein. In a native immune cell, one would in theory eliminate the trafficking and over expression problems, but would be limited to studies of the full-length protein, and elucidating the contribution of individual domains would be impossible. This endogenous system could still be used for acceptor photobleaching of heterotypic partners, and thus demonstrate if the TLR2 subfamily exists in the cell as a preformed dimer.

For the acceptor photobleaching system it is imperative that controls be determined for positive FRET and no FRET systems to ensure the values measure for TLR2 heterotypic interactions are not an artifact of crowding in the membrane due to over expression. Such controls should include positive and negative interacting proteins for both homotypic and heterotypic scenarios. For positive interactions the well studied GpA and T-cell receptor domains would be ideal choices.

Another item that needs to be completed is the problem with the nonphysical Gauge factor determined. Validating the EYFP and mCherry calibration curves for determining concentrations could allow for sensitized emission to be used for quantitative analysis. However, the acceptor

photobleaching system provides direct measurements of the FRET efficiency, which is the parameter of sensitized emission we could not calculate. If an accurate determination for linking fluorescence intensity in a membrane to absolute concentration of fluorescent proteins one would have accurate measurements of the total acceptor, $Acceptor_{pre}$ and donor, $Donor_{post}$, concentrations required to calculate dissociation constants. A method for correlating fluorescence intensity in supported lipid bilayers doped with a spectrally similar fluorophore to that of the membrane protein tagged with fluorescent proteins has been reported [56].

6.2 Directed Evolution Library Experiments

As the TLR2 library did not express at the cell surface, modifications in this library to traffic correctly are necessary. As transmembrane peptides for this domain have already been shown to regulate signaling in murine systems, [52], we would likely see inhibition in the reporter cells if it trafficked appropriately. We could then introduce diversity into this sequence using various techniques to identify more potent regulators of TLR2 signaling [134].

The E5 library should be confirmed that it is trafficking to the plasma membrane, as the published libraries do not utilize the HA-tag at the terminus, and a better methodology to ensure next round libraries have been properly assembled are critical.

Bibliography

[1] Mamoun Ahram, Zoi I Litou, Ruihua Fang, and Ghaith Al-Tawallbeh. Estimation of membrane proteins in the human proteome. In Silico Biology, 6:379–386, 2006.

[2] Nina Akrap, Thorsten Seidel, and B George Barisas. Förster distances for fret between mcherry and other visible fluorescent proteins. Analytical biochemistry, 402(1):105–106, 07 2010.

[3] Marina Ali, Michael Amon, Veronika Bender, and Nicholas Manolios. Hydrophobic transmembrane-peptide lipid conjugations enhance membrane binding and functional activity in t-cells. Bioconjug Chem, 16(6):1556–1563, Nov-Dec 2005.

[4] Michael A Amon and Nicholas Manolios. Hypothesis: Tcr signal transduction–a novel trimodular signaling system. Mol Immunol, 45(4):876–880, Feb 2008.

[5] Veerappan Anbazhagan and Dirk Schneider. The membrane environment modulates self-association of the human gpa tm domain - implications for membrane protein folding and transmembrane signaling. Biochimica et Biophysica Acta, 1798:1899–1907, 2010.

[6] Laurence Arbibe, Jean-Paul Mira, Nicole Teusch, Lois Kline, Mausumee Guha, Nigel Mackman, Paul J Godowski, Richard J Ulevitch, and Ulla G Knaus. Toll-like receptor 2-mediate NF-κB activation requires a Rac1-dependent pathway. Nature, 1:533–540, 2000.

[7] Ethan B Van Arnam, Henry A Lester, and Dennis A Dougherty. Dissecting the functions of conserved prolines within transmembrane helices of the d2 dopamine receptor. ACS Chemical Biology, 6:1063–1068, 2011.

[8] Gregory M Barton, Jonathan C Kagan, and Ruslan Medzhitov. Intracellular localization of Toll-like receptor 9 prevents recognition of self DNA but facilitates access to viral DNA. Nature Immunology, 7:49–56, 2006.

[9] Shaherin Basith, Balachandran Manavlalan, Gwang Lee, Sang Geon Kim, and Sandgdun Choi. Toll-like receptor modulators: a patent review (2006-2010). Expert Opinion on Therapeutic Patents, 21(6):927–944, 2011.

[10] A. Bennasroune, A. Gardin, C. Auzan, E. Clauser, S. Dirrig-Grosch, M. Meira, A. Appert-Collin, D. Aunis, G. Crémel, and P. Hubert. Inhibition by transmembrane peptides of chimeric insulin receptors. Cellular and Molecular Life Sciences CMLS, 62(18):2124–2131, 2005.

[11] Amar Bennasroune, Maria Fickova, Anne Gardin, Sylvie Dirrig-Grosch, Dominique Aunis, Gérard Crémel, and Pierre Hubert. Transmembrane peptides as inhibitors of erbb receptor signaling. Molecular Biology of the Cell, 15(7):3464–3474, 2004.

[12] Binyamin D Berkovits and Christine Mayr. Alternative 3' utrs act as scaffolds to regulate membrane protein localization. Nature, 522(7556):363–367, Jun 2015.

[13] Claude Berney and Gaudenz Danuser. FRET or no FRET: A quantitative comparison. Biophysical Journal, 84(6):3992 – 4010, 2003.

[14] G Böhm, H Muhr, and R Jaenicke. Quantitative analysis of protein far UV circular dichroism spectra by neural networks. Protein Engineering, 5:191–195, 1992.

[15] Istvan Botos, David M Segal, and David R Davies. The structural biology of Toll-like receptors. Structure, 19:447–459, 2011.

[16] Melanie M Brinkmann, Eric Spooner, Kasper Hoebe, Bruce Beutler, Hidde L Ploegh, and You-Me Kim. The interaction between the ER membrane protein UNC93B and TLR3, 7, and 9 is crucial for TLR signaling. The Journal of Cell Biology, 177:265–275, 2007.

[17] Bettina Brosig and Dieter Langosch. The dimerization motif of the glycophorin a transmembrane segment in membranes: Importance of glycine residues. Protein Science, 7:1052–1056, 1998.

[18] Tobin J Cammett, Susan J Jun, Emily B Cohen, Francisco N Barrera, Donald M Engelman, and Daniel Dimaio. Construction and genetic selection of small transmembrane proteins that activate the human erythropoietin receptor. Proc Natl Acad Sci U S A, 107(8):3447–3452, Feb 2010.

[19] Gregory A Caputo, Rustem I Litvinov, Wei Li, Joel S Bennett, Willaim F DeGrado, and Hang Yin. Computationally designed peptide inhibitors of protein-protein interactions in membranes. Biochemistry, 47(33):8600–8606, 2008.

[20] Gersende Caron, Dorothée Duluc, Isabelle Frémaux, Pascale Jeannin, Catherine David, Hugues Gascan, and Yves Delneste. Direct stimulation of human t cells via tlr5 and tlr7/8: Flagellin and r-848 up-regulate proliferation and ifn- production by memory cd4+ t cells. The Journal of Immunology, 175(3):1551–1557, 2005.

[21] Kelly M Chacon, Lisa M Petti, Elizabeth H Scheideman, Valentina Pirazzoli, Katerina Politi, and Daniel DiMaio. De novo selection of oncogenes. Proc Natl Acad Sci U S A, 111(1):E6–E14, Jan 2014.

[22] Lirong Chen, Lawrence Novicky, Mikhail Merzlyakov, Tihomir Hristov, and Kalina Hristova. Measuring the energetics of membrane protein dimerization in mammalian membranes. Journal of the American Chemical Society, 132:3628–3635, 2010.

[23] Lirong Chen, Jesse Placone, Lawrence Novicky, and Kalina Hristova. The extracellular domain of fibroblast growth factor receptor 3 inhibits ligand-independent dimerization. Science Signaling, 3(150):1–6, 2010.

[24] Kui Cheng, Meng Gao, James I. Godfroy, Peter N. Brown, Noah Kastelowitz, and Hang Yin. Specific activation of the tlr1-tlr2 heterodimer by small-molecule agonists. Science Advances, 1(3), 2015.

[25] Chen-Ni Chin, Jonathan N Sachs, and Donald M. Engelman. Transmembrane homodimerization of receptor-like protein tyrosine phosphatases. FEBS Letters, 579:3855–3858, 2005.

[26] Emily B Cohen, Susan J Jun, Zachary Bears, Francisco N Barrera, Miriam Alonso, Donald M Engelman, and Daniel DiMaio. Mapping the homodimer interface of an optimized, artificial, transmembrane protein activator of the human erythropoietin receptor. PLoS One, 9(4):e95593, 2014.

[27] Tomer Cohen, Shmuel Jaffe Cohen, Niv Antonovsky, Irun R. Cohen, and Yechiel Shai. Hiv-1 gp41 and tcr trans-membrane domains share a motif exploited by the hiv virus to modulate t-cell proliferation. PLoS Pathog, 6(9):e1001085, 09 2010.

[28] Jonathan W.D. Comeau, Santiago Costantino, and Paul W. Wiseman. A guide to accurate fluorescence microscopy colocalization measurements. Biophysical Journal, 91(12):4611 – 4622, 2006.

[29] Stefan N Constantinescu, Tzvia Keren, merav Socolovsky, Hyung song Nam, Yoav I Henis, and Harvey F Lodish. Ligand-independent oligomerization of cell-surface erythropoietin receptor is mediated by the transmembrane domain. PNAS, 98:4379–4384, 2001.

[30] Donald N Cook, David S Pisetsky, and David A Schwartz. Toll-like receptors in the pathogenesis of human disease. Nature Immunology, 5(10):975–979, 2004.

[31] Natasha K Crellin, Rosa V Garcia, Omeed Hadisfar, Sarah E Allan, Theodore S Steiner, and Megan K Levings. Human cd4+ t cells express tlr5 and its ligand flagellin enhances the suppressive capacity and expression of foxp3 in cd4+cd25+ t regulatory cells. J Immunol, 175(12):8051–8059, Dec 2005.

[32] Florian Cymer, Gunnar von Heijne, and Stephen H White. Mechanisms of integral membrane protein insertion and folding. J Mol Biol, 427(5):999–1022, Mar 2015.

[33] Sándor Damjanovich, László Bene, János Matkó, Abdelkrim Alileche, Carolyn K. Goldman, Susan Sharrow, and Thomas A. Waldmann. Preassembly of interleukin 2 (il-2) receptor subunits on resting kit 225 k6 t cells and their modulation by il-2, il-7, and il-15: A fluorescence resonance energy transfer study. Proceedings of the National Academy of Sciences, 94(24):13134–13139, 1997.

[34] Sándor Damjanovich, László Bene, János Matkó, Abdelkrim Alileche, Carolyn K. Goldman, Susan Sharrow, and Thomas A. Waldmann. Preassembly of interleukin 2 (il-2) receptor subunits on resting kit 225 k6 t cells and their modulation by il-2, il-7, and il-15: A fluorescence resonance energy transfer study. Proceedings of the National Academy of Sciences, 94(24):13134–13139, 1997.

[35] P Dasari, I C Nicholson, and H Zola. Toll-like receptors. Journal of Biological Regulators and Homeostatic Agents, 22(1):17–26, 2008.

[36] Mohan R. Dasu, Sridevi Devaraj, Samuel Park, and Ishwarlal Jialal. Increased Toll-like receptor (TLR) activation and TLR ligands in recently diagnosed type 2 diabetic subjects. Diabetes Care, 33(4):861–863, 2010.

[37] David L Daugherty and Samuel H Gellman. A fluorescence assay for leucine zipper dimerization: Avoiding unintended consequences of fluorophore attachment. Journal of the American Chemical Society, 121:4325–4333, 1999.

[38] Jessica P. Dawson, Roman A. Melnyk, Charles M. Deber, and Donald M. Engelman. Sequence context strongly modulates association of polar residues in transmembrane helices. Journal of Molecular Biology, 331(1):255 – 262, 2003.

[39] Jessica P Dawson, Joshua S Weinger, and Donald M Engelman. Motifs of serine and threonine can drive association of transmembrane helices. Journal of Molecular Biology, 316(3):799 – 805, 2002.

[40] Kevin M Dean and Amy E Palmer. Advances in fluorescence labeling strategies for dynamic cellular imaging. Nat Chem Biol, 10(7):512–523, 07 2014.

[41] William F. DeGrado, Holly Gratkowski, and James D. Lear. How do helix–helix interactions help determine the folds of membrane proteins? perspectives from the study of homo-oligomeric helical bundles. Protein Science, 12(4):647–665, 2003.

[42] Jean-Pierre Duneau, Attila P Vegh, and James N Sturgis. A dimerization hierarcy in the transmembrane domains of the HER receptor family. Biochemistry, 46:2010–2019, 2007.

[43] Kenneth W Dunn, Malgorzata M Kamocka, and John H McDonald. A practical guide to evaluating colocalization in biological microscopy. Am J Physiol Cell Physiol, 300:C723–C742, 2011.

[44] Mylinh T Duong, Todd M Jaszewski, Karen G Fleming, and Kevin R MacKenzie. Changes in apparent free energy of helix-helix dimerization in a biological membrane due to point mutations. Journal of Molecular Biology, 371:422–434, 2007.

[45] P Duplay, S Szmelcman, H Bedouelle, and M Hofnung. Silent and functional changes in the periplasmic maltose-binding protein of Escherichia coli K12. I. Transport of maltose. Journal of Molecular Biology, 194:663–673, 1987.

[46] H Durchschlag and P Zipper. Calculation of the partial volume of organic compounds and polymers. Progress in Colloid and Polymer Science, 90:20–39, 1994.

[47] Alexandra Z Ebie and Karen G Fleming. Dimerization of the erythropoietin receptor transmembrane domains in micelles. Journal of Molecular Biology, 366:517–524, 2007.

[48] Anne P B Edwards, Yanhua Xie, Lara Bowers, and Daniel DiMaio. Compensatory mutants of the bovine papillomavirus e5 protein and the platelet-derived growth factor beta receptor reveal a complex direct transmembrane interaction. J Virol, 87(20):10936–10945, Oct 2013.

[49] Nicholas F Endres, Rahul Das, Adam W Smith, Anton Arkhipov, Erika Kovacs, Yongjian Huang, Jeffrey G Pelton, Yibing Shan, David E Shaw, David E Wemmer, Jay T Groves, and John Kuriyan. Conformational coupling across the plasma membrane in activation of the egf receptor. Cell, 152(3):543–556, Jan 2013.

[50] Ryan Ferrao, Jixi Li, Elisa Bergamin, and Hao Wu. Structural insights into the assembly of large oligomeric signalosomes in the Toll-like receptor-Interleukin-1 receptor subfamily. Science Signaling, 5, 2012.

[51] Carmen Finger, Claudia Escher, and Dirk Schneider. The single transmembrane domains of human receptor tyrosine kinases encode self-interactions. Science Signaling, 2(89):1–8, 2009.

[52] Avner Fink, Eliran M Reuven, Christopher J Arnusch, Liraz Shmuel-Galia, Niv Antonovsky, and Yechiel Shai. Assembly of the TLR2/6 transmembrane domains is essential for activation and is target for prevention of sepsis. The Journal of Immunology, 190:6410–6422, 2013.

[53] Avner Fink, Neta Sal-Man, Doron Gerber, and Yechiel Shai. Transmembrane domains interactions within the membrane milieu: Principles, advances and challenges. Biochimica et Biophysica Acta (BBA) - Biomembranes, 1818(4):974 – 983, 2012. Protein Folding in Membranes.

[54] T W Gadella and T M Jovin. Oligomerization of epidermal growth factor receptors on a431 cells studied by time-resolved fluorescence imaging microscopy. a stereochemical model for tyrosine kinase receptor activation. The Journal of Cell Biology, 129(6):1543–1558, 1995.

[55] D Galiana-Arnoux and J L Imler. Toll-like receptors and innate antiviral immunity. Tissue Antigens, 67:267–276, 2006.

[56] William J Galush, Jeffrey A Nye, and Jay T Groves. Quantitative fluorescence microscopy using supported lipid bilayer standards. Biophys J, 95(5):2512–2519, Sep 2008.

[57] Nicholas J. Gay, Martyn F. Symmons, Monique Gangloff, and Clare E. Bryant. Assembly and localization of toll-like receptor signalling complexes. Nat Rev Immunol, 14(8):546–558, 08 2014.

[58] Degui Geng, Sabina Kaczanowska, Alexnder Tsai, Kenisha Younger, Augusto Ochoa, Aaron P Rapoport, Suzanne Ostrand-Rosenberg, and Eduardo Davila. Tlr5 ligand-secreting t cells reshape the tumor microenvironment and enhance antitumor activity. Cancer Research, 2015.

[59] Susan R. George, Samuel P. Lee, George Varghese, Peter R. Zeman, Philip Seeman, Gordon Y. K. Ng, and Brian F. O'Dowd. A transmembrane domain-derived peptide inhibits d1 dopamine receptor function without affecting receptor oligomerization. Journal of Biological Chemistry, 273(46):30244–30248, 1998.

[60] Doron Gerber, Neta Sal-Man, and Yechiel Shai. Two motifs within a transmembrane domain, one for homodimerization and the other for heterodimerization. The Journal of Biological Chemistry, 20:21177–21182, 2004.

[61] Doron Gerber and Yechiel Shai. In vivo detection of hetero-assocation of glycophorin-a and its mutants within the membrane. The Journal of Biological Chemistry, 276(33):31229–31232, 2001.

[62] Giovanna Ghirlanda. Design of membrane proteins: toward functional systems. Current Opinion in Chemical Biology, 13:643–651, 2009.

[63] Daniel G Gibson, Lei Young, Ray-Yuan Chuang, J Craig Venter, Clyde A Hutchison, and Hamilton O Smith. Enzymatic assembly of dna molecules up to several hundred kilobases. Nat Meth, 6(5):343–345, 05 2009.

[64] Fui G. Goh and Kim S. Midwood. Intrinsic danger: activations of Toll-like receptors in rheumatoid arthritis. Rheumatology, pages 1–17, 2011.

[65] Holly Gratkowski, James D. Lear, and William F. DeGrado. Polar side chains drive the association of model transmembrane peptides. Proceedings of the National Academy of Sciences, 98(3):880–885, 2001.

[66] Yue Guan, Katherine Omueti-Ayoade, Sarita K. Mutha, Paul J. Hergenrother, and Richard I. Tapping. Identification of novel synthetic toll-like receptor 2 agonists by high throughput screening. Journal of Biological Chemistry, 285(31):23755–23762, 2010.

[67] Yue Guan, Diana Rose E Ranoa, Song Jiang, Sarita K Mutha, Xinyan Li, Jeorme Baudry, and Richard I Tapping. Human TLRs 10 and 1 share common mechanism of innate immune sensing but not signaling. Journal of Immunology, 184:5094–5103, 2010.

[68] Chunmei Guo, Steven K. Dower, David Holowka, and Barbara Baird. Fluorescence resonance energy transfer reveals interleukin (il)-1-dependent aggregation of il-1 type i receptors that correlates with receptor activation. Journal of Biological Chemistry, 270(46):27562–27568, 1995.

[69] Bryan E. Hart and Richard I. Tapping. Cell surface trafficking of tlr1 is differentially regulated by the chaperones prat4a and prat4b. Journal of Biological Chemistry, 287(20):16550–16562, 2012.

[70] Uzma Hasan, Claire Chaffois, Cladue Gaillard, Virginie Salunier, Estelle Merck, Sandra Tancredi, Chantal Guiet, Francine Briere, Jaromir Vlach, Serge Legecque, Giorgio Trinchieri, and Elizabeth E M Bates. Human TLR10 is a fucntional receptor, expressed by b cells and plasmacytoid dendritic cells, which activates gene transcription through myd88. Journal of Immunology, 174:2942–2950, 2005.

[71] Uzma A Hasan, Sandra Dollet, and Jaromir Vlach. Differential induction of gene promoter constructs by constitutively active human TLRs. Biochemical and Biophyscial Research Communications, 321:124–131, 2004.

[72] Lijuan He and Kalina Hristova. Pathogenic activation of receptor tyrosine kinases in mammalian membranes. J Mol Biol, 384(5):1130–1142, Dec 2008.

[73] Lijuan He and Kalina Hristova. Physical-chemical principles underlying rtk activation, and their implications for human disease. Biochim Biophys Acta, 1818(4):995–1005, Apr 2012.

[74] Terence E. Hebert, Serge Moffett, Jean-Pierre Morello, Thomas P. Loisel, Daniel G. Bichet, Cécile Barret, and Michel Bouvier. A peptide derived from a 2-adrenergic receptor transmembrane domain inhibits both receptor dimerization and activation. Journal of Biological Chemistry, 271(27):16384–16392, 1996.

[75] Ramanujan S Hegde and Harris D Bernstein. The surprising complexity of signal sequences. Trends Biochem Sci, 31(10):563–571, Oct 2006.

[76] Frank Hennecke, Arne Muller, Roland Meister, Astrid Strelow, and Susanne Behrens. A toxr-based two-hybrid system for the detection of periplasmic and cytoplasmic protein-protein interactions in escherichia coli: minimal requirements for specific dna binding and transcriptional activation. Protein Eng Des Sel, 18(10):477–486, Oct 2005.

[77] Elizabeth J Hennessy, Andrew E Parker, and Luke A J O'Neill. Taregting Toll-like receptors: emerging therapeutics? Nature Reviews Drug Discovery, 9:293–307, 2010.

[78] Jana R. Herrmann, Johanna C. Panitz, Stephanie Unterreitmeier, Angelika Fuchs, Dmitrij Frishman, and Dieter Langosch. Complex patterns of histidine, hydroxylated amino acids and the gxxxg motif mediate high-affinity transmembrane domain interactions. Journal of Molecular Biology, 385:912–923, 2009.

[79] Tara Hessa, Hyun Kim, Karl Bihlmaier, Carolina Lundin, Jorrit Boekel, Helena Andersson, Ingmarie Nilsson, Stephen H White, and Gunnar von Heijne. Recognition of transmembrane helices by the endoplasmic reticulum translocon. Nature, 433(7024):377–381, Jan 2005.

[80] Tara Hessa, Nadja M Meindl-Beinker, Andreas Bernsel, Hyun Kim, Yoko Sato, Mirjam Lerch-Bader, IngMarie Nilsson, Stephen H White, and Gunnar von Heijne. Molecular code for transmembrane-helix recognition by the sec61 translocon. Nature, 450(7172):1026–1030, Dec 2007.

[81] Eric S Hoffman, Richard E T Smith, and Ronald C Renaud Jr. Tlr-targeted therapeutics. Nature Reviews Drug Discovery, 4:879–880, 2005.

[82] Harald Husebye, Øyvind Halaas, Harald Stenmark, Gro Tunheim, Øystein Sandanger, Bjarne Bogen, Andreas Brech, Eicke Latz, and Terje Espevik. Endocytic pathways regulate Toll-like receptor 4 signaling and link innate and adaptive immunity. The EMBO Journal, 25:683–692, 2006.

[83] Nghi T Huynh, Rosemary A Ffrench, Ross A Boadle, and Nicholas Manolios. Transmembrane t-cell receptor peptides inhibit b- and natural killer-cell function. Immunology, 108(4):458–464, Apr 2003.

[84] James Isaac Godfroy III, Mohammad Roostan, Yurii S Moroz, Ivan V Korendovych, and Hang Yin. Isolated Toll-like receptor transmembrane domains are capable of oligomerizaiton. PLoS ONE, 7(11):e48875, 2012.

[85] Sung il Yoon, Oleg Kurnasov, Venkatesh Natarajan, Minsun Hong, Andrei V Gudkov, Andrei L Osterman, and Ian A Wilson. Structural basis of TLR5-Flagellin recognition and signaling. Science, 335:859, 2012.

[86] Jean-Luc Imler and Jules A Hoffman. Toll signaling: the TIReless quest for specificity. Nature Immunology, 4(2):105–106, 2003.

[87] John R James, Marta I Oliveira, Alexandre M Carmo, Andrea Iaboni, and Simon J Davis. A rigorous experimental framework for detecting protein oligomerization using bioluminescence resonance energy transfer. Nat Meth, 3(12):1001–1006, 12 2006.

[88] Elizabeth A Jares-Erijman and Thomas M Jovin. Fret imaging. Nat Biotech, 21(11):1387–1395, 11 2003.

[89] Elizabeth A Jares-Erijman and Thomas M Jovin. Imaging molecular interactions in living cells by fret microscopy. Current Opinion in Chemical Biology, 10:409–416, 2006.

[90] Simon Jaud, Monica Fernandez-Vidal, Ingmarie Nilsson, Nadja M Meindl-Beinker, Nadja C Hubner, Douglas J Tobias, Gunnar von Heijne, and Stephen H White. Insertion of short transmembrane helices by the sec61 translocon. Proc Natl Acad Sci U S A, 106(28):11588–11593, Jul 2009.

[91] Mi Sun Jin, Sung Eun Kim, Jin Young Heo, Mi Eun Lee, Ho Min Kim, Sang-Gi Paik, Hayyoung Lee, and Jie-Oh Lee. Crystal structure of the TLR1-TLR2 heterodimer induced by binding of a tri-acylated lipopeptide. Cell, 130:1071–1082, 2007.

[92] Mi Sun Jin and Jie-Oh Lee. Structure of the Toll-like receptor family and its ligand complexes. Immunity, 29:182–191, 2008.

[93] Rachel M. Johnson, Karen Hecht, and Charles M. Deber. Aromatic and cation interactions enhance helixhelix association in a membrane environment. Biochemistry, 46(32):9208–9214, 2007. PMID: 17658897.

[94] Jin Young Kang and Jie-Oh Lee. Structural biology of the toll-like receptor family. Annu Rev Biochem, 80:917–941, 2011.

[95] Jin Young Kang, Xuehua Nan, Mi Sun Jin, Suk-Jun Youn, Young Hee Ryu, Shinjee Mah, Seung Hyun Jan, Hayyoung Lee, Sang-Gi Paik, and Jie-Oh Lee. Recognition of lipopeptide patterns by Toll-like receptor 2-Toll-like receptor 6 heterodimer. Immunity, 31:873–884, 2009.

[96] Holger Kanzler, Franck J Barrat, Edith M Hessel, and Robert L Coffman. Therapeutic targeting of innate immunity with toll-like receptor agonists and antagonists. Nature Medicine, 13(5):552–559, 2007.

[97] Masaru Katoh and Hitoshi Nakagama. Fgf receptors: Cancer biology and therapeutics. Medicinal Research Reviews, 34(2):280–300, 2014.

[98] Federico Katzen, Todd C Peterson, and Wieslaw Kudlicki. Membrane protein expression: no cells required. Trends in Biotechnology, 27:455–460, 2009.

[99] Jennifer M Kavran, Jacqueline M McCabe, Patrick O Byrne, Mary Katherine Connacher, Zhihong Wang, Alexander Ramek, Sarvenaz Sarabipour, Yibing Shan, David E Shaw, Kalina Hristova, Philip A Cole, and Daniel J Leahy. How igf-1 activates its receptor. eLife, 3:e03772, 2014.

[100] Taro Kawai and Shizuo Akira. Tlr signaling. Cell Death and Differentiation, 13:816–825, 2006.

[101] Taro Kawai and Shizuo Akira. The role of pattern-recognition receptors in innate immunity: update on Toll-like receptors. Nature Immunology, 11(5):373–384, 2010.

[102] Anne K. Kenworthy. Imaging protein-protein interactions using fluorescence resonance energy transfer microscopy. Methods, 24(3):289 – 296, 2001.

[103] Christopher King, Sarvenaz Sarabipour, Patrick Byrne, Daniel J Leahy, and Kalina Hristova. The fret signatures of noninteracting proteins in membranes: simulations and experiments. Biophys J, 106(6):1309–1317, Mar 2014.

[104] Harald Kolmar, Frank Hennecke, Kerstin Götze, Birgit Janzer, Beate Vogt, Frank Mayer, and Hans-Joachim Fritz. Membrane insertion of the bacterial signal transduction protein ToxR and the requirements of transcription activation studied by modular replacement of different protein substructures. The EMBO Journal, 14:3895–3904, 1995.

[105] Ling Kong and Bao-Xue Ge. MyD88-independent activation of a novel actin-Cdc42/Rac pathway is require for Toll-like receptor-stimulated phagocytosis. Cell Research, 18:745–755, 2008.

[106] Arthur M Krieg and Jorg Vollmer. Toll-like receptors 7, 8, and 9: linking innate immunity to autoimmunity. Immunological Reviews, 220:251–269, 2007.

[107] Jayalakshmi Krishnan, Gwang Lee, and Sandgdun Choi. Drugs targeting Toll-like receptors. Archives of Pharmacalogical Research, 32(11):1485–1502, 2009.

[108] Egbert K O Kruithof, Nathalie Satta, Jia Wei Liu, Sylvie Dunoyer-Geindre, and Richard J Fish. Gene conversion limist divergence of mammalian TLR1 and TLR6. BMC Evolutionary Biology, 7:148–157, 2007.

[109] Nozomu Kurosaka, Andrea Bolte, Marina Ali, and Nicholas Manolios. T-cell antigen receptor assembly and cell surface expression is not affected by treatment with t-cell antigen receptor-alpha chain transmembrane peptide. Protein Pept Lett, 14(3):299–303, 2007.

[110] Dieter Langosch and Isaiah T Arkin. Interaction and conformational dynamics of membrane-spanning protein helices. Protein Science, 18(7):1343–1358, 2009.

[111] Dieter Langosch, Bettina Brosig, Harald Kolmar, and Han-Joachim Fritz. Dimerization of the glycophorin a transmembrane segment in membranes probed with the ToxR transcription activator. Journal of Molecular Biology, 263:525–530, 1996.

[112] Dieter Langosch and Jaap Heringa. Interaction of transmembrane helices by a knobs-into-holes packing characteristic of soluble coiled coils. Proteins: Structure, Function, and Bioinformatics, 31(2):150–159, 1998.

[113] Eicke Latz, Anjali Verma, Alberto Visintin, Mei Gong, Cherilyn M Sirois, Dionne C G Klein, Biran G Monks, C James McKnight, Marc S Lamphier, W Paul Duprex, Terje Espevik, and Douglas T Golenbock. Ligand-induced conformational changes allosterically activate Toll-like receptor 9. Nature Immunology, 8(7):772–779, 2007.

[114] Eicke Latz, Alberto Visintin, Egil Lien, Kate A Fitzgerald, Terje Espevik, and Douglas T Golenbock. The LPS receptor generates inflammatory signals from the cell surface. Journal of Endotoxin Research, 9(6), 2003.

[115] Eicke Latz, Alberto Visintin, Egil Lien, Kate A Fitzgerald, Brian G Monks, Evelyn A Kurt-Jones, Douglas T Golenbock, and Terje Espevik. Lipopolysaccharide rapidly traffics to and from the Golgi Apparatus with the Toll-like receptor 4-MD-2-CD-14 complex that is distinct from the initiation of signal transduction. The Journal of Biological Chemistry, 49:47834–47843, 2002.

[116] J Lebowitz, M S Lewis, and P Schuck. Modern analytical ultracentrifugation in protein science: A tutorial review. Protein Science, 11:2067–2079, 2002.

[117] Bettina L Lee, Joanne E Moon, Jeffrey H Shu, Lin Yuan, Zachary R Newman, Randy Schekman, and Gregory M Barton. UNC93B1 mediates differential trafficking of endosomal TLRs. eLife, 2:e00291, 2013.

[118] Clarissa C Lee, Ana M Avalos, and Hidde L Ploegh. Accessory molecules for Toll-like receptors and their function. Nature Reviews Immunology, 12:168–179, 2012.

[119] Jongsoon Lee, Masaya Miyazaki, Giulio R. Romeo, and Steven E. Shoelson. Insulin receptor activation with transmembrane domain ligands. Journal of Biological Chemistry, 289(28):19769–19777, 2014.

[120] Mark A Lemmon, John M Flanagan, John F Hunt, Brian D Adair, Barbara-Jean Bormann, Christopher E Dempsey, and Donald M. Engelman. Glycophorin a dimerization is driven by specific interactions between transmembrane α-helices. The Journal of Biological Chemistry, 267:7683–7689, 1992.

[121] Joshua N. Leonard, Rodolfo Ghirlando, Janine Askins, Jessica K Bell, David H Margulies, David R Davies, and David M Segal. The TLR3 signaling complex forms by cooperative receptor dimerization. PNAS, 105(1):258–263, 2007.

[122] Ilya Levental, Michal Grzybek, and Kai Simons. Raft domains of variable properties and compositions in plasma membrane vesicles. PNAS, 108:11411–11416, 2011.

[123] Ilya Levental, Daniel Lingwood, Michal Grzybek, Ünal Coskun, and Kai Simons. Palmitoylation regulates raft affinity for the majority of integral raft proteins. PNAS, 107:22050–22054, 2010.

[124] Edwin Li and Kalina Hristova. Role of receptor tyrosine kinase transmembrane domains in cell signaling and human pathologies. Biochemistry, 45(20):6241–6251, 2006. PMID: 16700535.

[125] Edwin Li and Kalina Hristova. Receptor tyrosine kinase transmembrane domains. Cell Adhesion & Migration, 4(2):249–254, 2010.

[126] Edwin Li, Jesse Placone, Mikhail Merzlyakov, and Kalina Hristova. Quantitative measurements of protein interactions in a crowded cellular environment. Anal Chem, 80(15):5976–5985, Aug 2008.

[127] Edwin Li, Min You, and Kalina Hristova. Sodium dodecyl sulfate-polyacrylamide gel electrophoresis and forster resonance energy transfer suggest weak interactions between fibroblast growth factor receptor 3 (fgfr3) transmembrane domains in the absence of extracellular domains and ligands. Biochemistry, 44:352–360, 2005.

[128] Renhao Li, Roman Gorelik, Vikas Nanda, Peter B Law, James D Lear, Willaim F DeGrado, and Joel S Bennett. Dimerization of the transmembrane domain of integrin α_{IIb} subunit in cell membranes. The Journal of Biological Chemistry, 279(24):26666–26673, 2004.

[129] Egil Lien and Danny Zipris. The role of toll-like receptor pathways in the mechanism of type 1 diabetes. Current Molecular Medicine, 9:52–68, 2009.

[130] Su-Chang Lin, Yu-Chih Lo, and Hao Wu. Helical assembly in the myd88-irak4-irak2 complex in tlr/il-1r signalling. Nature, 465(7300):885–890, Jun 2010.

[131] Eric Lindner and Dieter Langosch. A toxr-based dominant-negative system to investigate heterotypic transmembrane domain interactions. PROTEINS: Structure, Function, and Bioinformatics, 65:803–807, 2006.

[132] Jennifer Lippincott-Schwartz and George H. Patterson. Development and use of fluorescent protein markers in living cells. Science, 300(5616):87–91, 2003.

[133] Lin Liu, Istvan Botos, Yan Wang, Joshua N. Leonard, Joseph Shiloach, David M Segal, and David R Davies. Structural basis of Toll-like receptor 3 signaling with double-stranded rna. Science, 320:379–381, 2008.

[134] Matthew W Lluis, James Isaac Godfroy III, and Hang Yin. Protein engineering methods applied to membrane protein targets. Protein Engineering, Design & Selection, 26:91–100, 2013.

[135] N Manolios. Hierarchy of t cell antigen receptor assembly. Immunol Cell Biol, 73(6):544–548, Dec 1995.

[136] N Manolios, J S Bonifacino, and R D Klausner. Transmembrane helical interactions and the assembly of the t cell receptor complex. Science, 249(4966):274–277, Jul 1990.

[137] N Manolios, S Collier, J Taylor, J Pollard, L C Harrison, and V Bender. T-cell antigen receptor transmembrane peptides modulate t-cell function and t cell-mediated disease. Nat Med, 3(1):84–88, Jan 1997.

[138] N Manolios, O Kemp, and Z G Li. The t cell antigen receptor alpha and beta chains interact via distinct regions with cd3 chains. Eur J Immunol, 24(1):84–92, Jan 1994.

[139] N Manolios and Z G Li. The t cell antigen receptor beta chain interacts with the extracellular domain of cd3-gamma. Immunol Cell Biol, 73(6):532–536, Dec 1995.

[140] Nicholas Manolios, Marina Ali, Michael Amon, and Veronika Bender. Therapeutic application of transmembrane t and natural killer cell receptor peptides. Adv Exp Med Biol, 640:208–219, 2008.

[141] Nicholas Manolios, Marina Ali, and Vera Bender. T-cell antigen receptor (tcr) transmembrane peptides: A new paradigm for the treatment of autoimmune diseases. Cell Adh Migr, 4(2):273–283, Apr-Jun 2010.

[142] Sara A Marlatt, Yong Kong, Tobin J Cammett, Gregory Korbel, James P Noonan, and Daniel Dimaio. Construction and maintenance of randomized retroviral expression libraries for transmembrane protein engineering. Protein Eng Des Sel, 24(3):311–320, Mar 2011.

[143] Damien Maurel, Laetitia Comps-Agrar, Carsten Brock, Marie-Laure Rives, Emmanuel Bourrier, Mohammed Akli Ayoub, Herve Bazin, Norbert Tinel, Thierry Durroux, Laurent Prezeau, Eric Trinquet, and Jean-Philippe Pin. Cell-surface protein-protein interaction analysis with time-resolved fret and snap-tag technologies: application to gpcr oligomerization. Nat Meth, 5(6):561–567, 06 2008.

[144] Emily C McCusker, Steven E Bane, Michelle A O'Malley, and Anne Skaja Robinson. Heterlogous GPCR expression: A bottleneck to obtaining crystal structures. Biotechnology Progress, 23:540–547, 2007.

[145] Anne F McGettrick and Luke A J O'Neill. Localisation and trafficking of Toll-like receptors: an important mode of regulation. Current Opinion in Immunology, 22:20–27, 2010.

[146] Ruslan Medzhitov. Toll-like receptors and innate immunity. Nature Reviews Immunology, 1:135–145, 2001.

[147] Ruslan Medzhitov. Recognition of microorganisms and activation of the immune response. Nature, 449:819–826, 2007.

[148] Jeannine M. Mendrola, Mitchell B. Berger, Megan C. King, and Mark A. Lemmon. The single transmembrane domains of erbb receptors self-associate in cell membranes. Journal of Biological Chemistry, 277(7):4704–4712, 2002.

[149] Mikhail Merzlyakov, Lirong Chen, and Kalina Hristova. Studies of receptor tryosine kinase transmembrane domain interactions: The emex-fret method. Journal of Membrane Biology, 215:93–103, 2007.

[150] Konstantin S Mineev, Sergey A Goncharuk, and Alexander S Arseniev. Toll-like receptor 3 transmembrane domain is able to perform various homotypic interactions: an nmr structural study. FEBS Lett, 588(21):3802–3807, Nov 2014.

[151] David T Moore, Bryan W Berger, and Willaim F DeGrado. Protein-protein interactions in the membrane: sequence, structural, and biological motifs. Structure, 16:991–1001, 2008.

[152] Johanna Napetschnig and Hao Wu. Molecular basis of nf-κb signaling. Annual Review of Biophysics, 42:19.1–19.26, 2013.

[153] Wataru Nemoto and Hiroyuki Toh. Membrane interactive α-helices in GPCRs as a novel drug target. Current Protein and Peptide Science, 7:561–575, 2006.

[154] Chung Truong Nguyen, Seol Hee Hong, Jeong-Im Sin, Hong Van Dinh Vu, Kwangjoon Jeong, Kyoung Oh Cho, Satoshi Uematsu, Shizuo Akira, Shee Eun Lee, and Joon Haeng Rhee. Flagellin enhances tumor-specific cd8(+) t cell immune responses through tlr5 stimulation in a therapeutic cancer vaccine model. Vaccine, 31(37):3879–3887, Aug 2013.

[155] Nadra J Nilsen, Susanne Deininger, Unni Nonstad, Frode Skjeldal, Harald Husebye, Dmitri Rodionov, Sonja von Aulock, Thomas Hartung, Egil Lien, Oddmund Bakke, and Terje Espevik. Cellular trafficking of lipoteichoic acid and Toll-like receptor 2 in relation to signaling; role of CD14 and CD36. Journal of Leukocyte Biology, 84:280–291, 2008.

[156] Tadashi Nishiya and Anthony L DeFranco. Ligand-regulated chimeric receptor approach reveals distinctive subcellular localization and signaling properties of the Toll-like receptors. The Journal of Biological Chemistry, 279(18):19008–19017, 2004.

[157] Umeharu Ohto, Takuma Shibata, Hiromi Tanji, Hanako Ishida, Elena Krayukhina, Susumu Uchiyama, Kensuke Miyake, and Toshiyuki Shimizu. Structural basis of CpG and inhibitory DNA recognition by toll-like receptor 9. Nature, 520:702–705, 2015.

[158] Karin Ojemalm, Takashi Higuchi, Yang Jiang, Ulo Langel, IngMarie Nilsson, Stephen H White, Hiroaki Suga, and Gunnar von Heijne. Apolar surface area determines the efficiency of translocon-mediated membrane-protein integration into the endoplasmic reticulum. Proc Natl Acad Sci U S A, 108(31):E359–64, Aug 2011.

[159] Luke A J O'Neill. Immunity's early-warning system. Scientific American, 292(1):38–45, 2005.

[160] Luke A J O'Neill and Andrew G Bowie. The family of five: Tir-domain-containing adaptors in toll-like receptor signalling. Nat Rev Immunol, 7(5):353–364, May 2007.

[161] Luke A J O'Neill, Clare E Bryant, and Sarah L Doyle. Therapeutic targeting of toll-like receptors for infectious and inflammatory disease and cancer. Pharmacological Reviews, 61:177–197, 2009.

[162] Marije Oosting, Shih-Chin Cheng, Judith M Bolscher, Rachel Vestering-Stenger, Theo S Plantinga, Ineke C Verschueren, Peer Arts, Anja Garritsen, Hans van Eenennaam, Patrick Sturm, Bart-Jan Kullberg, Alexander Hoischen, Gosse J Adema, Jos W M van der Meer, Mihai G Netea, and Leo A B Joosten. Human tlr10 is an anti-inflammatory pattern-recognition receptor. Proc Natl Acad Sci U S A, 111(42):E4478–84, Oct 2014.

[163] John P Overington, Bissan Al-Lazikani, and Andrew L Hopkins. How many drug targets are there? Nature Reviews Drug Discovery, 5:993–996, 2006.

[164] Adrian Ozinsky, David M Underhill, Jason D Fontenot, Adeline M Hajjar, Kelly D Smith, Christopher B Wilson, Leas Schroeder, and Alan Aderem. The repertoire for pattern recognition of pathogens by the innate immune system is defined by cooperation between Toll-like receptors. PNAS, 97(25):13766–13771, 2000.

[165] E M Palsson-McDermott and Luke A J O'Neill. Building an immune system from nine domains. Biochemical Society Transactions, 35:1437–1444, 2007.

[166] Gabriela Panter and Roman Jerala. The ectodomain of the Toll-like receptor 4 prevents constitutive receptor activation. The Journal of Biological Chemistry, 286(26):23334–23344, 2011.

[167] Beom Seok Park, Dong Hyun Song, Ho Min Kim, Byong-Seok Choi, Hayyoung Lee, and Jie-Oh Lee. The structural basis of lipopolysacchardie regonition by the TLR4-MD-2 complex. Nature, 458:1191–1195, 2009.

[168] Seung-Yeol Park, Jia-Shu Yang, Angela B Schmider, Roy J Soberman, and Victor W Hsu. Coordinated regulation of bidirectional COPI transport at the Golgi by CDC42. Nature, 521:529–532, 2015.

[169] Lisa M Petti, Kristina Talbert-Slagle, Megan L Hochstrasser, and Daniel DiMaio. A single amino acid substitution converts a transmembrane protein activator of the platelet-derived growth factor beta receptor into an inhibitor. J Biol Chem, 288(38):27273–27286, Sep 2013.

[170] David W. Piston and Gert-Jan Kremers. Fluorescent protein fret: the good, the bad and the ugly. Trends in Biochemical Sciences, 32(9):407 – 414, 2007.

[171] Jesse Placone, Lijuan He, Nuala Del Piccolo, and Kalina Hristova. Strong dimerization of wild-type erbb2/neu transmembrane domain and the oncogenic val664glu mutant in mammalian plasma membranes. Biochim Biophys Acta, 1838(9):2326–2330, Sep 2014.

[172] Jesse Placone and Kalina Hristova. Direct assessment of the effect of the gly380arg achondroplasia mutation on fgfr3 dimerization using quantitative imaging fret. PLoS One, 7(10):e46678, 2012.

[173] Jennifer B Ptacek, Anne P B Edwards, Lisa L Freeman-Cook, and Daniel DiMaio. Packing contacts can mediate highly specific interactions between artificial transmembrane proteins and the pdgfbeta receptor. Proc Natl Acad Sci U S A, 104(29):11945–11950, Jul 2007.

[174] Yan Qin, Philip J Dittmer, J Genevieve Park, Katarina B Jansen, and Amy E Palmer. Measuring steady-state and dynamic endoplasmic reticulum and golgi zn2+ with genetically encoded sensors. Proc Natl Acad Sci U S A, 108(18):7351–7356, May 2011.

[175] Anne-Catherine Raby, Benjamin Holst, Emmanuel Le Bouder, Constantino Diaz, Edgardo Ferran, Laurence Conraux, Jean-Claude Guillemot, Barbara Coles, Ann Kift-Morgan, Chantal S Colmont, Tamas Szakmany, Pascual Ferrara, Judith E Hall, Nicholas Topley, and Mario O Labéta. Targeting the TLR co-receptor CD14 with TLR2-derived peptides modulates immune responses to pathogens. Science Translational Medicine, 5(185ra64), 2013.

[176] Ingrid Remy, Ian A Wilson, and Stephen W Michnick. Erythropoietin receptor activation by a ligand-induced conformational change. Science, 283:990–993, 1999.

[177] Eliran Moshe Reuven, Avner Fink, and Yechiel Shai. Regulation of innate immune responses by transmembrane interactions: Lessons from the {TLR} family. Biochimica et Biophysica Acta (BBA) - Biomembranes, 1838(6):1586 – 1593, 2014. Membrane Structure and Function: Relevance in the Cell's Physiology, Pathology and Therapy.

[178] William P Russ and Donald M. Engelman. The gxxxg motif: A framework for transmembrane helix-helix association. Journal of Molecular Biology, 296:911–916, 2000.

[179] T Rutledge, P Cosson, N Manolios, J S Bonifacino, and R D Klausner. Transmembrane helical interactions: zeta chain dimerization and functional association with the t cell antigen receptor. EMBO J, 11(9):3245–3254, Sep 1992.

[180] Neta Sal-Man, Doron Gerber, Itai Bloch, and Yechiel Shai. Specificity in transmembrane helix-helix interactions mediated by aromatic residues. Journal of Biological Chemistry, 282(27):19753–19761, 2007.

[181] Neta Sal-Man, Doron Gerber, and Yechiel Shai. The identification of a minimal dimerization motif qxxs that enables homo- and hetero-association of transmembrane helices in vivo. Journal of Biological Chemistry, 280(29):27449–27457, 2005.

[182] Neta Sal-Man, Doron Gerber, and Yechiel Shai. Proline localized to the interaction interface can mediate self-association of transmembrane domains. Biochim Biophys Acta, 1838(9):2313–2318, Sep 2014.

[183] Neta Sal-Man and Yechiel Shai. Arginine mutations within a transmembrane domain of tar, an escherichia coli aspartate receptor, can drive homodimer dissociation and heterodimer association in vivo. Biochemical Journal, 385(Pt 1):29–36, 01 2005.

[184] Deanne W Sammond, Catherine Joce, Ryan Takeshita, Sara E McQuate, Nilanjan Ghosh, Jennifer M Martin, and Hang Yin. Transmembrane peptides used to investigage the homo-oligomeric interface and binding hotspot of latent membrane protein 1. Biopolymers, 95(11):772–784, 2011.

[185] Sarvenaz Sarabipour, Robin B. Chan, Bowen Zhou, Gilbert Di Paolo, and Kalina Hristova. Analytical characterization of plasma membrane-derived vesicles produced via osmotic and chemical vesiculation. Biochimica et Biophysica Acta (BBA) - Biomembranes, 1848(7):1591 – 1598, 2015.

[186] Sarvenaz Sarabipour and Kalina Hristova. Glycophorin a transmembrane domain dimerization in plasma membrane vesicles derived from cho, hek 293t, and a431 cells. Biochim Biophys Acta, 1828(8):1829–1833, Aug 2013.

[187] Elizabeth H. Scheideman, Sara A. Marlatt, Yanhua Xie, Yani Hu, Richard E. Sutton, and Daniel DiMaio. Transmembrane protein aptamers that inhibit ccr5 expression and hiv coreceptor function. Journal of Virology, 86(19):10281–10292, 2012.

[188] Dirk Schneider and Donald M. Engelman. Involvement of transmembrane domain interactions in signal transduction by α/β integrins. The Journal of Biological Chemistry, 279:9840–9846, 2004.

[189] RE Scott. Plasma membrane vesiculation: a new technique for isolation of plasma membranes. Science, 194(4266):743–745, 1976.

[190] Alessandro Senes, Mark Gerstein, and Donald M. Engelman. Statistical analysis of amino acid patterns in transmembrane helices: The gxxxg motif occurs frequently and in association with β-branched residues at neighboring positions. Journal of Membrane Biology, 296:921–936, 2000.

[191] Erdinc Sezgin, Hermann-Josef Kaiser, Tobias Baumgart, Petra Schwille, Kai Simons, and Ilya Levental. Elucidating membrane structure and protein behavior using giant plasma membrane vesicles. Nature Protocols, 7:1042–1051, 2012.

[192] W R Sherman and E Robins. Fluorescence of substituted 7-hydroxycoumarins. Anal Chem, 40:803–805, 1968.

[193] Peter F Slivka, Johnny Wong, Gregory A Caputo, and Hang Yin. Peptide probes for transmembrane domains. ACS Chemical Biology, 3:402–411, 2008.

[194] Ricky Soong, Mikhail Merzlyakov, and Kalina Hristova. Hill coefficient analysis of transmembrane helix dimerization. Journal of Membrane Biology, 230:49–55, 2009.

[195] Timothy J Stevens and Isaiah T Arkin. Do more complex organisms have a greater proportion of membrane proteins in their genomes? PROTEINS: Structure, Function, and Genetics, 39:417–420, 2000.

[196] Cameron R Stewart, Lynda M Stuart, Kim Wilkinson, Janine M van Gils, Jiusheng Deng, Annett Halle, Katey J Rayner, Laurent Boyer, Ruiqin Zhong, Willaim A Frazier, Adam Lacy-Hulbert, Joseph El Khoury, Douglas T Golenbock, and Kathryn J Moore. Cd36 ligands promote sterile inflammation through assembly of a Toll-like receptor 4 and 6 heterodimer. Nature Immunology, 11(2):155–161, 2010.

[197] Koichi Tabeta, Kasper Hoebe, Edith M Janssen, Xin du, Philippe George, Karine Crozat, Suzanne Mudd, Navjiwan Mann, Sosathya Sovath, Jason Goode, Louis Shamel, Anat A Herskovits, Daniel A Portnoy, Michael Cooke, Lisa M Tarantino, Tim Wiltshire, Benjamin E

Steinberg, Sergio Grinstein, and Bruce Beutler. The Unc93b1 mutation 3d disrupts exogenous antigen presentation and signaling via Toll-like receptors 3, 7 and 9. Nature Immunology, 7(2):156–164, 2006.

[198] Michiaki Takagi. Toll-like receptor - a potent driving force behind rheumatoid arthritis. Journal of Clinical and Experimental Hematopathology, 51:77–84, 2011.

[199] Koichiro Takahashi, Takuma Shibata, Sachiko Akashi-Takamura, Takashi Kiyokawa, Yasutaka Wakabayashi, Natsuko Tanimura, Toshihiko Kobayashi, Fumi Matsumoto, Ryutaro Fukui, Taku Kouro, Yoshinori Nagai, Kiyoshi Takatsu, Shin-ichiroh Saitoh, and Kensuke Miyake. A protein associated with toll-like receptor (tlr) 4 (prat4a) is required for tlr-dependent immune responses. The Journal of Experimental Medicine, 204(12):2963–2976, 2007.

[200] Shogo Takashiba, Thomas E Van Dyke, Salomon Amar, Yoji Murayama, Aubrey W Soskolne, and Lior Shapira. Differentiation of monocytes to macrophages primes cells for lipopolysaccharide stimulation via accumulation of cytoplasmic nuclear factor b. Infection and Immunity, 67(11):5573–5578, 11 1999.

[201] Osamu Takeuchi and Shizuo Akira. Pattern recognition receptors and inflammation. Cell, 140:805–820, 2010.

[202] Kristina Talbert-Slagle and Daniel DiMaio. The bovine papillomavirus e5 protein and the pdgf beta receptor: it takes two to tango. Virology, 384(2):345–351, Feb 2009.

[203] Kristina Talbert-Slagle, Sara Marlatt, Francisco N Barrera, Ekta Khurana, Joanne Oates, Mark Gerstein, Donald M Engelman, Ann M Dixon, and Daniel Dimaio. Artificial transmembrane oncoproteins smaller than the bovine papillomavirus e5 protein redefine sequence requirements for activation of the platelet-derived growth factor beta receptor. J Virol, 83(19):9773–9785, Oct 2009.

[204] Natsuko Tanimura, Shinichiroh Saitoh, Fumi Matsumoto, Sachiko Akashi-Takamura, and Kensuke Miyake. Roles for LPS-dependent interaction and relocation of TLR4 and TRAM in TRIF-signaling. Biochemical and Biophyscial Research Communications, 368:94–99, 2008.

[205] Hiromi Tanji, Umeharu Ohto, Takuma Shibata, Kensuke Miyake, and Toshiyuki Shimizu. Structural reorganization of the Toll-like receptor 8 dimer induced by agonistic ligands. Science, 339:1426–1429, 2013.

[206] Richard I. Tapping. Innate immune sensing and activation of cell surface Toll-like receptors. Seminars in Immunology, 21:175–184, 2009.

[207] Sandra Thibault, Michaël Imbeault, Mélanie R. Tardif, and Michel J. Tremblay. TLR5 stimulation is sufficient to trigger reactivation of latent hiv-1 provirus in t lymphoid cells and activate virus gene expression in central memory cd4+ t cells. Virology, 389(1–2):20 – 25, 2009.

[208] Nathalie Thieblemont and Samuel D Wright. Transport of bacterial lipopolysaccharide to the Golgi Apparatus. Journal of Experimental Medicine, 190:523–534, 1999.

[209] Mireille Treeby, Jožica Vašl, Peter Ota, Jožica Friedrich, and Roman Jerala. Different functional role of domain boundaries of Toll-like receptor 4. Biochemical and Biophyscial Research Communications, 381:65–69, 2009.

[210] Martha Triantafilou, Frederick G J Gamper, Rowenna M Haston, Marios Angelos Mouratis, Siegfried Morath, Thomas Hartung, and Kathy Triantafilou. Membrane sorting of Toll-like receptor (TLR)-2/6 and TLR2/1 heterodimers at the cell surface determines heterotypic assoications with CD36 and intracellular targeting. The Journal of Biological Chemistry, 281:331002–31011, 2006.

[211] Martin B Ulmschneider, Jakob P Ulmschneider, Nina Schiller, B A Wallace, Gunnar von Heijne, and Stephen H White. Spontaneous transmembrane helix insertion thermodynamically mimics translocon-guided insertion. Nat Commun, 5:4863, 2014.

[212] Himesha Vandebona, Marina Ali, Michael Amon, Veronika Bender, and Nicholas Manolios. Immunoreceptor transmembrane peptides and their effect on natural killer (nk) cell cytotoxicity. Protein Pept Lett, 13(10):1017–1024, 2006.

[213] M T Montero Vega and A de Andres Martin. The significance of toll-like receptors in human diseases. Alergologia et immunopathologia, 37:252–263, 2009.

[214] G. Vereb, J. Szöllősi, J. Matkó, P. Nagy, T. Farkas, L. Vígh, L. Mátyus, T. A. Waldmann, and S. Damjanovich. Dynamic, yet structured: The cell membrane three decades after the singer–nicolson model. Proceedings of the National Academy of Sciences, 100(14):8053–8058, 2003.

[215] Gunnar von Heijne. The membrane protein universe: what's out there and why bother? Journal of Internal Medicine, 261:543–557, 2007.

[216] Yasutaka Wakabayashi, Makiko Kobayashi, Sachiko Akashi-Takamura, Natsuko Tanimura, Kazunori Konno, Koichiro Takahashi, Takashi Ishii, Taketoshi Mizutani, Hideo Iba, Taku Kouro, Satoshi Takaki, Kiyoshi Takatsu, Yoshiya Oda, Yasushi Ishihama, Shin-ichiroh Saitoh, and Kensuke Miyake. A protein associated with toll-like receptor 4 (prat4a) regulates cell surface expression of tlr4. The Journal of Immunology, 177(3):1772–1779, 2006.

[217] Xin M Wang, Julianne T Djordjevic, Veronica Bender, and Nicholas Manolios. T cell antigen receptor (tcr) transmembrane peptides colocalize with tcr, not lipid rafts, in surface membranes. Cell Immunol, 215(1):12–19, Jan 2002.

[218] Xin M Wang, Julianne T Djordjevic, Nozomu Kurosaka, Stephen Schibeci, Lianne Lee, Peter Williamson, and Nicholas Manolios. T-cell antigen receptor peptides inhibit signal transduction within the membrane bilayer. Clin Immunol, 105(2):199–207, Nov 2002.

[219] Stephen H White. Translocons, thermodynamics, and the folding of membrane proteins. FEBS Lett, 555(1):116–121, Nov 2003.

[220] Stephen H White. The progress of membrane protein structure determination. Protein Science, 13:1948–1949, 2004.

[221] Stephen H White and Gunnar von Heijne. The machinery of membrane protein assembly. Curr Opin Struct Biol, 14(4):397–404, Aug 2004.

[222] Stephen H White and Gunnar von Heijne. Transmembrane helices before, during, and after insertion. Curr Opin Struct Biol, 15(4):378–386, Aug 2005.

[223] Stephen H White and Gunnar von Heijne. How translocons select transmembrane helices. Annu Rev Biophys, 37:23–42, 2008.

[224] Remigiusz Worch, Christian Bökeland Sigfried Höfinger, Petra Schwille, and Thomas Weidemann. Focus on composition and interaction potential of single-pass transmembrane domains. Proteomics, 10:4196–4208, 2010.

[225] Hao Wu. Higher-order assemblies in a new paradigm of signal transduction. Cell, 153, 2013.

[226] Fang Xiao Zhou, Melanie J. Cocco, William P. Russ, Axel T. Brunger, and Donald M. Engelman. Interhelical hydrogen bonding drives strong interactions in membrane proteins. Nature Structure Mol Biology, 7(2):154–160, 02 2000.

[227] Yi Yang, Bei Liu, Jie Dai, Pramod K Srivastava, David J Zammit, Leo Lefrançois, and Zihai Li. Heat shock protein gp96 is a master chaperone for Toll-like receptors and is important in the innate function of macrophages. Immunity, 26:215–226, 2007.

[228] Muhammed A Yildirim, Kwang-Il Goh, Michael E Cusick, Albert-László Barabási, and Marc Vidal. Drug-target network. Nature Biotechnology, 25:1119–1126, 2007.

[229] Hang Yin, Rustem I. Litvinov, Gaston Vilaire, Hua Zhu, Wei Li, Gregory A. Caputo, David T. Moore, James D. Lear, John W. Weisel, William F. DeGrado, and Joel S. Bennett. Activation of platelet iib3 by an exogenous peptide corresponding to the transmembrane domain of iib. Journal of Biological Chemistry, 281(48):36732–36741, 2006.

[230] Hang Yin, Joanna S Slusky, Bryan W Berger, Robin S Walters, Gaston Vilaire, Rustem I Litvinov, James D Lear, Gregory A Caputo, Joel S Bennett, and Willaim F DeGrado. Computational design of peptides that target transmembrane helices. Science, 315:1817–1822, 2007.

[231] Qian Yin, Tian-Min Fu, Jixi Li, and Hao Wu. Structural biology of innate immunity. Annual Review of Immunology, 33:13.1–13.24, 2015.

[232] Min You, Edwin Li, William C Wimley, and Kalina Hristova. Forster resonance energy transfer in liposomes: measurements of transmembrane helix dimerization in the native bilayer environment. Anal Biochem, 340(1):154–164, May 2005.

[233] Tomasz Zal and Nicholas R J Gascoigne. Using live fret imaging to reveal early protein-protein interactions during t cell activation. Curr Opin Immunol, 16(5):674–683, Oct 2004.

[234] Ivan Zanoni, Renato Ostuni, Lorri R Marek, Simona Barresi, Roman Barbalat, Gregory M Barton, Francesca Granucci, and Jonathan C Kagan. Cd14 controls the LPS-induced endocytosis of Toll-like receptor 4. Cell, 147:868–880, 2011.

[235] Kol A Zarember and Paul J Godowski. Tissue expression of human Toll-like receptors and differential regulation of Toll-like receptor mRNAs in Leukocytes in response to microbes, their products, and cytokines. Journal of Immunology, 168:554–561, 2002.

[236] Fangfa Zeng, Wen Yang, Jie Huang, Yuan Chen, and Yong Chen. Determination of the lowest concentrations of aldehyde for completely fixing various cellular structures by real-time imaging and quantification. Histochemical Cell Biology, 139:735–749, 2013.

[237] Haifeng Zhang, Puei Nam Tay, Weiping Cao, Wei Li, and Jinhua Lu. Integrin-nucleated Toll-like receptor (TLR) dimerization revelas subcellular targeting of TLRs and distinct mechanisms of TLR4 activation and signaling. FEBS Letters, 532:171–176, 2002.

[238] Gang Zheng, Allan M Torres, Marina Ali, Nicholas Manolios, and William S Price. Nmr study of the structure and self-association of core peptide in aqueous solution and dpc micelles. Biopolymers, 96(2):177–180, 2011.

[239] Hua Zhu, Douglas G Metcalf, Craig N Streu, Paul C Billings, Willaim F DeGrado, and Joel S Bennett. Specificity for homooligomer versus heterooligomer formation in integrin transmembrane helices. Journal of Molecular Biology, 401:882–891, 2010.

Appendix A

Isolated Toll-like receptor transmembrane domains are capable of oligomerization Supplementary Information

This appendix contains the supplementary text, figures, and tables that were published as J. I. Godfroy III, M. Roostan, Y. S. Moroz, I. V. Korendovych, and H. Yin. "Isolated Toll-like receptor transmembrane domains are capable of oligomerization" *PLoS ONE.* 7:e48875, **2012**. [84]

A.1 Supplementary Material and Methods

A.1.1 Proper membrane insertion of chimeric proteins

To verify that the TMD constructs for the Toll-like receptors were being properly integrated in the bacterial membrane, a minimal media growth assay was performed. In this assay, a bacterial strain that lacks the maltose protein, PD28 [45], were transformed with the plasmids encoding the TMD of interest. The PD28 bacteria were grown in minimal media with maltose as the sole carbon source. Cell density was monitored at OD_{595} and corresponds to the efficiency of membrane integration. We saw that all designed TLR TMDs were able to properly insert into the bacterial membranes as indicated by the increasing OD_{595} (Figure A.2). The ΔTM construct was not capable of inserting and showed no growth as was expected.

A.1.2 Analytical ultracentrifugation

Equilibrium sedimentation was used primarily to determine the association state of TLR2, TLR6, and TLR2-TLR6. The experiments were performed in a Beckman XL-I analytical ultracen-

trifuge (Beckman Coulter) using six-channel carbon-epoxy composite centerpieces at 25°C. Peptides were co-dissolved in trifluoroethanol (TFE) and C14-betaine. The organic solvent was removed using dry nitrogen gas and the resulting thin film of peptide/detergent mixture was dried overnight. The sample was then dissolved in buffer previously determined to match the density of the detergent component (100 mM HEPES buffer, pH = 7.4, containing 25% D_2O). The final concentration of C14-betaine is 10 mM in all of the samples. Peptide concentrations were determined by UV-Vis on the Beckman Coulter XL-I and dilutions were carried out to get concentrations in the desired absorbance ranges of the instrument (0.3-1) using the following extinction coefficients: 39,300 M^{-1} cm^{-1} at 400 nm for coumarin labeled peptides and 69,000 M^{-1} cm^{-1} at 495 nm for FITC labeled peptides. Data at different measurement speeds (30, 35 krpm) and different peptide:detergent ratios were analyzed by global curve-fitting of radial concentration gradients (measured using optical absorption) to the sedimentation equilibrium equation. Absorbance at both 400 nm and 495 nm was measured. Peptide partial specific volumes were calculated using previously described methods [46] and residue molecular weights corrected for the 25% D_2O exchange expected for the density-matched buffer. The solvent density (1.031 g/ml) was calculated using the program Sednterp [116]. These coefficients were multiplied by the molar detergent ratio concentration units.

In order to estimate the association state of the peptides, the sedimentation equilibrium was fitted to a single species model:

$$Abs = E + \epsilon * c_0 * l * exp[\frac{\omega^2}{2 * R * T} * M * (r^2 - r_0^2)] \tag{A.1}$$

where E = baseline (zero concentration) absorbance, c_o is the peptide:detergent ratio of the peptide at r_o, ϵ is the molar extinction coefficient, l is the optical path length, $\omega = 2\pi * RPM$, R= $8.3144 * 10^7$ erg K^{-1} mol^{-1} , T is temperature in K, M is the buoyant molecular weight of the peptide.

Molecular weight was obtained from the buoyant molecular weight using:

$$M_w = M(1 - \bar{\nu} * \rho) \tag{A.2}$$

where M is the buoyant molecular weight, $\bar{\nu}$ is the partial specific volume, and ρ is the solution density.

The results showed that TLR2 exists in a monomer-dimer-tetramer equilibrium and TLR6 exists in a monomer-dimer equilibrium. For the heterotypic interaction, when TLR2 and TLR6 were both present in the same sample cell, the apparent smaller average molecular weight of the species monitored at 495 nm (where only TLR2 absorbs) indicates that TLR2 and TLR6 are also interacting. The resulting fits are shown in Supplementary Figures A.3-A.5.

A.2 Supplementary Tables

Table A.1: Homotypic TLR interaction grouping information using Tukey-Kramer method and 95.0% confidence level (p = 0.05).

TMD	**N**	**Mean**	**Grouping**					
GpA	21	1.000	A					
ΔTM	22	0.0922						F
TLR1	22	0.0922				E		
TLR2	17	0.7829	A	B	C			
TLR3	22	0.8032	A	B	C			
TLR4	22	0.5620			C	D	E	
TLR5	23	0.6087		B	C	D	E	
TLR6	21	0.5764		B	C	D	E	
TLR7	22	0.4947				D	E	
TLR8	19	0.7486		B	C	D		
TLR9	23	0.7992	A	B	C			
TLR10	19	0.8259	A	B				

Means that do not share a letter in grouping correspond to homotypic TMD interactions that are not significantly different at 95% confidence (p<0.05).

Table A.2: Homotypic TMD interaction p-values using Tukey-Kramer method

TMD	*GpA*	ΔTM	*TLR1*	*TLR2*	*TLR3*	*TLR4*	*TLR5*	*TLR6*	*TLR7*	*TLR8*	*TLR9*	*TLR10*
GpA	-	0.0000	0.0000	0.1824	0.2156	0.0000	0.0000	0.0000	0.0000	0.0433	0.1782	0.4526
ΔTM	0.0000	-	0.0000	0.0000	0.0000	0.0000	0.0000	0.0000	0.0000	0.0000	0.0000	0.0000
TLR1	0.0000	0.0000	-	0.0081	0.0009	0.9936	0.8362	0.9781	1.0000	0.0255	0.0009	0.0005
TLR2	0.1824	0.0000	0.0081	-	1.0000	0.2032	0.5585	0.3131	0.0176	1.0000	1.0000	1.0000
TLR3	0.2156	0.0000	0.0009	1.0000	-	0.0593	0.2686	0.1126	0.0024	0.9999	1.0000	1.0000
TLR4	0.0000	0.0000	0.9936	0.2032	0.0593	-	1.0000	1.0000	0.9992	0.4108	0.0626	0.0346
TLR5	0.0000	0.0000	0.8362	0.5585	0.2686	1.0000	-	1.0000	0.9309	0.8114	0.2826	0.1737
TLR6	0.0000	0.0000	0.9781	0.3131	0.1126	1.0000	1.0000	-	0.9957	0.5607	0.1190	0.0680
TLR7	0.0000	0.0000	1.0000	0.0176	0.0024	0.9992	0.9309	0.9957	-	0.0518	0.0024	0.0013
TLR8	0.0433	0.0000	0.0255	1.0000	0.9999	0.4108	0.8114	0.5607	0.0518	-	1.0000	0.9985
TLR9	0.1782	0.0000	0.0009	1.0000	1.0000	0.0626	0.2826	0.1190	0.0024	1.0000	-	1.0000
TLR10	0.4526	0.0000	0.0005	1.0000	1.0000	0.0346	0.1737	0.0680	0.0013	0.9985	1.0000	-

Intersections correspond to the p-value for the TLR homotypic interaction being compared.

Table A.3: GpA heterotypic interaction grouping information using Tukey-Kramer Method and 95% confidence interval ($p<0.05$).

TMD*	**N**	**Mean**	**Grouping**		
*Poly-Leu**	30	1.000	A	B	
*TMD5**	28	1.1703	A		
Integrin α_{IIb}*	26	1.0189	A	B	C
*TLR1**	28	0.8934		B	C
*TLR2**	28	0.7284			C
*TLR4**	26	1.1905	A		
*TLR5**	28	0.8934		B	C
*TLR6**	23	1.0451	A	B	C
*TLR10**	30	1.1244	A	B	

Means that do not share a letter in grouping correspond to heterotypic GpA-TMD* interactions that are not significantly different at 95% confidence ($p<0.05$).

Table A.4: GpA TMD heterotypic interaction p-values using Tukey-Kramer method

TMD*	*Poly-Leu**	*TMD5**	*Integrin α_{IIb}**	*TLR1**	*TLR2**	*TLR4**	*TLR5**	*TLR6**	*TLR10**
*Poly-Leu**	-	0.5564	1.000	0.9464	0.0454	0.4245	0.9464	0.9999	0.5564
*TMD5**	0.5564	-	0.7450	0.0445	0.0001	1.0000	0.0446	0.9108	0.9998
*Integrin α_{IIb}**	1.000	0.7450	-	0.8933	0.0337	0.6182	0.8933	1.0000	0.9546
*TLR1**	0.9464	0.0445	0.8933	-	0.6212	0.0268	1.0000	0.7763	0.1568
*TLR2**	0.0454	0.0001	0.0337	0.6212	-	0.0000	0.6211	0.0192	0.0002
*TLR4**	0.4245	1.0000	0.6182	0.0268	0.0000	-	0.0268	0.8277	0.9979
*TLR5**	0.9464	0.0046	0.8933	1.0000	0.6211	0.0268	-	0.7763	0.1569
*TLR6**	0.9999	0.9108	1.0000	0.7763	0.0192	0.8277	0.7763	-	0.9940
*TLR10**	0.5564	0.9998	0.9546	0.1568	0.0002	0.9979	0.1569	0.9940	-

Intersections correspond to the p-value for the GpA-TMD* homotypic interaction being compared.

Table A.5: TLR2 heterotypic interaction grouping information using Tukey-Kramer Method and 95% confidence interval ($p<0.05$).

TMD*	**N**	**Mean**	**Grouping**			
*Poly-Leu**	30	1.0000	A	B		
*TMD5**	21	1.1904	A			
Integrin α_{IIb}*	19	0.7609			C	
*TLR1**	26	0.2198				D
*TLR2**	25	0.1930				D
*TLR4**	23	1.1386	A			
*TLR5**	25	0.9233		B	C	
*TLR6**	30	0.2588				D
*TLR10**	26	0.3877				D

Means that do not share a letter in grouping correspond to heterotypic TLR2-TMD* interactions that are not significantly different at 95% confidence ($p<0.05$).

Table A.6: TLR2 TMD heterotypic interaction p-values using Tukey-Kramer method

TMD*	*Poly-Leu**	*TMD5**	*Integrin α_{IIb}**	*TLR1**	*TLR2**	*TLR4**	*TLR5**	*TLR6**	*TLR10**
*Poly-Leu**	-	0.1080	0.0179	0.0000	0.0000	0.4574	0.9546	0.0000	0.0000
*TMD5**	0.1080	-	0.0000	0.0000	0.0000	0.9983	0.0050	0.0000	0.0000
*Integrin α_{IIb}**	0.0179	0.0000	-	0.0000	0.0000	0.0000	0.3651	0.0000	0.0000
*TLR1**	0.0000	0.0000	0.0000	-	1.0000	0.0000	0.0000	0.9995	1.0000
*TLR2**	0.0000	0.0000	0.0000	1.0000	-	0.0000	0.0000	0.9822	0.0816
*TLR4**	0.4574	0.9983	0.0000	0.0000	0.0000	-	0.0449	0.0000	0.0000
*TLR5**	0.9546	0.0050	0.3651	0.0000	0.0000	0.0449	-	0.0000	0.0000
*TLR6**	0.0000	0.0000	0.0000	0.9995	0.9822	0.0000	0.0000	-	0.5136
*TLR10**	0.0000	0.0000	0.0000	0.2033	0.0816	0.0000	0.0000	0.5136	-

Intersections correspond to the p-value for the TLR2-TMD* homotypic interaction being compared.

Table A.7: TLR1 heterotypic interaction grouping information using Tukey-Kramer Method and 95% confidence interval ($p<0.05$).

TMD*	**N**	**Mean**	**Grouping**			
*Poly-Leu**	29	1.0000	A	B		
*TMD5**	28	1.0921	A			
Integrin α_{IIb}*	28	0.7583		B	C	
*TLR1**	28	0.3722				D
*TLR2**	30	0.3243				D
*TLR4**	28	0.8709	A	B	C	
*TLR5**	30	0.6805	A	B	C	
*TLR6**	30	0.3349				D
*TLR10**	28	0.3608				D

Means that do not share a letter in grouping correspond to heterotypic TLR1-TMD* interactions that are not significantly different at 95% confidence ($p<0.05$).

Table A.8: TLR1 TMD heterotypic interaction p-values using Tukey-Kramer method

TMD*	*Poly-Leu**	*TMD5**	*Integrin α_{IIb}**	*TLR1**	*TLR2**	*TLR4**	*TLR5**	*TLR6**	*TLR10**
*Poly-Leu**	-	0.9673	0.0665	0.0000	0.0000	0.8026	0.0018	0.0000	0.0000
*TMD5**	0.9673	-	0.0013	0.0000	0.0000	0.1386	0.0000	0.0000	0.0000
*Integrin α_{IIb}**	0.0665	0.0013	-	0.0001	0.0000	0.9031	0.0000	0.0000	
*TLR1**	0.0000	0.0000	0.0001	-	0.9996	0.0000	0.0036	0.9999	1.0000
*TLR2**	0.0000	0.0000	0.0000	0.9996	-	0.0000	0.0002	1.0000	1.0000
*TLR4**	0.8026	0.1386	0.9031	0.0000	0.0000	-	0.2914	0.0000	0.0000
*TLR5**	0.0018	0.0000	0.9881	0.0036	0.0002	0.2914	-	0.0000	0.0020
*TLR6**	0.0000	0.0000	0.0000	0.9999	1.0000	0.0000	0.0004	-	1.0000
*TLR10**	0.0000	0.0000	0.0000	1.0000	1.0000	0.0000	0.0020	1.0000	-

Intersections correspond to the p-value for the TLR1-TMD* homotypic interaction being compared.

Table A.9: TLR6 heterotypic interaction grouping information using Tukey-Kramer Method and 95% confidence interval ($p<0.05$).

TMD*	**N**	**Mean**	**Grouping**		
*Poly-Leu**	28	1.0000	A		
*TMD5**	30	1.1235	A		
Integrin α_{IIb}*	28	0.6106		B	
*TLR1**	28	0.3316			C
*TLR2**	30	0.2802			C
*TLR4**	30	0.9610	A		
*TLR5**	28	0.6106		B	
*TLR6**	30	0.2564			C
*TLR10**	28	0.3445			C

Means that do not share a letter in grouping correspond to heterotypic TLR6-TMD* interactions that are not significantly different at 95% confidence ($p<0.05$).

Table A.10: TLR6 TMD heterotypic interaction p-values using Tukey-Kramer method

TMD*	*Poly-Leu**	*TMD5**	*Integrin α_{IIb}**	*TLR1**	*TLR2**	*TLR4**	*TLR5**	*TLR6**	*TLR10**
*Poly-Leu**	-	0.0000	0.4378	0.0000	0.0000	0.9990	0.0000	0.0000	0.0000
*TMD5**	0.4378	-	0.0000	0.0000	0.0000	0.0930	0.0000	0.8671	0.0000
*Integrin α_{IIb}**	0.0007	0.0000	-	0.0000	0.0000	0.0079	0.2792	0.0000	0.0000
*TLR1**	0.0000	0.0000	0.0000	-	0.9932	0.0000	0.0001	0.9287	1.0000
*TLR2**	0.0000	0.0000	0.0000	0.9932	-	0.0000	0.0000	1.0000	0.9712
*TLR4**	0.9990	0.0930	0.0079	0.0000	0.0000	-	0.0000	0.0000	0.0000
*TLR5**	0.0000	0.0000	0.2792	0.0001	0.0000	0.0000	-	0.0000	0.0002
*TLR6**	0.0000	0.8671	0.0000	0.9287	1.0000	0.0000	0.0000	-	0.8390
*TLR10**	0.0000	0.0000	0.0000	1.0000	0.9712	0.0000	0.0002	0.8390	-

Intersections correspond to the p-value for the TLR6-TMD* homotypic interaction being compared.

Table A.11: Helical content analysis of synthetic TLR1, TLR2, and TLR6 TMD peptides

TLR1	*200-260 nm*	*205-260 nm*	*210-260 nm*
Helix	99.70%	99.90%	99.90%
Antiparallel	0.00%	0.00%	0.00%
Beta-Turn	2.60%	2.40%	2.20%
Random Coil	0.40%	0.20%	0.30%
Total Sum	102.80%	102.60%	102.50%

TLR2	*200-260 nm*	*205-260 nm*	*210-260 nm*
Helix	99.80%	99.90%	99.90%
Antiparallel	0.00%	0.00%	0.10%
Beta-Turn	2.50%	2.20%	2.00%
Random Coil	0.30%	0.20%	0.30%
Total Sum	102.60%	102.40%	102.30%

TLR6	*200-260 nm*	*205-260 nm*	*210-260 nm*
Helix	99.90%	100.00%	100.00%
Antiparallel	0.00%	0.00%	0.00%
Beta-Turn	2.00%	1.70%	1.60%
Random Coil	0.10%	0.10%	0.20%
Total Sum	102.10%	101.80%	101.80%

A.3 Supplementary Figures

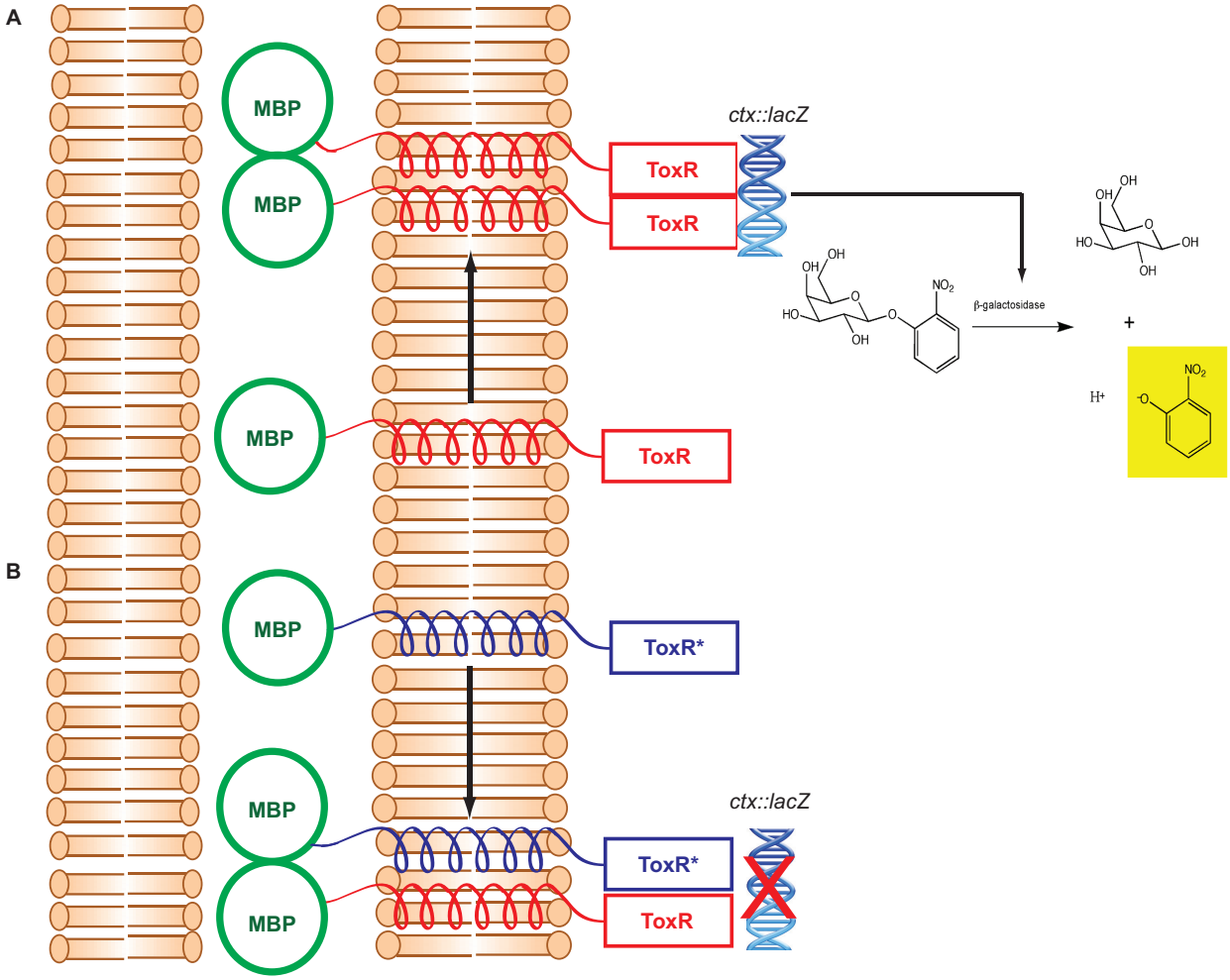

Figure A.1: ToxR assay schematic.
(A) Homotypic interactions are studied using a plasmid that encodes a TMD of interest between a functional ToxR transcriptional activator and a periplasmic directing maltose binding protein. TMD-TMD interactions leads to binding of the cholera toxin promoter that controls lacZ expression in the FHK12 E. coli strain used [104]. Lysis of the cells and addition of the sugar ONPG allows enzyme activity to be monitored by the production of a yellow colorimetric compound. (B) Heterotypic interactions are studied using a knockdown reporter in which two plasmids are expressed, one with the functional ToxR domain, and one with a nonfunctional ToxR* domain that contains a S87H mutation. TMD-TMD interactions involving the TMD encoded along with the ToxR* domain prevent binding of the promoter and enzyme production leading to a reduced signal. MBP maltose binding protein, ctx cholera toxin promoter, lacZ β-galactosidase reporter gene.

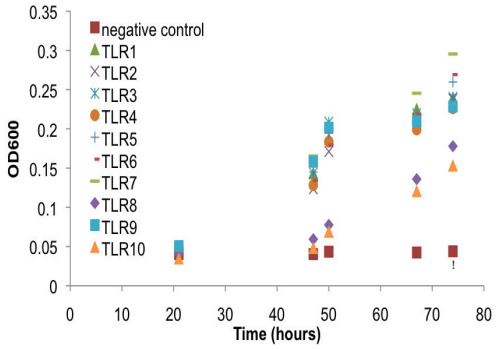

Figure A.2: Control for proper membrane insertion of chimeric TLR ToxR constructs.
Maltose deficient PD28 cells were transformed with plasmids and grown in minimal media. Growth kinetics were monitored over 3 days to determine if constructs were inserting and allowing cells to grown with maltose as the sole carbon source. Growth was observed for all TLR constructs, but not for the TM construct, as expected.

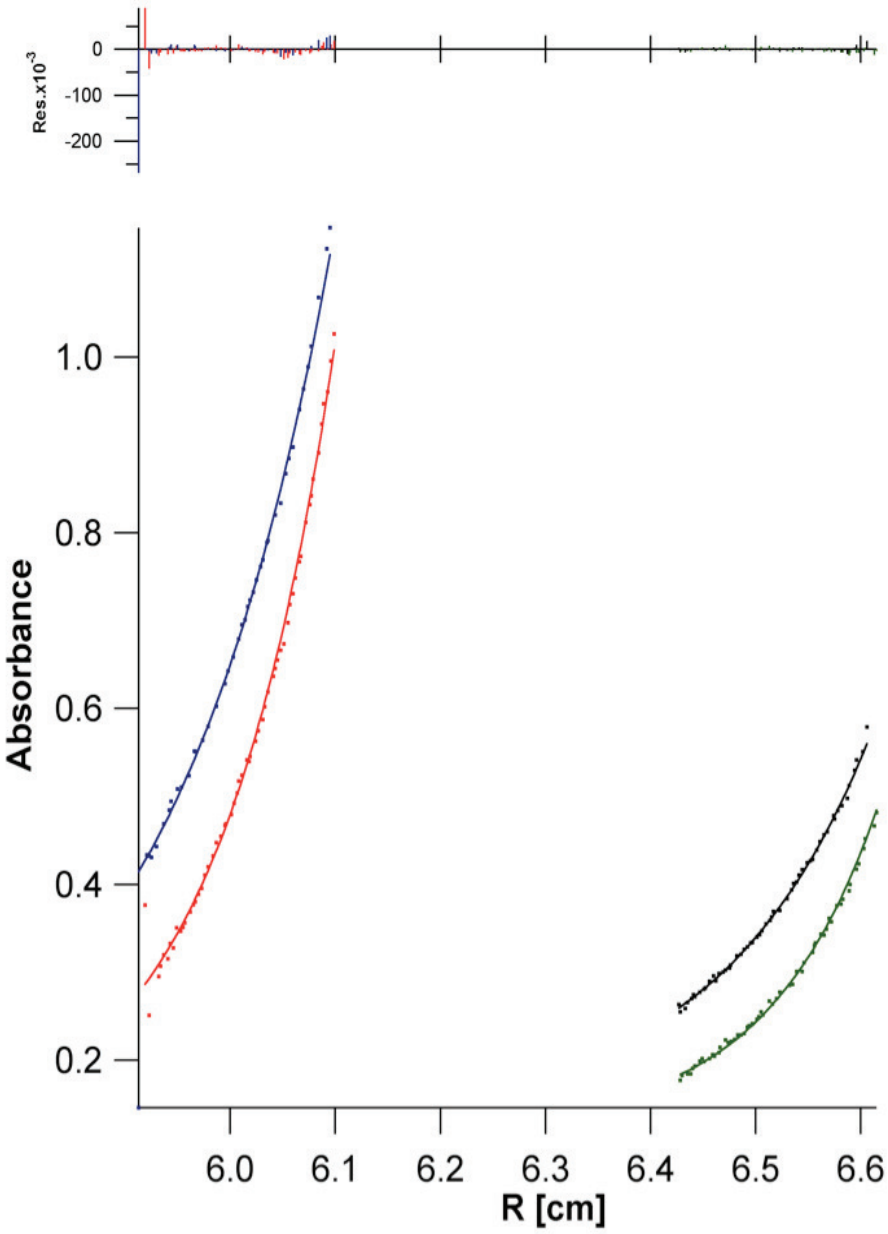

Figure A.3: TLR2 homotypic sedimentation equilibrium AUC.
Sedimentation equilibrium profile at 495 nm of FITC-labeled TLR2 in density matched C14-betaine micelles (10 mM) in HEPES buffer (100 mM, pH 7.4). The partial specific volume and the solution density were fixed at 0.78730 mL/g and 1.031 g/mL, respectively. The data was analyzed using a global fitting routine. The average molecular weight obtained from the fit (14135 $\pm$ 370 Da) corresponds well with TLR2 in a monomer-dimer-tetramer equilibrium.

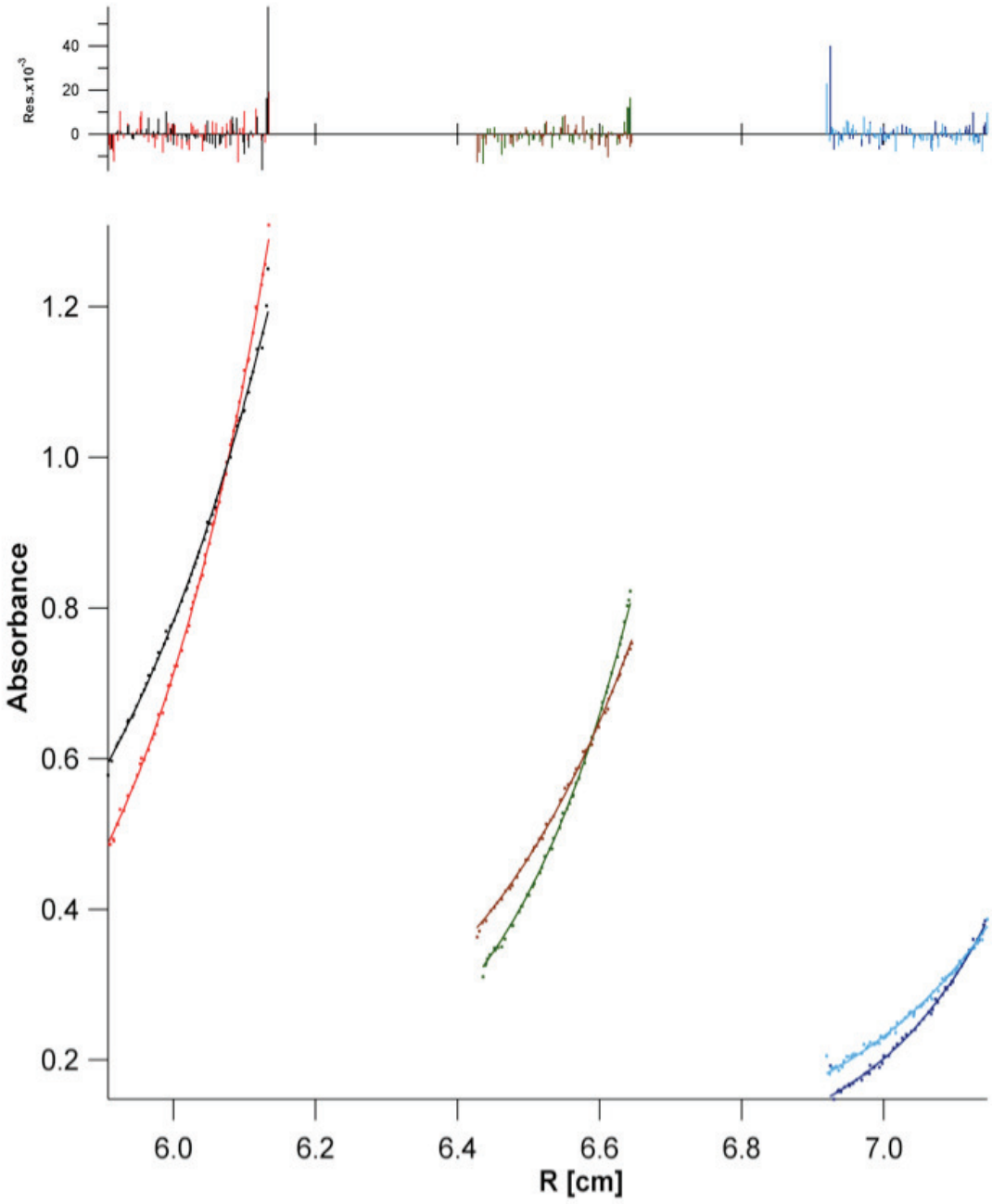

Figure A.4: TLR6 homotypic sedimentation equilibrium AUC.
Sedimentation equilibrium profile at 400 nm of coumarin-labeled TLR6 in density matched C14-betaine micelles (10 mM) in HEPES buffer (100 mM, pH 7.4). The partial specific volume and the solution density were fixed at 0.78705 mL/g and 1.031 g/mL, respectively. The data was analyzed using a global fitting routine. The average molecular weight obtained from the fit (7680 ± 866 Da) corresponds well with TLR6 in a monomer-dimer equilibrium.

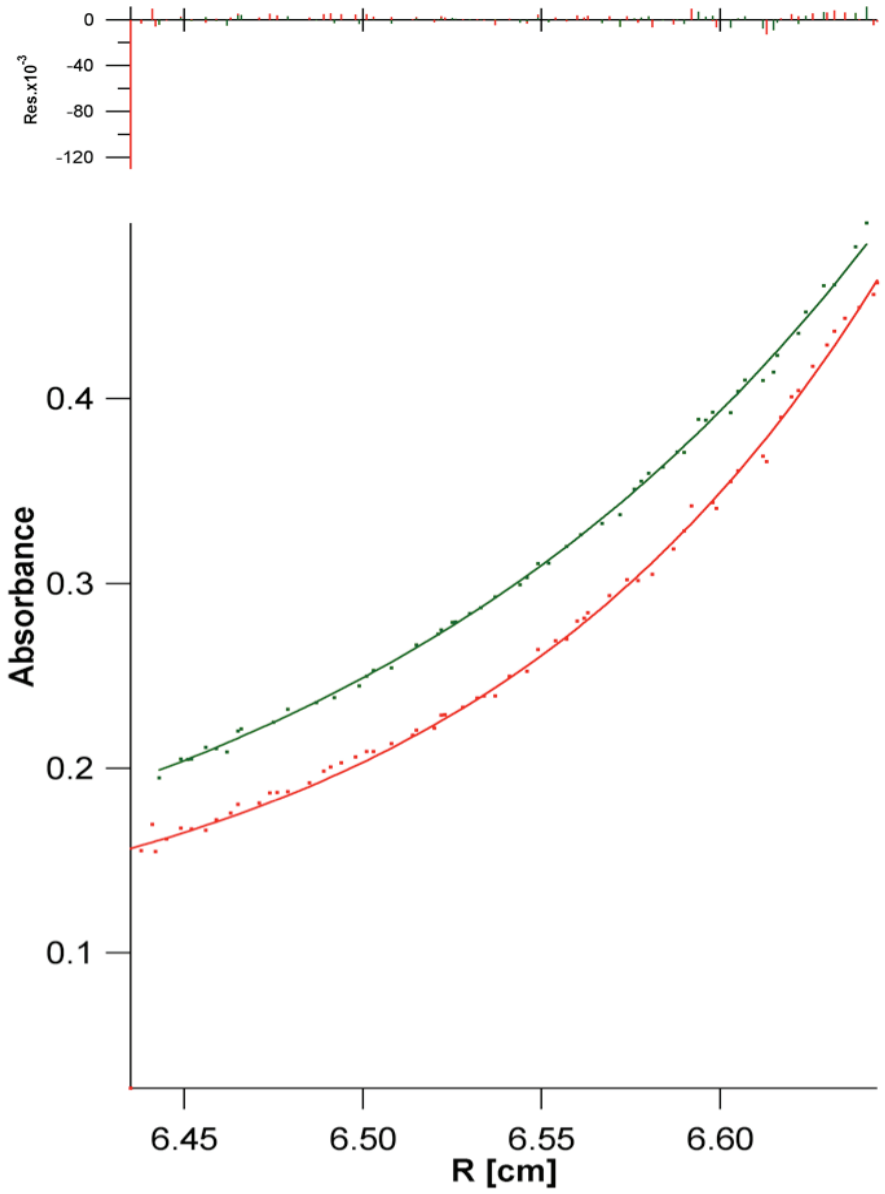

Figure A.5: TLR2-TLR6 heterotypic sedimentation equilibrium AUC.
Sedimentation equilibrium profile at 495 nm of of FITC-labeled TLR2 in density matched C14-betaine micelles (10 mM) in HEPES buffer (100 mM, pH 7.4) in the presence of 2 equiv. of coumarin-labeled TLR6 peptide. The partial specific volume and the solution density were fixed at 0.78730 mL/g and 1.031 g/mL, respectively. The data was analyzed using a global fitting routine. The average molecular weight obtained from the fit (12330 $\pm$ 506 Da) indicates that TLR6 shifts the monomer-dimer equilibrium of TLR2.

Appendix B

Studying interaction and trafficking of Toll-like receptor transmembrane domains in mammalian membranes Supporting Information

B.1 Supplementary Figures

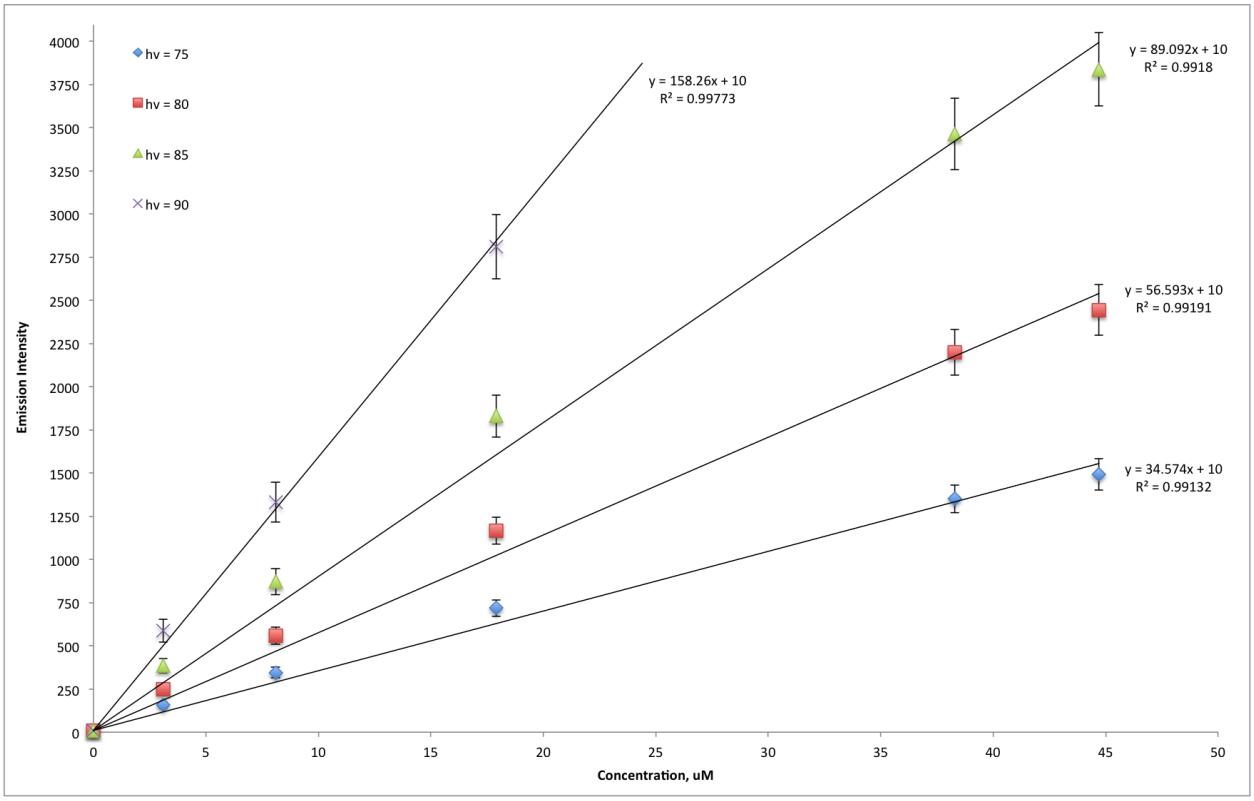

Figure B.1: Calibration curves for EYFP.
EYFP was expressed, purified, and suspended in vesiculation buffer. Protein concentrations were determined by UV-VIS using 83,500 M^{-1} cm^{-1} as the extinction coefficients. EYFP intensity was measured using a 488 nm excitation and a 525/50 nm filter. The slopes from the fits are used to determine the apparent concentration of EYFP inside each vesicle for a given microscope gain setting.

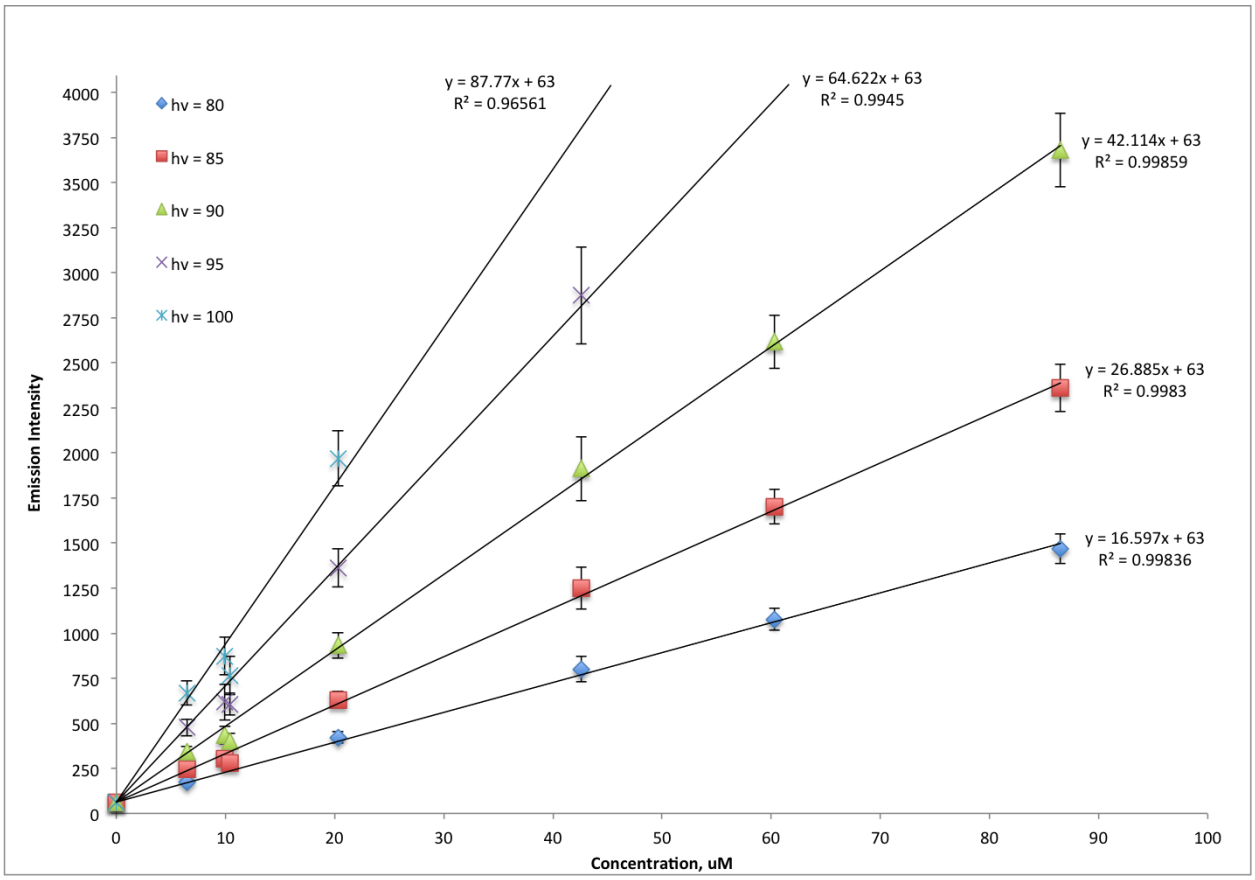

Figure B.2: Calibration curves for mCherry.
mCherry was expressed, purified, and suspended in vesiculation buffer. Protein concentrations were determined by UV-VIS using 72,000 M^{-1} cm^{-1} as the extinction coefficients. mCherry intensity was measured using a 561 nm excitation and a 650 nm LP filter. The slopes from the fits are used to determine the actual concentration of mCherry inside each vesicle.

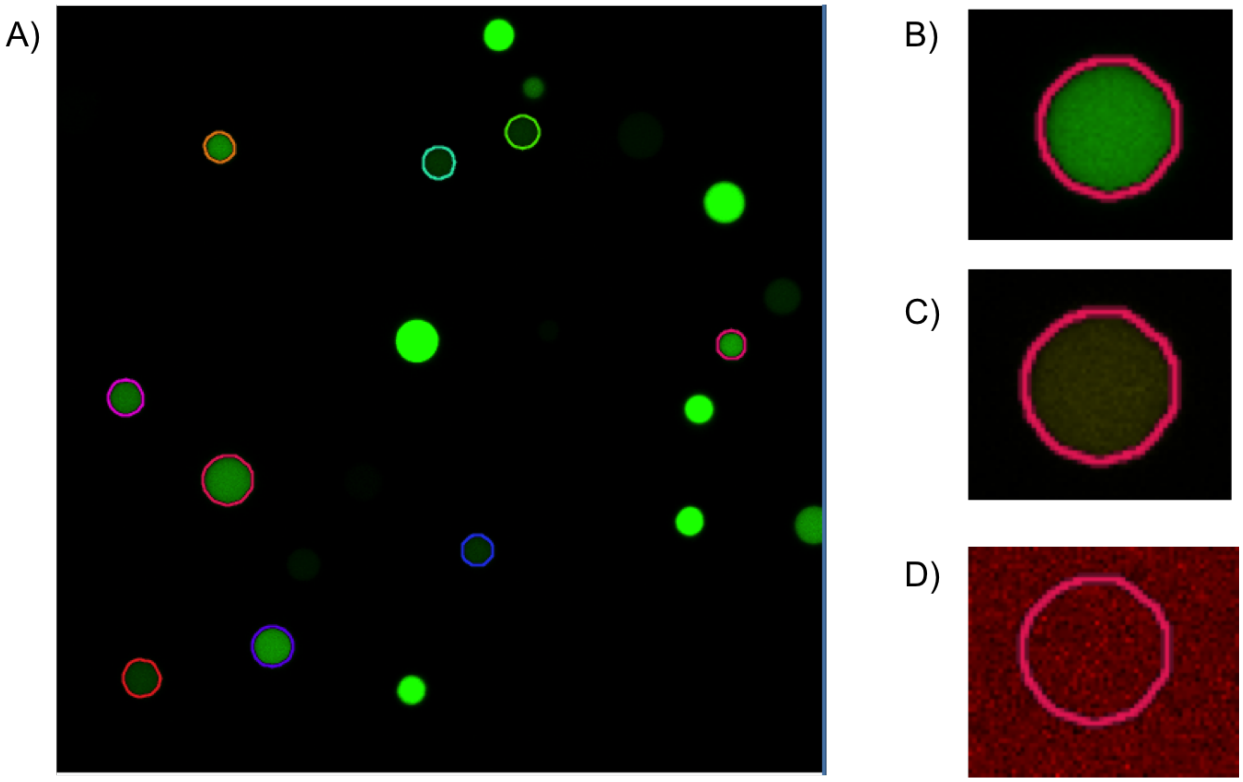

Figure B.3: Donor bleedthrough vesicles.
A) A representative field of view for vesicles produced from cells transfected with pcDNA-EYFP. Three scans were performed in channel series for data collection and analysis. B) Donor scan for EYFP using 488 nm laser and 525/50 filter. C) Sensitized emission scan using the FRET channel, 488 nm laser and 600/50 filter. D) Acceptor scan using a 561 nm laser and 650 LP filter. To determine the bleedthrough the intensity in the Donor scan and FRET scan were compared according to Equation 3.3.

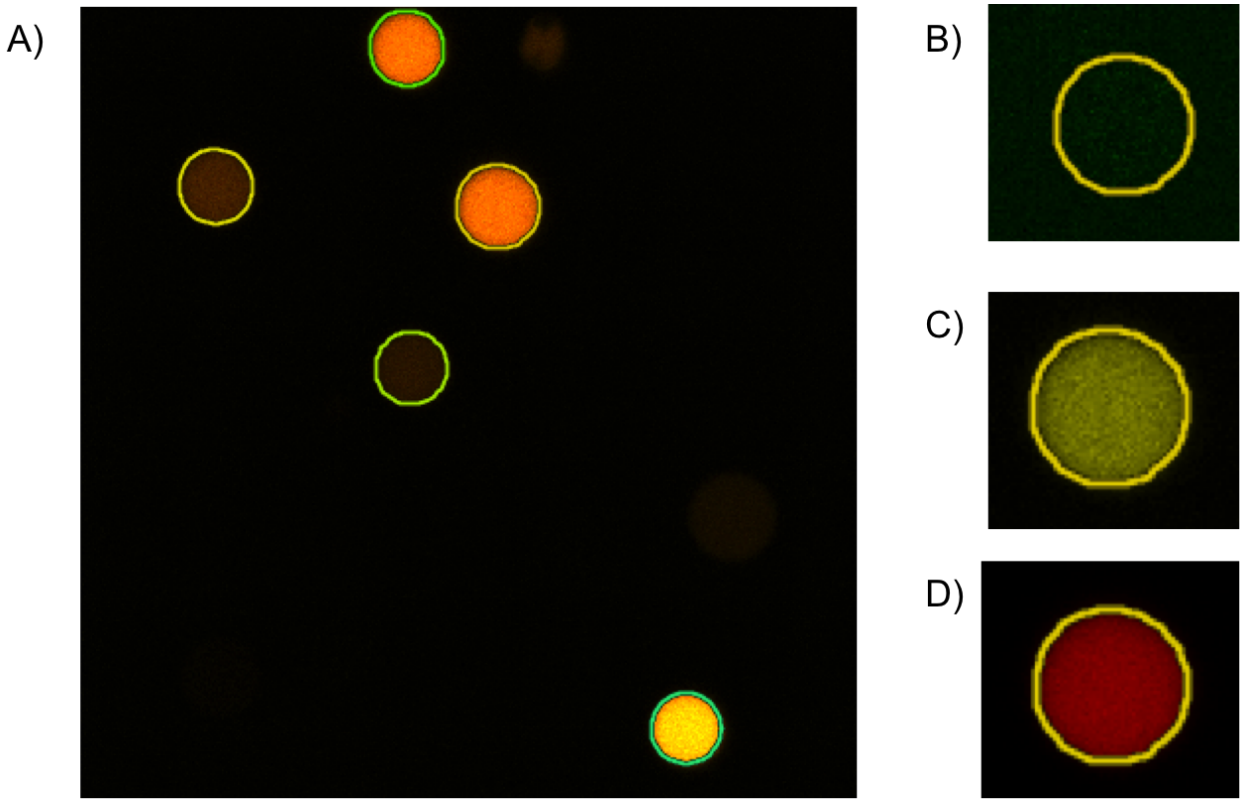

Figure B.4: Acceptor bleedthrough vesicles.
A) A representative field of view for vesicles produced from cells transfected with pcDNA-mCherry. Three scans were performed in channel series for data collection and analysis. B) Donor scan for EYFP using 488 nm laser and 525/50 filter. C) Sensitized emission scan using the FRET channel, 488 nm laser and 600/50 filter. D) Acceptor scan using a 561 nm laser and 650 LP filter. To determine the bleedthrough the intensity in the Donor scan and FRET scan were compared according to Equation 3.4.

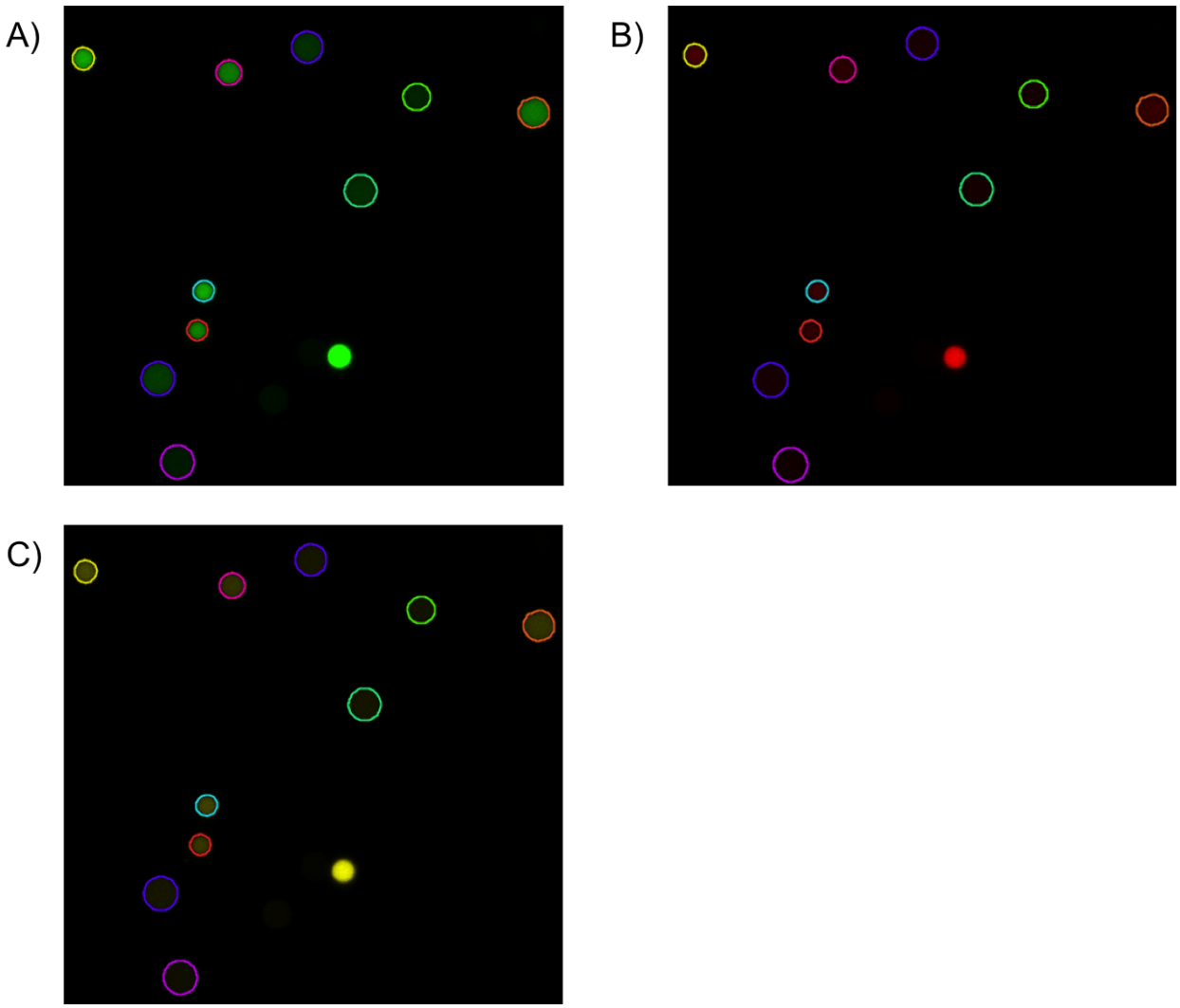

Figure B.5: Gauge factor vesicles.
Vesicles were produced from cells that were transfected with a pcDNA-EYFP-mCherry fusion construct. Three scans were performed in channel series for data collection and analysis. A) Donor scan for EYFP using 488 nm laser and 525/50 filter. B) Acceptor scan using a 561 nm laser and 650 LP filter. C) Sensitized emission scan using the FRET channel, 488 nm laser and 600/50 filter. The sensitized emission was calculated based on the intensity in each channel according to Equation 3.2. These calculated values were then used to determine the gauge factor according to Equation 3.8.

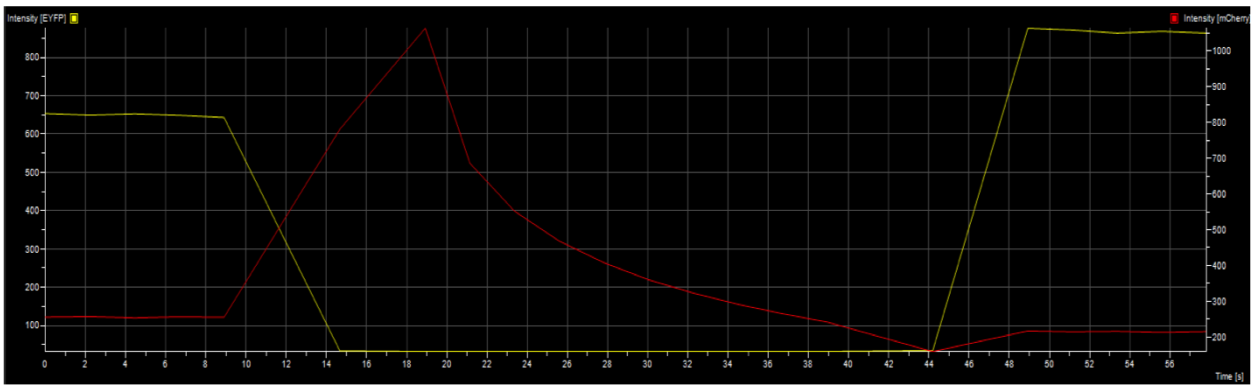

Figure B.6: Photobleaching scan timecourse.
A representative image of a cell undergoing FRET as scanned according to the acceptor photobleaching protocol. Donor fluorescence is not affected during normal scan periods, and the high intensity bleach step rapidly decreases the intensity of acceptor present. After the bleach, a significant change in donor intensity is seen.

Appendix C

Transmembrane peptides as regulators of Toll-like receptor signaling Supporting Information

C.1 Supplementary Figures

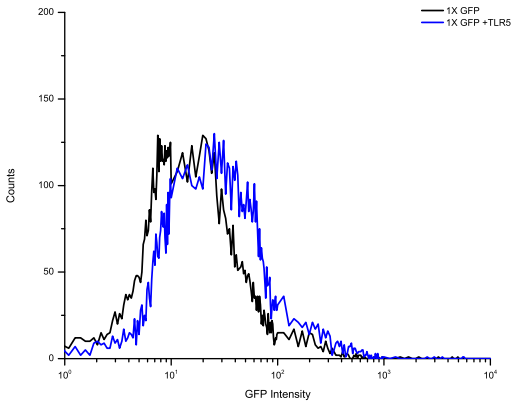

Figure C.1: Jurkat initial response to TLR5 agonist, flagellin.
Jurkat cells were stably transfected with the pGreenFire reporter plasmid. Treatment with the TLR5 agonist flagellin (100 ng/mL) showed a small activation of the reporter. Cells were sorted by collecting the top 10% of activated cells.

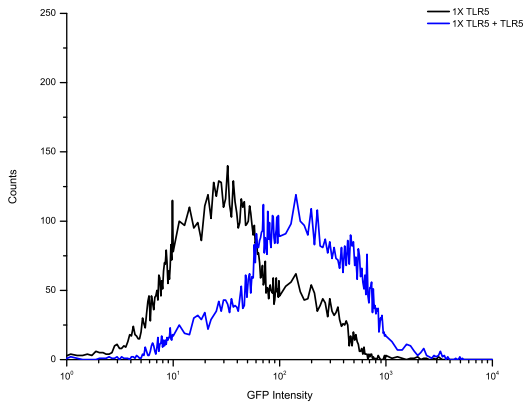

Figure C.2: Jurkat response to TLR5 agonist after one sort.
Jurkat cells sorted for response to TLR5 were grown up and treated again with TLR5 agonist, flagellin (100 ng/mL), and the top 10% of activated cells were collected.

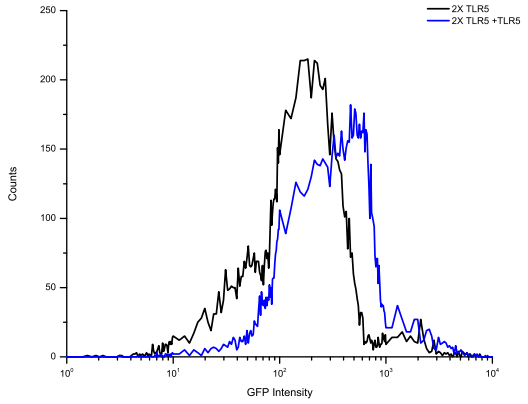

Figure C.3: Jurkat response to TLR5 agonist after two sort.
Jurkat cells twice sorted for response to TLR5 were grown up and treated again with TLR5 agonist, flagellin (100 ng/mL), and the top 10% of activated cells were collected.

Appendix D

Common Experimental Methods and Images

This appendix includes methods and representative images of Western blots, PCR gels, purification of proteins, and purification and characterization of synthetic transmembrane peptides.

D.1 Western Blots

All western blots were run on homemade SDS-PAGE gels. These gels were cast at a single concentration of polyacrylamide, which ranges from 8-15% depending on the size of the protein of interest being detected. All gels are run at a constant voltage,140 V, for 1 hr and 15 min in standard Tris-Glycine-SDS running buffer, before transfer to nitrocellulose membranes (Invitrogen). Transfers to membranes were carried out in a Tris-Glycine buffer containing 20% methanol for 1 hr at a constant current, 100 mA. Membranes were stained with Ponceau red to verify the transfer, then washed 3 times for 10 min with Tris-buffered saline containing Tween-20 (TBST). Membranes were blocked in 5% nonfat milk in Tris-buffered saline for 2 hrs at room temperature with gentle rocking. The membrane was washed 3 times for 10 minutes with TBST before incubation with primary antibody. Primary antibody dilutions were done according to manufacturer recommendations and allowed to incubate overnight at 4°C with gentle rocking. The next morning, the membrane was washed 3 times for 10 minutes with TBST, prior to incubation with horseradish peroxidase conjugates secondary antibodies against the primary antibody host species. The secondary antibody is diluted in 5% milk according to manufacturer recommendations, and allowed to incubate for 2 hr at room temp with gentle rocking. The membrane is again washed 3 times for 10 min with TBST

before addition of chemiluminescent substrates (Invitrogen). The membrane luminescence is then detected using a LAS-4000 (GE Healthcare) CCD camera imager. A representative image of this process from the ToxR assay is shown below (Figure D.1).

D.2 Agarose Gels

All DNA plasmids and PCR products are verified for size and concentration on a 1% agarose gel using a GelRed stain (Phenix Research Products) and a Generuler 1 kb plus DNA ladder (Thermo). For DNA to be used in cloning reactions, PCR reactions were carried out with primers designed for the sequence of interest using a high-fidelity DNA polymerase, Phusion (Thermo), a standard gel result is shown in (Figure D.2A). All PCR annealing and cycle times are varied depending on primers and expected size of PCR product. These products are exchanged into water using a PCR clean-up kit (Omega), and concentration determined using a Nanodrop-2000 (Invitrogen).

To verify proper insertion of DNA, primers for the plasmid backbone were used with a low-fidelity polymerase, DreamTaq (Thermo), to confirm inserts were of the expected size in the cloning site by colony PCR (Figure D.2B). A negative control for empty vector using the backbone primers on the original plasmid should always be used for verification of no insert during standard colony PCR protocols. Colony PCR is performed by picking a single colony from plates grown overnight and smearing the bacteria in the bottom of a PCR tube. The remainder of the colony is grown in media containing appropriate antibiotics overnight for plasmid purification. Colonies in PCR tubes are combined with a master mix PCR reaction mixture, thermocycled, and then analyzed on a gel to determine which colonies should be used for plasmid purification. After mini-prep plasmid purification (Omega), DNA is sent for Sanger sequencing (Genewiz) to verify the plasmid construct.

D.3 Protein Purification

For protein expression and purification, DNA encoding the protein of interest was cloned into the pET-15b expression vector (EMD Millipore) using the NdeI and BamHI restriction sites.

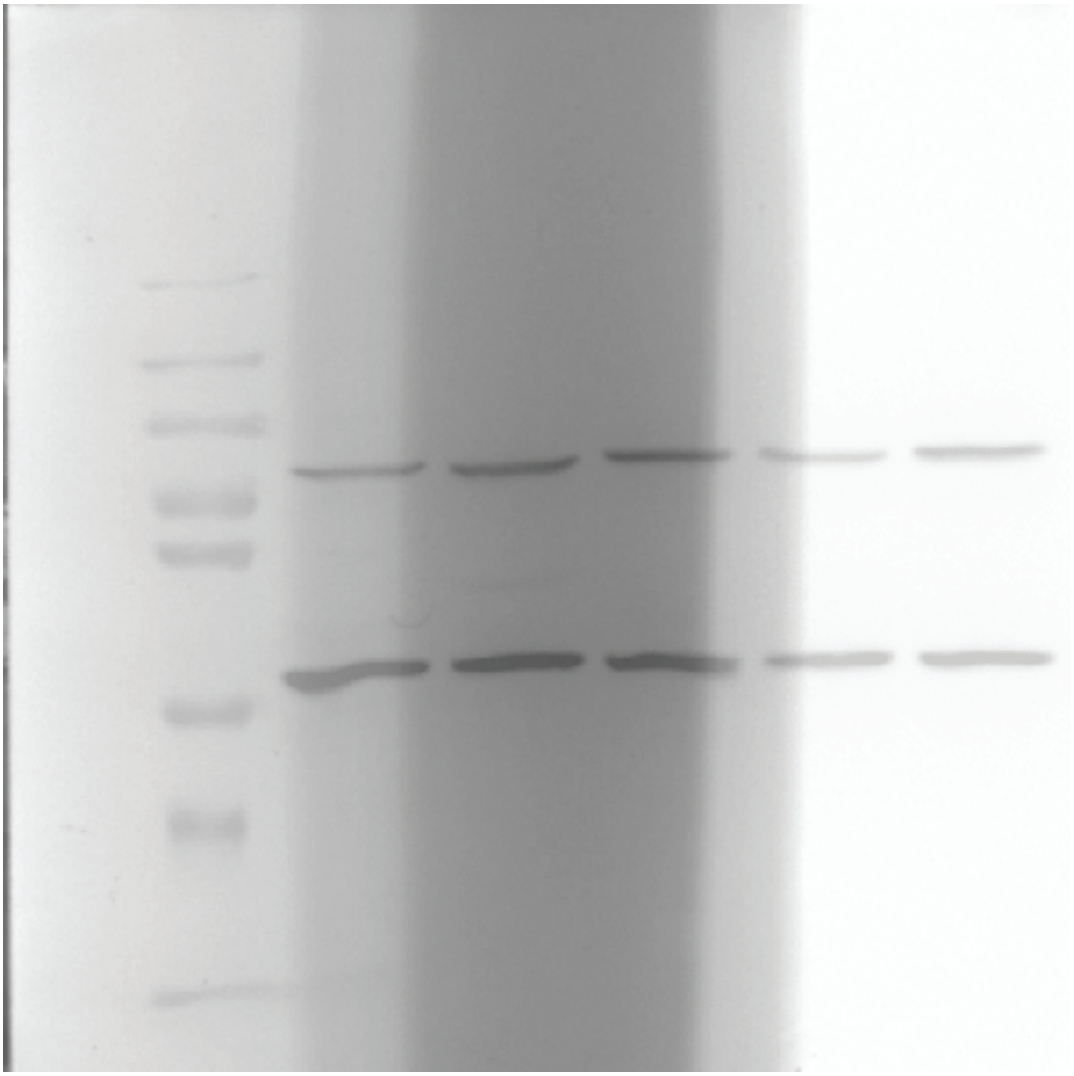

Figure D.1: Maltose binding protein Western blot.
A representative image of the Western blots determined for the ToxR assay homotypic interactions. In a gel there are two bands that express the Maltose binding protein (MBP). The band at approximately 70 kDa is the chimeric transmembrane construct of interest, the band at approximately 45 kDa is endongenous MBP. One can normalize to expression levels and loading using the chimeric and endogenous intensities as determined from ImageJ analysis.

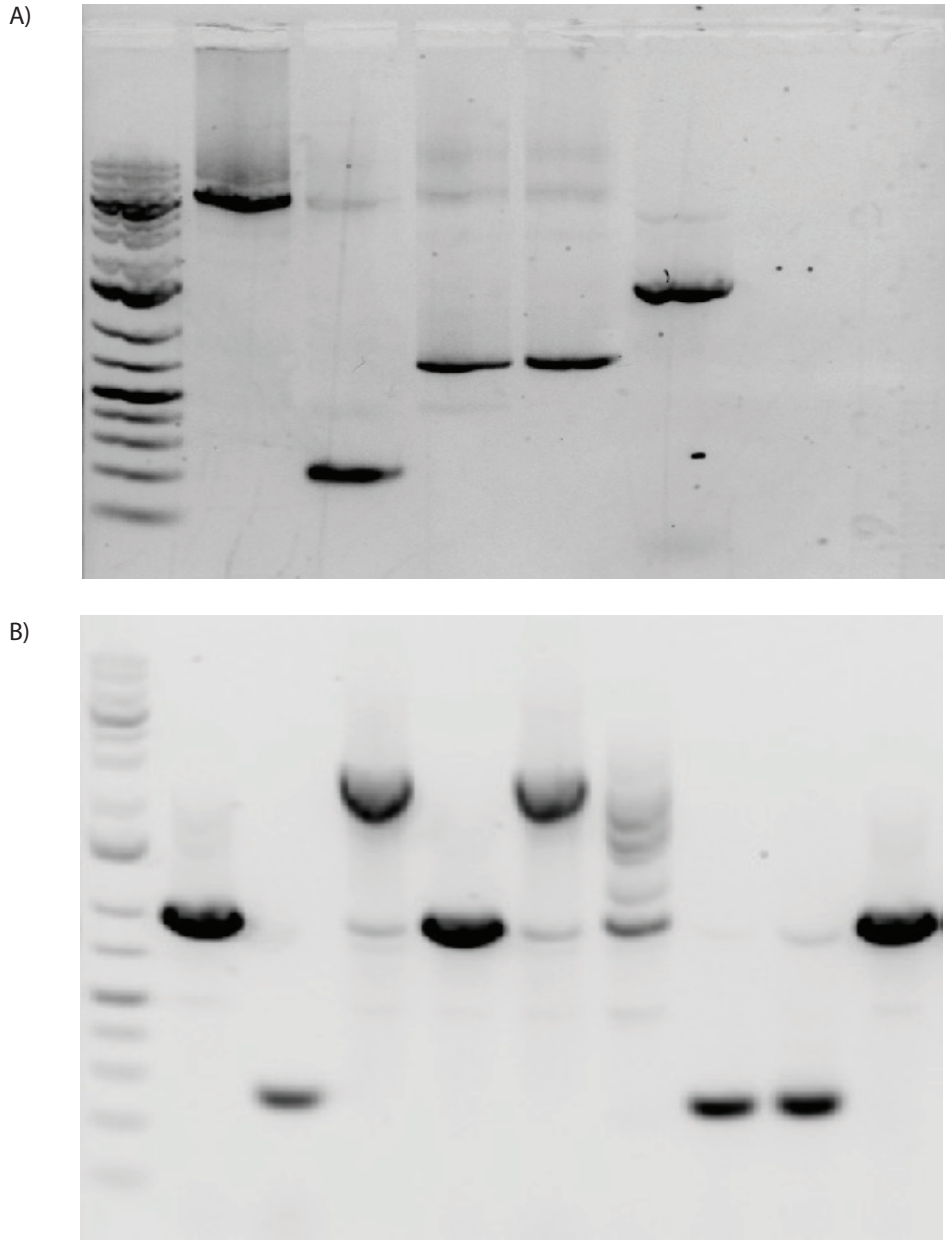

Figure D.2: Agarose gel analysis of PCR products.
A) A representative gel of PCR amplification of inserts for a Gibson assembly reaction using Phusion polymerase. The gel is loaded as ladder, vector product, TLR2 signal peptide, EYFP, mCherry, TLR2 TM+TIR. All samples show the most intense band at the expected product size of interest. B) A representative gel of a colony PCR amplification using DreamTaq polymerase. This gel shows a colony screen for a Gibson reaction to make a pcDNA-FP-TLR2-TM+TIR construct. The gel is loaded as ladder, FP only control, empty vector control, colonies. Results show that only two picked colonies show proper assembly of constructs of the expected size. These colonies were purified and verified by sequencing.

This plasmid was transformed in DH5α bacteria for production, purificitation, and verification of the correct inserts. The correct constructs were then transformed in the BL21(DE3) bacterial expression strain and plated at a 1:10 dilution on LB + Ampicillin plates. Single colonies were selected for starter growths in 5 mL LB + Ampicillin growth media, and allowed to grow overnight at 37°C, 225 rpm. The starter growths were transferred to 250 mL of LB media with no antibiotic the next morning and allowed to grow until a density of $OD_{600} = 0.6$ was reached at which point the cells were induced with 1 mM IPTG. The induction was carried out for 4 hrs at 37 °C, 225 rpm before the cells were pelleted. The bacterial pellet was resuspended in 15 mL of loading buffer (300 mM NaCl, 5 mM imidazole in PBS, pH 7.4) containing protease inhibitors (Roche). The pellets were lysed by sonication (Misonix) using an amplitude of 90% for 6 cycles of 20 sec on, 10 sec off. The lysis was ultracentrifuged by spinning at 14,000 rpm for 30 min in a Sorvall RC 5C Plus centrifuge using the SA600 rotor. The clarified supernatant was used for purification on Talon cobalt columns (Clontech) using an AKTA-10 FPLC (GE). Proteins were purified using a gradient of binding buffer (300 mM NaCl, 5 mM imidazole in PBS, pH 7.4) and elution buffer (300 mM NaCl, 250 mM imidazole in PBS, pH 7.4). For the mCherry protein, Figure D.3A, the protein was eluted using a 2.5% elution buffer mixture for washing (6 column volumes) followed by a 25% elution buffer mixture to recover the protein, and a final wash with 100% elution buffer. For the EYFP protein, Figure D.3B, a similar gradient was used, but to avoid the long tail once the UV trace began to drop at 25% elution buffer, it was quickly ramped to 50% elution buffer until baseline on UV was established, and then a final wash with 100% elution buffer was performed. Samples of fractions from the flow through during column loading, the 2.5% washing step, and 25-50% elution steps were analyzed by Coomassie staining. For Coomassie staining, 15 μL of collected fractions were loaded on a 10% SDS-PAGE gel and ran at 180V for 40 min. Gels were then stained using Coomassie G250, and destained (70% water, 20% methanol, 10% acetic acid) overnight. Images were collected on a LAS-4000 imager (GE).

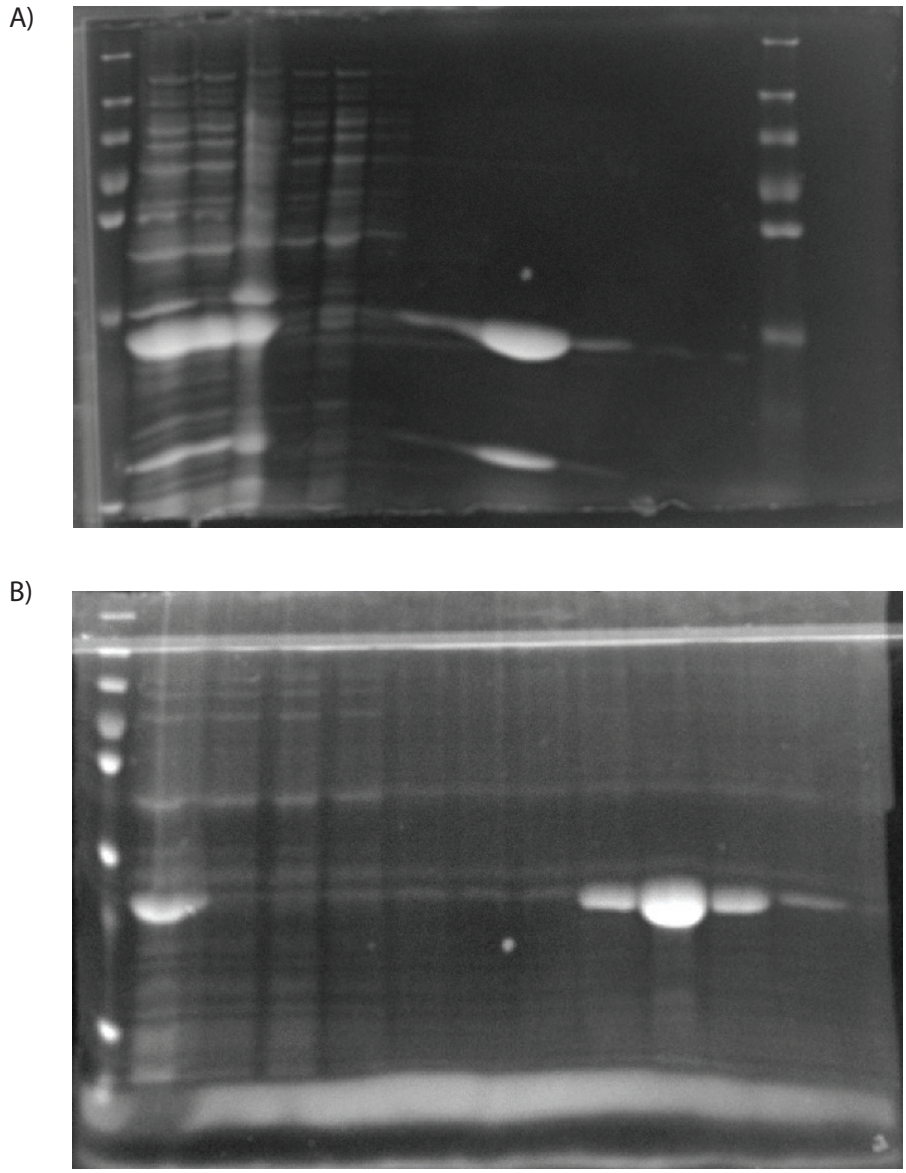

Figure D.3: Fluorescent protein purification.
The mCherry (A) and EYFP (B) proteins were purified using FPLC. Fractions collected were analyzed by Coomassie stain to verify purity and protein of interest. A) The mCherry samples were loaded as ladder, lysate, supernatant, pellet, 3 lanes of column loading flowthrough, 2.5% wash start, 2.5% wash end, 25% start, 25% end, 100% wash, ladder. mCherry is expected to be approximately 30 kDa in size, of which an overexpressed band is seen for the lysate, supernatant, and pellet. mCherry protein binds the column and isn't seen in the flow through, a small amount leaks of during the 2.5% wash, before all of the protein comes off during the 25% elution. B) The EYFP samples were loaded as ladder, supernatant, 3 lanes of column loading flowthrough, 3 lanes of 2.5% wash, 2 lanes of 25% elution, and 2 lanes of 50% elution. The EYFP protein is clearly present as an overexpressed band in the supernatant and only shows up in the expected elution fractions.

D.4 Peptide Purification

Peptides were synthesized at a 0.1 mmol scale using Rink Amide resin 0.36 mmol / g loading capacity using a CEM Liberty automated synthesizer with a Disocery microwave module. Solubility of the peptides was enhanced by including a di-Lysine motif at both termini. For peptides labeled with fluorescent dyes, a 6-atom flexible spacer was added to the N-terminus and dyes were conjugated as previously reported [230, 19]. Side chain deprotection and cleavage from the resin was done using a mixture of trifluoroacetic acid/water/1,2-ethanedithiol/thioanisole/phenol/triisopropylsilane (81.5:5:5:2.5:1 v/v) at room temperature under a N_2 blanket for 2 h. The crude peptides were collected by precipitation with cold (-20°C) diethyl ether. The peptides were then purified on an Agilent 1200 series semi-preparative reverse phase high-performance liquid chromatography system with a Vydac Protein C4 column. Peptides were purified using two different solvent systems. Peptides could be dissolved in a 6:3:1 isopropanol/acetonitrile/water containing 0.1% trifluoroacetic acid solvent or in 100% dimethylsulfoxide. Peptides could then be purified using a linear gradient of solvent A (Millipore water with 0.1% trifluoracetic acid) and solvent B (6:3:1 isopropanol/acetonitrile/water containing 0.1% trifluoroacetic acid), Figure D.4 and D.5, or using a linear gradient of solvent A (Millipore water with 0.1% trifluoracetic acid) and solvent B (Acetonitrile with 0.1% trifluoracetic acid), Figure **??**. The identities of the purified peptides were confirmed by MALDI-TOF mass spectrometry on a Voyager-DE-STR Biospectrometry Workstation (Perseptive Biosystems). All peptides were lyophilized using a Labconoco FreeZone 4.5 freeze drier to yield the purified peptides as their TFA salts.

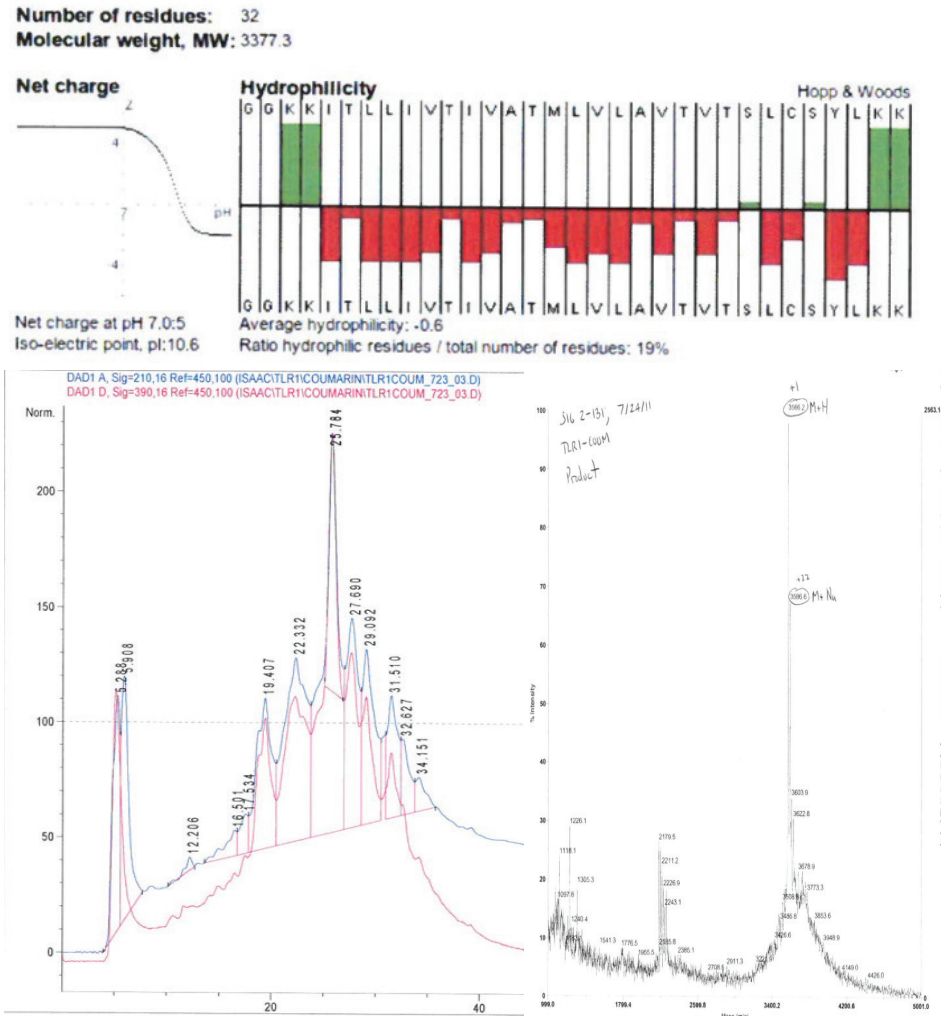

Figure D.4: TLR1 peptide purification.
The TLR1 peptide was synthesized by solid-phase synthesis. A coumarin fluorescent dye was added to the N-terminus for monitoring. The TLR1-coumarin peptide was purified on a Vydac Protein C4 column using a linear gradient of solvent A (Millipore water with 0.1% trifluoracetic acid) and solvent B (6:3:1 isopropanol/acetonitrile/water containing 0.1% trifluoroacetic acid). MALDI was used to verify the products in the chromatogram peaks with the desired peptide product being in the approximately 25.7 min retention time peak.

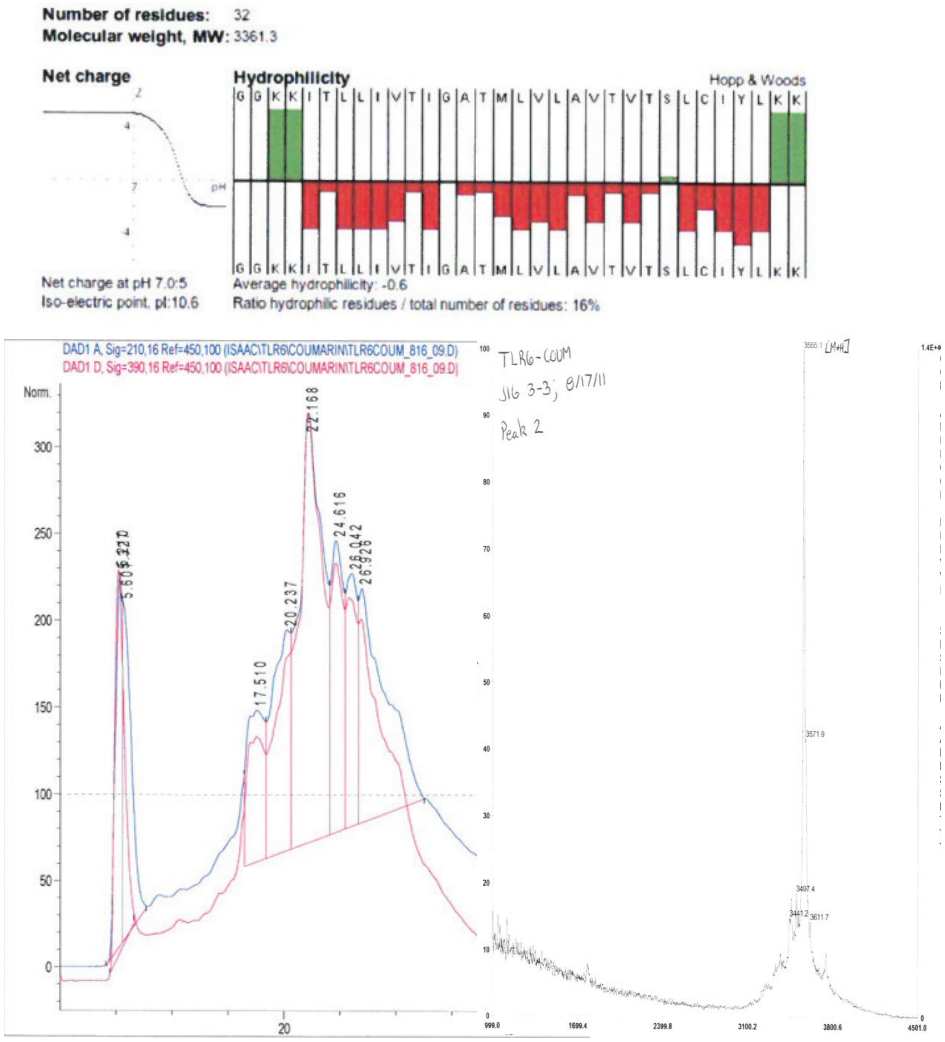

Figure D.5: TLR6 peptide purification.
The TLR6 peptide was synthesized by solid-phase synthesis. A coumarin fluorescent dye was added to the N-terminus for monitoring. The TLR6-coumarin peptide was purified on a Vydac Protein C4 column using a linear gradient of solvent A (Millipore water with 0.1% trifluoracetic acid) and solvent B (6:3:1 isopropanol/acetonitrile/water containing 0.1% trifluoroacetic acid). MALDI was used to verify the products in the chromatogram peaks with the desired peptide product being in the approximately 22.2 min retention time peak.

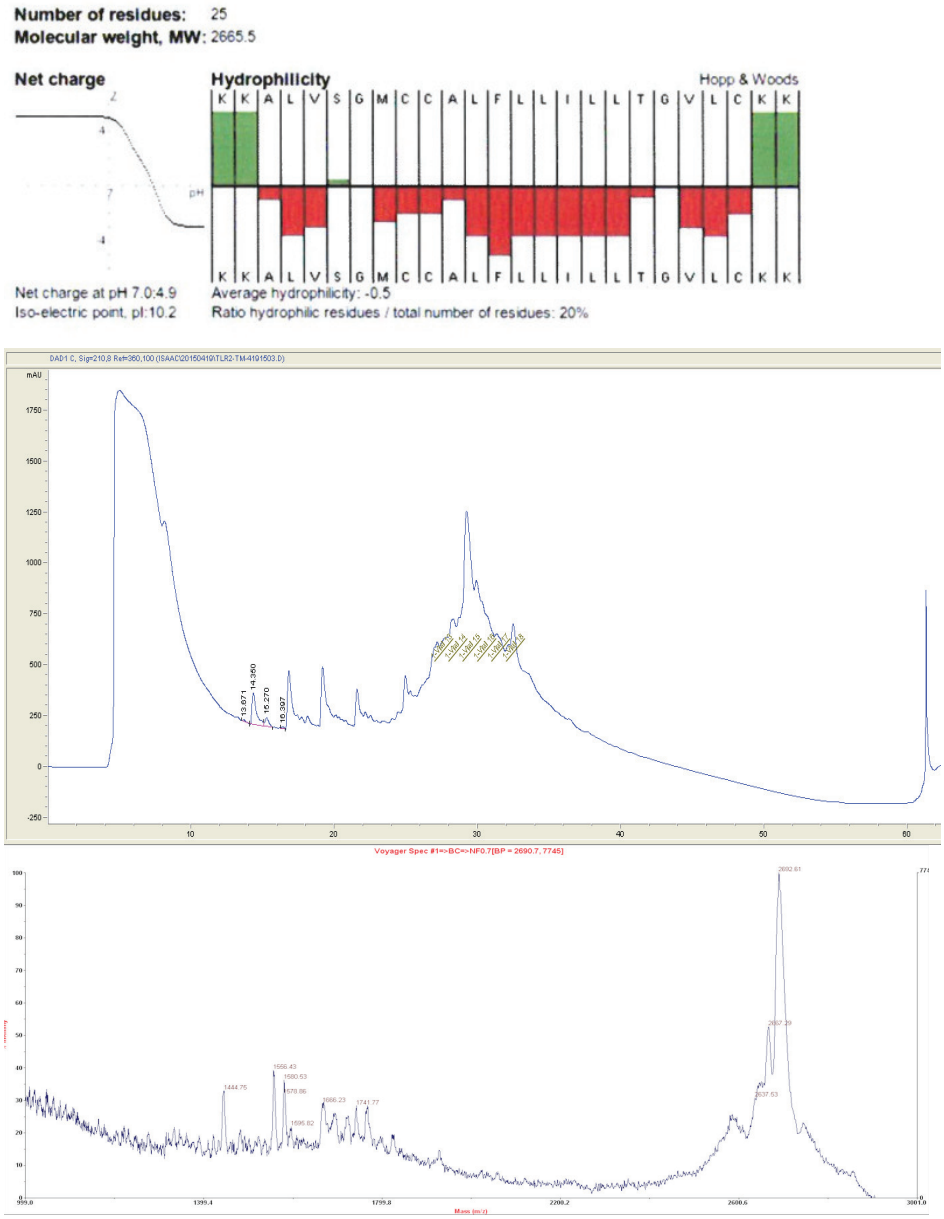

Figure D.6: TLR2 peptide purification.
The TLR2 peptide was synthesized by solid-phase synthesis. The TLR2 peptide was dissolved in 10% DMSO and purified on a Vydac Protein C4 column using a linear gradient of solvent A (Millipore water with 0.1% trifluoracetic acid) and solvent B (Acetonitrile with 0.1% trifluoracetic acid). MALDI was used to verify the products in the chromatogram peaks with the desired peptide product being in the approximately 30 min retention time peak.